THE BEHAVIOR OF TRANSPIRED TURBULENT BOUNDARY LAYERS

Robert J. Moffat, et al

Stanford University

Prepared for:

Office of Naval Research
National Science Foundation
National Aeronautics and Space Administration

April 1975

DISCLAIMER NOTICE

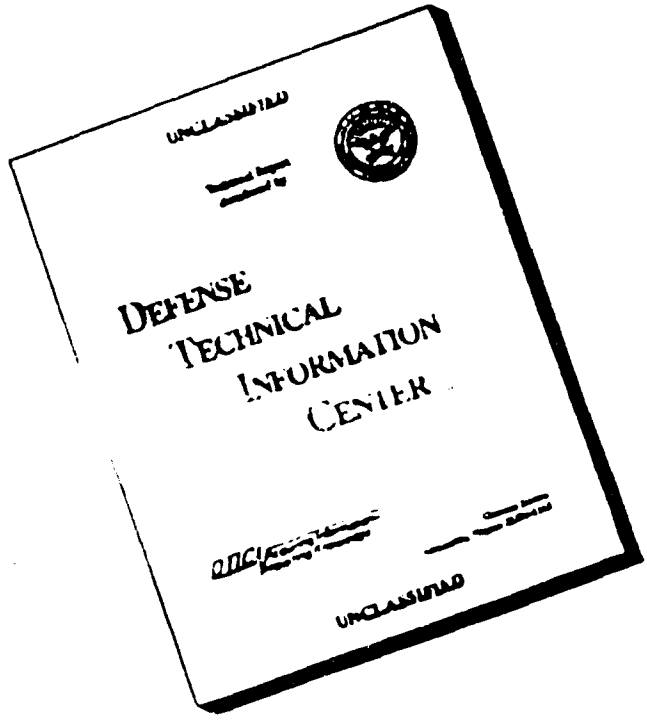

THIS DOCUMENT IS BEST QUALITY AVAILABLE. THE COPY FURNISHED TO DTIC CONTAINED A SIGNIFICANT NUMBER OF PAGES WHICH DO NOT REPRODUCE LEGIBLY.

(1)

THE BEHAVIOR OF TRANSPIRED TURBULENT BOUNDARY LAYERS

By

W. M. Kays and R. J. Moffat

Report No. HMT-20

A summary of studies
supported by

The National Science Foundation
NSF GK534 and NSF GK2201

The National Aeronautics and Space Administration
NGR-05-020-134

The Office of Naval Research
N00014-67-A-0112-0072

Thermosciences Division
Department of Mechanical Engineering
Stanford University
Stanford, California

April 1975

Department of Mechanical Engineering
Thermosciences Division
Stanford University
Stanford, California

ERRATA FOR HMT-20

(W. M. Kays and R. J. Moffat)

Page	Line	Mistake	Should read
11	Eq. 14	where $m_p \cong n - 0.2$ if $c_f/2 \propto Re_x^{-.2}$	where $m_p = -(1+n)\frac{b}{1+b}$ and $c_f/2 \propto Re_m^{-b}$
24	Eq. 28	$t^+ = \frac{t-t_o}{t-t_o}$	$t^+ = \frac{t-t_o}{t_\infty - t_o}$
44	Eq. 53	otherwise $b = 2.0$	otherwise $b = 2.9$
45	Eq. 54	$= (A^+_{eff} - A^+_{eq})/C$	$= -(A^+_{eff} - A^+_{eq})/C$

Errata sheet for HMT-20 on p. 12.

THE BEHAVIOR OF TRANSPIRED TURBULENT BOUNDARY LAYERS

By

W. M. Kays and R. J. Moffat

Report HMT-20

A summary of studies
supported by

The National Science Foundation
NSF GK534 and NSF GK2201

The National Aeronautics and Space Administration
NGR-05-020-134

The Office of Naval Research
N00014-67-A-0112-0072

Thermosciences Division
Department of Mechanical Engineering
Stanford University
Stanford, California

April 1975

ABSTRACT

This report summarizes almost seven years of experimental and analytical studies of the heat transfer behavior of the turbulent boundary layer. The principal objective has been the acquisition of a reliable data base and its modeling by means of a finite-difference computer program. Experimental results are provided to the computer in terms of values and variations of mixing length parameters and turbulent Prandtl numbers. The data base covers a wide range of boundary conditions and free stream conditions:

--- Free stream velocities:--uniform velocity; accelerations at constant K up to "relaminarization"; decelerations at constant B, but not including separation.
--- Transpiration:--blowing and suction at constant blowing fraction F; at constant blowing parameter B; and with stepwise and arbitrary variations.
--- Wall temperature:--uniform, stepwise and arbitrary distributions.

It is shown that a single pair of functions (one for A^+ and one for turbulent Prandtl number) suffice to recover all of the data. Both the surface data (skin friction and Stanton number) and the profiles of mean velocity and temperature are predictable with acceptable accuracy.

ACKNOWLEDGMENTS

This report summarizes the contributions of several doctoral programs: R. J. Moffat, R. L. Simpson, D. G. Whitten, W. H. Thielbahr, H. L. Julien, R. J. Loyd, D. W. Kearney, P. S. Andersen, B. F. Blackwell and A. F. Orlando. Each has contributed both to the data base and to our conceptual understanding of the processes involved. It is surely true that without the individual diligence, imagination, and thought contributed by these men, that we could not have assembled such a complete picture of behavior of the turbulent boundary layer in such a short time.

It is also true that just as "...an army marches on its stomach", so a research program progresses on its apparatus and equipment. Robin A. Birch, George Yoshida, and Tots Ikebe have done yeomen service in fabrication and assembly of everything from the basic structures to the hot wire probes. Our secretaries, Jan Moffat and Ruth Korb, have met many a fleeting deadline for reports and theses, in spite of the perennial hazards of last minute changes and disasters: we really appreciate their "beyond the call of duty" assistance.

This program has been funded by several organizations during its career. The original apparatus for porous wall studies were developed under a National Science Foundation grant, NSF GK534, which also supported the studies of the constant velocity problem, both heat transfer and hydrodynamics. The National Aeronautics and Space Administration funded the study of accelerated flows with NGR-05-020-134, in cooperation with the National Science Foundation NSF GK2201. Most recently, structural studies of decelerating flows were supported by NASA and by the Office of Naval Research, N00014-67-A-0112-0072. The authors hope that the breadth of support reflects the breadth of interest in these studies, and that these data are useful.

Nomenclature

English Letter Symbols

A^+	Dimensionless length scale for the damping function, Eq. (53).
B_h	Blowing parameter of the heat transfer problem, Eq. (5).
B_m	Blowing parameter of the momentum problem, Eq. (3).
c	Specific heat at constant pressure, Btu/lb_m°F.
c_f	Coefficient of skin friction.
c_{f_o}	Coefficient of skin friction with no transpiration, other factors remaining constant, Eq. (47).
D	Damping function for mixing length.
F	Blowing fraction, $\rho_o v_o / \rho_\infty U_\infty$.
g_c	Gravitational constant, ft/sec^2 lb_f/lb_m.
G	Clauser shape factor, Eq. (11).
G_∞	Mass velocity of the free stream, $lb_m/ft^2 sec$.
H	Shape factor, δ_1/δ_2.
k	Mixing length constant.
K	Acceleration parameter, Eq. (15).
ℓ	Mixing length.
ℓ_T	Length scale of turbulence.
m	Exponent describing free stream velocity variation in decelerating flows, Eq. (1).
$\dot{m}''$	Transpiration rate, $lb_m/sec\ ft^2$.
p	Pressure.
p^+	Dimensionless pressure, $\frac{\nu}{\rho U_\tau^3} \frac{dp}{dx}$
Pr	Prandtl number.
Pr_t	Turbulent Prandtl number, Eq. (59).
$\dot{q}''$	Heat transfer rate, Btu/sec ft^2.

English
Letter
Symbols

Re_h	Enthalpy thickness Reynolds number, $G_\infty \Delta_2/\nu$.
Re_m	Momentum thickness Reynolds number, $G_\infty \delta_2/\nu$.
Re_t	Turbulence Reynolds number, Eq. (50).
St	Stanton number.
St_o	Stanton number with no transpiration, other factors remaining constant.
t	Temperature.
t_o	Surface temperature, °F.
$\bar{t}$	Dimensionless temperature, Eq. (28).
t^+	Dimensionless temperature, Eq. (28).
t_d^+	Dimensionless temperature defect, Eq. (18).
t_∞	Temperature of free stream, °F.
u	Velocity, ft/sec.
u'	Fluctuating component of u, ft/sec.
$\bar{u}$	Dimensionless velocity, u/U_∞, or time-averaged velocity.
u^+	Dimensionless velocity, u/U_τ.
U_∞	Velocity of the free stream, ft/sec.
U_τ	Shear velocity, $\sqrt{g_c \tau_o/\rho}$.
v_o	Velocity of the transpired fluid, at the wall.
v_o^+	Velocity of the transpired fluid, at the wall, dimensionless, v_o/U_τ.
v'	Fluctuating component of v.
$\bar{v}$	Dimensionless velocity, v/U_∞, or time-averaged velocity.
x	Distance in the stream-wise direction, ft.
y	Distance normal to the wall, ft.
z	Distance normal to the flow, parallel to the surface, ft.
y^+	Dimensionless distance from the wall, yU_τ/ν.

Greek Letter Symbols

α	Thermal diffusivity, $k/\rho c$.
β	Pressure gradient parameter, Eq. (6).
$\delta( )$	Uncertainty in ( ), Eq. (29).
δ_{99}	Boundary layer thickness to the location of $u/U_\infty = 0.99$.
δ_1	Displacement thickness.
δ_2	Momentum thickness.
δ_3	Clauser thickness, Eq. (10).
ϵ_h	Turbulent diffusivity for heat, Eq. (58).
ϵ_m	Turbulent diffusivity for momentum, Eq. (44).
Δ_2	Enthalpy thickness.
Δ_3	Defect enthalpy thickness, Eq. (19).
λ	Mixing length proportionality factor, Eq. (55).
ρ_0	Density evaluated at the surface, lb_m/ft^3.
ρ_∞	Density evaluated in the free stream, lb_m/ft^3.
τ	Shear stress, lb_f/ft^2.
τ_0	Shear stress at the surface, lb_f/ft^2.
τ_t	Turbulent shear stress.
ν	Kinematic viscosity, ft^2/sec.

INTRODUCTION

The boundary layer with transpiration thru the solid surface is a variant of the general boundary layer problem that has been of considerable interest in technical applications for at least two decades. In the early 1950's transpiration was being extensively investigated as a means of cooling aerodynamic surfaces under high velocity flight conditions. But transpiration from a solid surface over which a fluid is flowing, and on which a boundary layer is developing, is of interest in a large number of quite different types of applications, of which transpiration cooling is only one.

In the typical transpiration cooling application, the solid surface is constructed of some kind of porous solid material. Cooling fluid, which may be chemically the same as the free-stream, is then forced through the surface with the objective of protecting the surface from a hot free-stream. This is a boundary layer problem for which the normal component of velocity at the solid-fluid interface is non-zero, but otherwise the same momentum and energy boundary layer differential equation must be solved as for the nontranspired boundary layer. A variation on this problem occurs when the cooling fluid is a chemically different specie than the free-stream fluid. For example, helium might be injected as a coolant to protect a surface from a high temperature air free-stream. In this case the mass-diffusion equation of the boundary layer must be solved in addition to the momentum and energy equations. There are obviously similarities between these two types of problems, but also fundamental differences. Both are "mass transfer" problems in the sense that mass is transferred across the fluid-solid interface, but the latter is also a mass-diffusion problem, while the former is not.

Another transpiration problem arises when there is evaporation or sublimation from an interface into a boundary layer, or condensation onto the interface. A further variation on the problem arises when there is chemical reaction either within the boundary layer or at the surface.

In any of the cases cited, the direction of the flow normal to the surface at the interface could be into the surface, or it could be out of the surface. The terms "blowing" and "suction" are frequently used to

denote the direction of flow at the interface, while the word "transpiration" generally is taken to embrace both cases. Suction is sometimes used as a scheme for aerodynamic boundary layer control because it is possible to inhibit or prevent boundary layer separation by suction.

These various types of applications suggest why chemical, mechanical and aeronautical engineers have all made significant contributions to the theory, and the terminology to a certain extent reflects these various origins of interest.

In the class of problem considered here it is assumed that the surface is aerodynamically smooth, and that the holes or pores in the surface through which the transpiration fluid flows are sufficiently small relative to the boundary layer thickness so that the velocity normal to the surface may be treated as uniform over every small region. (If the holes are large, with large spacing, the boundary layer structure is altered. Although the resulting boundary layer may have some of the characteristics of the transpired boundary layer, that problem will not be considered here.)

The transpired boundary layer may be laminar or turbulent. The laminar boundary layer with transpiration has been extensively studied, resulting in a large number of exact mathematical solutions for certain fundamental cases where similarity in velocity profiles, and in temperature profiles, is obtained, and various approximate methods have been developed to handle cases when similarity does not exist. More recently finite difference solutions have become so easy to obtain with digital computers, for any kind of boundary conditions, that further investigation of the laminar boundary layer does not appear very fruitful, except for some very special cases. The turbulent boundary layer, on the other hand, is not nearly so well understood, even without transpiration. Up until about ten years ago there were remarkably few experimental data available for the transpired turbulent boundary layer. Mickley et al. (1954, 1957) at MIT had, during the 1950's, studied the momentum and concentration boundary layers; very little had been done with the thermal boundary layer. Certainly there were insufficient data of adequate accuracy to provide the basis for anything approaching a complete turbulent boundary layer theory. In the 1960's experimental activity went forward with increasing intensity in various parts of the world, and in 1965 the authors joined in this effort.

At the present time the behavior of the turbulent transpired momentum boundary layer for an essentially incompressible fluid is fairly well understood for a sufficient range of boundary conditions to make it worthwhile to attempt to summarize the available data, and the state-of-the-art in boundary layer analytic prediction. A similar statement can be made about the thermal boundary layer, but only for fluids with Prandtl number near unity. This is not to say that predictions adequate for most engineering design cannot be made for other fluids, but experimental confirmatory data are lacking. Data on the turbulent transpired concentration boundary layer are considerably more scarce. The concentration boundary layer problem is complicated by the fact that strong transpiration is usually accompanied by large fluid property gradients caused by large concentration gradients, and this adds more variables to the experiments. Of course if concentrations, and thus concentration gradients, are small, and if Lewis number is near unity, the behavior of the concentration boundary layer should be identical to that of the thermal boundary layer.

In order to restrict this paper to a range of variables and boundary conditions for which there is now a considerable body of data, the scope of the paper will be restricted to the following:

(a) Momentum and thermal boundary layers only
(b) Constant fluid properties, so that the momentum and energy equations are effectively de-coupled.
(c) Low velocity flows, with a similar result as in (b).
(d) Two-dimensional boundary layers.
(e) Steady flow.
(f) Aerodynamically smooth surface
(g) Injection or suction velocity uniform over each small area of surface (though possibly varying in the streamwise direction on a larger scale)

Within this scope, the objective of the paper will be to summarize the present status of our experimental knowledge of this family of boundary layer flows, and to demonstrate how these flows can be predicted by a reasonably simple mathematical model and a finite-difference calculation procedure. Because the authors themselves have contributed much of the available data to the literature, the main line of experimental data to be presented will

be author's own. However, wherever practicable, comparisons will be made with the data of others, because there are indeed some discrepancies and, consequently, some differences of opinion. The mathematical model to be proposed is only one of several eddy-viscosity, eddy-conductivity models discussed in the literature, all of which are actually very similar. However, it is one that has been used with considerable success by the authors, as will be demonstrated. It is not a purpose of this paper to critically evaluate various prediction schemes. It is suggested that others might find the experimental data summarized here to be useful for such an evaluation.

The general problem considered is illustrated by reference to Fig. 1. A fluid flows at a steady rate along a flat surface which is porous, and through which fluid with the same composition can be forced into the boundary layer or withdrawn from the boundary layer (blowing or suction). Reynolds number is sufficiently high so that the boundary layer is turbulent. It is presumed that the surface is aerodynamically smooth and that the velocity normal to the surface, whether positive or negative, is uniform over an area large relative to the sublayer thickness. It is presumed that the solid surface is a heat conductor, and that heat can be conducted to or from the surface. It is further presumed that the surface construction is such that the transpired fluid is in thermal equilibrium with the solid surface at the interface. In general, our long range objective would be to consider the case where the mass transfer rate $\dot{m}''$ (i.e., the transpiration rate) is any arbitrary function of distance x along the surface, where the convection heat transfer $\dot{q}''$ is any arbitrary function of distance x along the surface (or the surface temperature t_o is any arbitrary function of x). We would like, ultimately, to consider the case where the free-stream velocity U_∞ may vary in any arbitrary manner with x , but we will restrict free-stream temperature t_∞ to a constant. The boundary layer is two-dimensional, with the co-ordinate y used to measure the distance normal to the surface (i.e., all properties are uniform with respect to the Z-direction). Under these conditions we are interested in the development and properties of a momentum boundary layer, characterized by a thickness δ_2 , and a thermal boundary layer characterized by a thickness Δ_2.

It is apparent that solution of the general problem described above is going to require a theory incorporating some broadly applicable hypotheses about the turbulent transport mechanisms. The number of independent variables, and the infinite possibilities for varying boundary conditions, make it impractical to consider the totally experimental approach wherein experimental data are generalized by dimensional analysis and then applied directly to particular problems. This raises the question as to what kinds of experiments should be carried out to provide the experimental basis for a general theory. What are the more fundamental cases that should be tested to provide firm bench-marks and from which the various constants and functions necessary to a more general theory can be derived? What are some critical experiments that should be carried out to provide a severe test of a general theory?

Experience with the laminar boundary layer, which can of course be completely handled analytically, has pointed the way to certain fundamental cases that also arise with turbulent boundary layers. Certain parameters can be maintained constant, which makes it easier to derive the critical constants and to determine their functional dependence. In laminar boundary layer theory the concept of velocity profile similarity leads to a very considerable mathematical simplification, and to a whole family of simple solutions for some particular cases of transpiration and free-stream velocity variation. Clauser (1954) demonstrated that for a turbulent boundary layer without transpiration a family of "equilibrium" boundary layers exist which have partial velocity profile similarity, and Bradshaw (1967) demonstrated that essentially the same free-stream velocity variation that yields the laminar boundary layer "similarity" solutions also leads to "equilibrium" boundary layers in the turbulent case. Anderson (1972) has shown that essentially the same situation exists for transpired turbulent boundary layers. Thus the family of "equilibrium" transpired turbulent boundary layers appears to provide a fundamental set, and will be used in this paper for the main presentation of experimental data. The constants and functions for use in a more general theory will be derived from these "equilibrium" experiments. Then, to provide some severe tests of general theories, a small amount of data for "non-equilibrium" cases will be presented.

In the section immediately following, the concept of the "equilibrium" boundary layer will be discussed more precisely. The available experimental data for "equilibrium" transpired boundary layers will then be presented in

three groups, starting with the case of a constant free-stream velocity, then the case of an accelerating free-stream velocity (favorable pressure gradient), and finally the case of decelerating free-stream velocity (adverse pressure gradient).

After presentation of some data on "non-equilibrium" flows, mathematical models for both the momentum and energy equations will be discussed, and the appropriate constants and functions derived from the "equilibrium" experiments will be presented. Finally some examples of predictions based on this particular theory will be presented.

As a final word of introduction, it should be pointed out that although the primary subject of this paper is the turbulent boundary layer with transpiration, the case of the impermeable wall, i.e., non-transpiration, is a valid member of the family of flows considered. The data presented for this case, which of course has been extensively studied by many workers over the years, was obtained in the authors' laboratory. However, in all essentials it is virtually identical to that reported by most other workers, and thus can probably be considered as definitive.

EQUILIBRIUM BOUNDARY LAYERS

The motivation which has guided the choice of parameters for the so-called equilibrium turbulent boundary layers has its roots in the similarity variables of laminar boundary layer theory. In laminar boundary layers, fixing the value of an appropriate ratio of boundary conditions allows the reduction of the partial differential equation to an ordinary one for some flow conditions, and permits a relatively simple, mathematical solution. The resulting velocity and temperature profiles are exactly self-similar, and there is no uncertainty as to the efficacy of the parameters chosen: the results speak for themselves. No such drastic benefit is realized in turbulent studies. Combinations of boundary conditions can be proposed as being likely to lead to self-similar behavior of the boundary layer, but the profiles must be found experimentally and they are not usually exactly self-similar, only approximately so. Turbulent boundary layers driven by these carefully chosen combinations of boundary conditions are known as "equilibrium" or "asymptotic" boundary layers: not truly similar, but closely so.

The best-known class of flows leading to laminar similarity solutions is the Falkner-Skan family, which results when the free-stream velocity, U_∞, varies as x^m (m positive or negative) and v_o varies in a related manner, i.e.,

$$U_\infty \propto x^m \tag{1}$$

and

$$v_o \propto U_\infty(c_f/2) \tag{2}$$

It is particularly important to note that similarity is not obtained in general when v_o is a constant, independent of x. The special case of $v_o = 0.0$ and U_∞ a constant does yield similarity in velocity profiles, but, in general, a constant value of v_o is an "arbitrary" variation of blowing as far as similarity is concerned. Note further that similarity is achieved only if $v_o/(U_\infty c_f/2)$ is a constant with respect to x. This dimensionless group is usually called the "blowing parameters", and will be termed B_m. Thus,

$$B_m = \frac{\rho_o v_o}{\rho_\infty U_\infty (c_f/2)} = \frac{\dot{m}''/G_\infty}{c_f/2} \tag{3}$$

The physical significance of holding B_m constant can be appreciated if it is observed that B_m can be rearranged to display:

$$B_m \triangleq \frac{(\rho_o v_o)U_\infty}{\tau_o} \tag{4}$$

In this form it can be seen that B_m is the ratio of the transpired momentum deficit to the surface shear force. When these are kept in a fixed ratio along a surface, then the laminar boundary layer develops in such a way as to produce similar velocity profiles. It seems likely that this ratio would also be important in turbulent boundary layers.

The energy equation can also be cast in such form as to reveal its similarity variables. Similar temperature profiles result when, in a laminar boundary layer having hydrodynamic similarity, the wall and free-stream temperatures are constant and the "heat transfer blowing parameter" B_m is held fixed. This parameter reflects the ratio of the transpired energy deficit to the surface heat transfer and is defined by:

$$B_h \triangleq \frac{\rho_o v_o}{\rho_\infty U_\infty St} = \frac{\dot{m}''/G_\infty}{St} = \frac{\dot{m}'' c(t_o - t_\infty)}{\dot{q}_o''} \tag{5}$$

The blowing parameter B_m and the heat transfer blowing parameter B_h both arise in the reduction of the partial differential equations of the laminar boundary layer to the ordinary differential equation of the similarity situation. Both, however, are also visible in the integral equations of the boundary layer: a form which applies also to turbulent boundary layers.

The condition of Eq. (1) can be shown to result in a pressure gradient parameter, β, which remains constant when m, is constant. The parameter β is defined as follows:

$$\beta \triangleq \frac{\delta_1}{\tau_0}\left(\frac{dP}{dx}\right) \tag{6}$$

β may be interpreted as the ratio of the axial pressure force acting on the boundary layer to the shear force at the wall. Thus B_m and β should have similar influences upon the development of the momentum boundary layer, and indeed if one examines the following form of the momentum integral equation of the boundary layer, this is seen to be the case:

$$\frac{d(U_\infty^2 \delta_2)}{dx} = \left(\frac{g_c \tau_0}{\rho_\infty}\right) (1 + B_m + \beta) \tag{7}$$

Equation (7) expresses the rate of growth of the momentum deficit of the boundary layer. If B_m and β are held constant along a surface, it is not surprising that the boundary layer maintains a similarity of structure as it develops.

The energy integral equation can be manipulated in such a way as to show the importance of B_h :

$$\frac{d[c\Delta_2 U_\infty (t_0 - t_\infty)]}{dx} = \frac{\dot{q}''_0}{\rho_\infty} (1 + B_h) \tag{8}$$

Equation (8) expresses the rate of growth of the axially flowing energy flux in the thermal boundary layer, and B_h is seen to have the same influence on the thermal boundary layer as B_m has on the momentum boundary layer. However, note that the pressure gradient parameter β has no direct effect on the thermal boundary layer.

Let us now turn to the turbulent boundary layer. It would be convenient to be able to define some kind of similarity that would lead to a classifiable group of flows. The problem is not quite so straightforward as for laminar boundary layers, because with turbulent boundary layers there are two distinct regions to consider: the inner and the outer regions behave differently. It is possible to have inner region similarity independent of the outer part of the boundary layer, though this latter may comprise most of the boundary layer thickness. The existence of a local "law-of-the-wall" which seems to hold under many conditions regardless of upstream history is witness to this fact. Put another way, we have been discussing some condi-

tions of ratios of forces acting on the boundary layer that lead to similar structure in laminar boundary layers. With the turbulent boundary layer it is possible for the inner region, near the wall, to be in equilibrium while the outer region continues to develop. This inner region equilibrium appears to be associated with an equality between the rate of production of turbulent energy and the rate of dissipation of turbulent energy.

Clauser (1954) proposed that boundary layers having outer region similarity be called equilibrium boundary layers, and that an equilibrium boundary layer be one for which the outer region velocity profile, plotted in velocity-defect co-ordinates was universal. This condition can be expressed by:

$$\frac{U-U_\infty}{U_\tau} = f\left(\frac{y}{\delta_3}\right) \quad \text{only} \tag{9}$$

where

$$\delta_3 = \int_0^\infty \frac{(U-U_\infty)}{U_\tau}\, dy \tag{10}$$

Clauser also proposed a shape factor, G, that would be a constant, independent of x, under these conditions:

$$G = \frac{1}{\delta_3} \int_0^\infty \left(\frac{U-U_\infty}{U_\tau}\right)^2 dy \tag{11}$$

Experimentally, it has been found that if β is held constant, G remains constant. Similarly, it has been found that holding B_m constant also yields constant G profiles. More recently it has been shown (Andersen, 1972) that if $(B_m + \beta)$ is maintained constant, G will be constant. Thus it appears that the same relationship among the forces acting on the boundary layer that yields similarity solutions for laminar boundary layers yields equilibrium boundary layers, in the Clauser sense, for turbulent boundary layers.

It is not surprising that the experimental condition leading to the constant β (and thus constant G) boundary layers is, again,

$$U_\infty \propto x^m \tag{12}$$

If there is transpiration in addition, B_m must be constant in order to yield constant G, and this requires that

$$v_0 \propto U_\infty(c_f/2) \tag{13}$$

which may readily be shown to reduce, to a good approximation, to

$$v_0 \tilde{\propto} x^{m_F} \tag{14}$$

$$\text{where } m_F \simeq n - 0.2 \text{ if } c_f/2 \propto Re_x^{-.2}$$

Figure 2 shows an example of a series of velocity-defect profiles for a blown adverse pressure gradient equilibrium boundary layer for which B_m, G, β, m, and m_F are all constant. Figure 3 shows the additive character of B_m and β for 18 equilibrium boundary conditions.

A rather special case of equilibrium turbulent boundary layers occurs in accelerating flows where the acceleration parameter, K, is maintained constant.

$$K \triangleq \frac{\nu}{U_\infty^2}\frac{dU_\infty}{dx} \tag{15}$$

The significance of constant K can be appreciated if the momentum integral equation of the boundary layer is written in the following form:

$$\frac{dRe_m}{U_\infty dx/\nu} = c_f/2 + v_0/U_\infty - K(1 + H)Re_m \tag{16}$$

If K and v_0/U_∞ are maintained constant, independent of x, and if K is finite and positive, the flow must inevitably approach a state of equilibrium for which Re_m is constant. This is often spoken of as an asymptotic-accelerating flow; a special case of an equilibrium boundary layer in which there is not only outer region similarity (constant G),

but also inner region similarity. The velocity profiles are similar all the way to the wall, with the result that not only is Re_m constant, but so also are $c_f/2$ and the shape factor H. Thus, constant K and constant v_o/U_∞ together yield a family of similarity solutions for laminar boundary layers and a family of asymptotic-accelerating layers for the turbulent case. An interesting feature of Eq. (16) is the fact that for each positive value of K and each value of F there exists a definite value of Re_m: as K increases, Re_m decreases. Experiments indicate that it is impossible to maintain a turbulent boundary layer if Re_m is below about 300. The corresponding value for K is about 3×10^{-6}. In other words, if K is of the order of 3×10^{-6}, or greater, the turbulent boundary layer will tend to revert to a laminar boundary layer. Evidence of this trend will be demonstrated in some of the experimental data to be presented.

If K is negative (i.e., a decelerating flow), no such asymptotic equilibrium can exist (except as discussed below). Note also that for a given value of K the rate of transpiration, whether positive or negative, will have a substantial influence on the asymptotic value of Re_m.

Another related type of asymptotic flow can be recognized in Eq. (16). If v_o/U_∞ is negative, Re_m will approach a constant when K is zero or negative, so long as the v_o/U_∞ term is larger in the absolute sense than the last term. This type of boundary layer is frequently referred to as the "asymptotic suction layer", and may be either laminar or turbulent, depending upon the magnitude of Re_m at the asymptotic condition. Note that for $K = 0.0$, $c_f/2$ approaches an asymptote, $-v_o/U_\infty$. Physically, the surface shear force is then precisely equal to the loss of momentum of the fluid that is brought from the free-stream to zero velocity at the surface. This represents a lower limit on $c_f/2$.

The energy integral equation of the boundary layer can be put in a form similar to that of Eq. (16), for the case of constant surface and free-stream temperatures.

$$\frac{dRe_h}{U_\infty dx/\nu} = St + v_o/U_\infty \qquad (17)$$

The important difference is that there is no term corresponding to the acceleration term (or pressure gradient term). Thus if K is a positive constant, the momentum boundary layer will come to equilibrium, with Re_m constant,

but the thermal boundary layer will continue to grow. In fact if K is maintained constant for sufficient distance the thermal boundary layer will grow outside of the momentum boundary layer as Re_h increases indefinitely.

As Eq. (17) suggests, an asymptotic thermal boundary layer exists in the case of negative v_o/U_∞ : an "asymptotic-suction-layer" similar to the momentum boundary layer case.

The general question of equilibrium turbulent thermal boundary layers, i.e., thermal boundary layers having outer region temperature profile similarity, has not, so far as the authors are aware, been systematically explored, although Blackwell (1972) has studied adverse pressure gradient equilibrium boundary layers with constant surface temperature. If surface temperature is allowed to vary, additional possibilities for similarity arise. In order to restrict this paper to a few classifiable types of boundary layers, consideration will be restricted to thermal boundary layers on constant temperature surfaces, with a constant temperature free-stream.

There is no question that the turbulent thermal boundary layer which forms on a constant temperature surface when the free-stream velocity is constant does have outer region similarity. There is also a fixed ratio (for a given Prandtl number) of enthalpy thickness Reynolds number to momentum thickness Reynolds number. Even when the boundary layer starts with widely differing enthalpy and momentum thickness Reynolds numbers, this ratio of sizes will be approached at points downstream.

When there is blowing or suction with constant free-stream velocity, and the blowing parameter B_m is maintained constant, it is observed experimentally that B_h will also approach a constant. The thermal boundary layer will approach an equilibrium state with a fixed ratio of enthalpy to momentum Reynolds numbers, regardless of the starting conditions.

Blackwell (1972) observed the same situation for an adverse pressure gradient flow for which β was held constant. Examination of the integral equations, (7) and (8), might suggest that analogous behavior for both boundary layers would be unlikely when there is a pressure gradient, because β appears in only one of the equations. However, the adverse pressure gradient is accompanied by a decrease in the surface shear stress (and in $c_f/2$), but no significant change in heat flux (and St), with the result

that the rate of growth of both boundary layers becomes the same. A similar conclusion results from examination of Eqs. (16) and (17). For an equilibrium, or constant β, boundary layer, the final term in Eq. (16) tends to vary with x at the same rate as does $c_f/2$, and St in Eq. (17) also varies at the same rate.

The equilibrium thermal boundary layer can be defined in an analogous manner to the equilibrium momentum boundary layer, i.e., a thermal boundary layer having outer region temperature profile similarity. Following the form of Equations (9 and 10), temperature defect coordinates are defined,

$$t_d^+ = \frac{(t_\infty - t)}{(t_\infty - t_0)} \frac{\sqrt{c_f/2}}{St} = \left(\frac{y}{\Delta_3}\right) \tag{18}$$

where

$$\Delta_3 = \frac{\sqrt{c_f/2}}{St} \int_0^\infty \frac{(t_\infty - t)}{(t_\infty - t_0)}\, dy \tag{19}$$

Figure 4 shows three temperature profiles plotted in these coordinates for an adverse pressure gradient momentum boundary layer having velocity-defect similarity, i.e., an equilibrium momentum boundary layer. Note that the temperature profiles are universal everywhere outside of the sublayer. Thus a constant G, β, m equilibrium momentum boundary layer will also yield an equilibrium thermal boundary layer when surface temperature is constant. The same thing is true if there is transpiration with B_m constant: B_h will become constant and similar temperature profiles result.

This behavior might also be anticipated from experience with the laminar boundary layer similarity solutions. Recall that the condition of Eq. (1) leads to laminar similarity solutions for the thermal boundary layer, so it is not surprising that this condition leads also to equilibrium turbulent thermal boundary layers.

In summary, equilibrium turbulent momentum boundary layers, having outer region velocity profile similarity, can be achieved by holding con-

stant the pressure gradient parameter, β , and the blowing parameter, B_m . Experimentally, these conditions can be established by adjusting free-stream velocity, U_∞ , and transpiration velocity, v_0 , according to the condition of Eqs. (1) and (2).

A special case of momentum boundary layer equilibrium is approached for accelerating flows when the acceleration parameter, K , is maintained finite and positive. For this special case the velocity profiles possess both inner and outer similarity.

Equilibrium thermal boundary layers are obtained, if surface and free-stream temperature are maintained constant, under the same conditions leading to equilibrium momentum boundary layers.

The special case of a constant acceleration parameter, K , does <u>not</u> result in an equilibrium thermal boundary.

EXPERIMENTAL RESULTS

The objective of this section is to illustrate the hydrodynamic and heat transfer behavior of equilibrium and near-equilibrium turbulent boundary layers subject to blowing and suction, acceleration and deceleration of the free stream. These are the cases used to generate the differential correlations used in the mathematical model described in the later portions of this paper. They show the principal physical responses of the boundary layer and serve to illustrate the complexity of the prediction problem. No attempt has been made to present a complete survey of the available data. The reader interested in the complete data sets should acquire the referenced theses, which contain full, tabular, data sets. The objective here is simply to provide the reader with insight into the nature of the physical response of the boundary layer.

The Stanford experimental results all derive from the same basic apparatus, described by Moffat (1967), modified by subsequent authors to permit studies of accelerating and decelerating flows.

The apparatus is an open circuit wind-tunnel whose test section is 8 feet long, 20 inches wide and approximately 6 inches high at the inlet end. The lower surface of the test section is the porous working plate while the top is a control surface and can be adjusted to vary the free stream velocity in the streamwise direction. The porous plate is subdivided into 24 strips each 4.0 inches long in the flow direction and each provided with a transpiration flowmeter, a set of imbedded electric heaters, and temperature measuring instrumentation. Heat transfer rate is deduced from the measured electrical power by energy balance, accounting for the heat losses from the porous strip to its surroundings by conduction and radiation. All tests were conducted with air as the transpired fluid as well as the main stream fluid, and with small temperature differences (approximately 25°F) to minimize the effects of properties variation through the boundary layer.

The porous plates are known to be uniform within $\pm 6\%$ in permeability in the center 6-inch span, where the data are taken. The plates were custom made by sintering bronze particles together in a polished stainless steel mold cavity. The particles ranged in size from 0.002 to 0.005 inches in diameter. The fabrication technique resulted in a porous material whose surface feels smooth to the touch and which displays a roughness of 250

micro-inches on a standard Surfa-gage test. The plates were installed with an insulating spacer of 0.020 thickness between adjacent plates, with the joints finished by hand until they were not discernible to the touch.

Wall temperatures were held uniform to within $\pm$0.5°F in cases reported as "constant wall temperature" to reduce conduction transfer between plates. Main stream velocity was shown to be uniform in the span-wise direction within $\pm$.4% with the free stream turbulence intensity being about 1/2%. Span-wise tests of the boundary layer development show the momentum thickness to be uniform within $\pm$2% across the measuring portion of the tunnel. Three-dimensional effects on the heat transfer measurements were investigated by comparing boundary layer profile integrals with heat transfer integrals along the plate. Simpson (1967) concluded that the 3-D effect was not larger than 3%. It follows from the similarity between the energy and momentum equations that three-dimensional effects on skin friction data should be of the same order of magnitude.

Statements regarding the "relative uncertainty" of Stanton number have little meaning since blowing tends to force the Stanton number to zero. Absolute uncertainties have more meaning, and will be referred to here. The stochastic component of uncertainty in reported values of Stanton number is about $\pm$0.0001 Stanton number unit. This value was estimated by applying constant probability propagation of uncertainty to the data reduction program using standard uncertainty values for the input measurements. Values of the skin friction coefficient are more difficult to measure than heat transfer and tend to be less certain. In addition, the skin friction data tend to be sparse (for example, the Stanford results present only 4 or 5 values of skin friction per situation whereas 24 values of Stanton number are presented), and therefore admit of larger differences in opinion in interpretation. Thus, although the stochastic component of uncertainty in each measurement may be $\pm$5%, there may be differences in interpretation of the same data by different investigators due to differences in curve-fitting coordinates etc. which are as large as 10% or 15% (see Squire, 1970).

The Experimental Boundary Conditions

The overall program from which the present examples of data were taken covered accelerating and decelerating flows as well as variations in wall

temperature and blowing. This range precluded the use of x-Reynolds number as a useful correlating parameter and lead early to the use of the local boundary thickness Reynolds number (either momentum- or enthalpy-thickness) for presentation of the results. It was shown, by the study of Whitten (1967), that for uniform free stream velocity, the boundary layer would adjust to even a step change in blowing within 2-5 boundary layer thicknesses. It can be seen by comparing his data with those of Moffat (1967), that uniform blowing (constant F flows) produced the same value of Stanton number for a given enthalpy thickness Reynolds number as did constant B flows. With the validity of "local equilibrium" established to at least this extent, it was possible to conduct the remaining experiments with the simpler (experimentally) boundary condition of constant F rather than the true equilibrium situation of constant B. It is believed that any effects of this simplification will be found only in the velocity and temperature profiles, and then only in the outermost parts (i.e., the wake region), since the inner region responds so rapidly to the wall conditions.

Accelerations were characterized by a constant value of K, defined as $\frac{\nu}{U_\infty^2}\frac{dU_\infty}{dx}$. Such a flow is of fundamental value, as shown earlier, and also has the merit of being easy to establish since it naturally occurs in the case of a channel formed between two converging planes (except for second order effects due to the growth of the displacement thicknesses). It was hypothesized, at first, and then confirmed experimentally, that the asymptotic state would result in a constant value of $c_f/2$. This has the effect that constant F is also constant B hence, although the experiment was set up as constant F, it resulted in a completely equilibrium situation with both K and B reasonably well fixed in the accelerating region.

The decelerating flows were set to nearly constant β pressure gradients by fixing $U_\infty = U_1 x^m$ with m negative and x determined with respect to the virtual origin. Blowing was set by specifying constant F, relying upon the trend towards local equilibrium. The results showed no discernible effect of deceleration upon the relationship between Stanton number and enthalpy thickness Reynolds number: the same correlations which worked for the flat plate case works for constant β decelerations. Hence, it seems

safe to assume that the local relationship determined by an experiment at constant F is the same relationship which would have been found in a constant B experiment.

Constant wall temperature was used throughout the base-line tests reported here, with an average temperature difference of about 25°F between the free stream and the wall. No correction has been made for the effect of variable fluid properties except to the initial "qualification runs" which validated the apparatus in the flat plate, no-blowing test case. Some tests have been made to document the response of the boundary layer to steps and ramps in temperature and to arbitrary distributions of blowing: these serve as check runs, against which one can test models of boundary layer behavior based upon the differential and integral correlations derived from the equilibrium experiments.

Correlations of Results

The principal correlations deduced from the present data set are the differential ones: the correlations used to model the momentum mixing length and the turbulent Prandtl number in the finite difference computing method described in the latter part of this paper. There is, however, use for integral correlations such as "Stanton number as a function of enthalpy thickness Reynolds number, F , and K or β'' . The range of validity of such integral correlations is necessarily less than that of the differential correlations, since the latter have the differential equation to help cope with the changing boundary conditions. Within their limited range, and accuracy, however, such correlations are extremely useful, particularly when kept to simple functional forms.

The results of the present data set are, therefore, presented in both ways: integral and differential correlations. Discussion of the differential correlations is collected in the last two sections. The integral correlations are discussed with the data since they help to clarify the organization of the results.

Heat Transfer Results for U_∞ = Constant

The principal effects of transpiration on heat transfer thru a constant velocity boundary layer are shown in Figures 5 thru 7.

Figure 5 shows Stanton number as a function of x-Reynolds number for uniform blowing and suction. The blowing fraction, $F = \dot{m}''/G_\infty$, is the ratio of the mass velocity through the surface ($\dot{m}''$) to the free-stream mass velocity (G_∞). It is apparent that blowing ($\dot{m}''/G_\infty > 0$) and suction ($\dot{m}''/G_\infty < 0$) both have large effects: blowing tends to drive the Stanton number towards zero as the blowing fraction increases whereas suction tends to force the Stanton number to an asymptotic value numerically equal to (-F). This behavior is illustrated in Figure 6, which shows St as a function of $\dot{m}''/G$ parametric in x-Reynolds number. The region of boundary layer behavior is thus seen to lie between $\dot{m}''/G$ of roughly $F = +0.01$ for this range of Reynolds numbers.

It is worth noting that all of the features shown in Figures 5 thru 7 can be recovered, with good accuracy, from a finite difference program using a damped mixing-length closure: the damping needs only to be made a function of the transpiration rate - no other change need be made. The evidence is that the main effects of blowing are confined to the inner portion of the momentum boundary layer: blowing changes the shear stress distribution and reduces the effect of the sublayer. The diminished influence of the sublayer can be simulated by making the damping factor, A^+, smaller as the blowing fraction increases, producing velocity profiles which closely resemble those shown in Figure 13. Experiments show that the turbulent Prandtl number is not much affected by blowing, and the A^+ variation alone results in satisfactory prediction of the principal features of the heat transfer. This point is developed in the third section of this paper, and an empirical correlation is presented for A^+ as a function of the blowing and the pressure gradient conditions. Correlations of this sort, for use with finite difference programs, are described as "differential correlations" to distinguish them from the more conventional "output oriented" correlation.

Within the range of values covered by the present data set, the effect of blowing can also be described by a correlation in Stanton number coordinates.

The data show that the ratio of Stanton number with blowing, St, to Stanton number without blowing, St_o, is a unique function of the blowing parameter B. The comparison can be made at the same x-location (same Re_x) as given by Equations (20) and (21):

$$\left.\frac{St}{St_o}\right|_{Re_x} = \frac{\ell n(1 + B_h)}{B_h} \tag{20}$$

or, equivalently,

$$\left.\frac{St}{St_o}\right|_{Re_x} = \frac{b}{e^b - 1} \tag{21}$$

where

$$B_h = \frac{\dot{m}''}{G_\infty St} \tag{22}$$

and

$$b = \frac{\dot{m}''}{G_\infty St_o} \tag{23}$$

Equations (20) and (21) were presented during the early 1950's by several workers in the field as "stagnant film theory" or "Couette flow" models. The agreement between the data and Eq. (20) is shown in Figure 7. In part, the good agreement results from the implicit nature of Eq. 20 diminishing St reduces both St/St_o and $\ell n(1 + B_h)/B_h$, hence preserving "good agreement".

As mentioned earlier, the objective of the overall research program suggested an early search for local descriptors of boundary layer behavior. In particular, emphasis was focused upon the relationship between Stanton number and enthalpy thickness Reynolds number. It was natural, then, to seek a way of predicting the effect of blowing in local coordinates: i.e., St/St_o at constant enthalpy thickness Reynolds number.

The data of Figure 5 have been re-cast to show Stanton number versus enthalpy thickness Reynolds number and plotted as Figure 8. Values of enthalpy thickness for this plot were calculated from the measured Stanton number data and the blowing fraction by integrating the two-dimensional energy integral equation but values derived by this method agree well (5-6%) with values deduced by traversing the boundary layers. An empirical form could be deduced from this figure but a better guide is at hand.

Whitten (1967) showed that Eq. (20) could be combined with the two-dimensional energy integral equation and with an equation describing the variation of St_o with Re_x to yield the following form:

$$\left.\frac{St}{St_o}\right|_{Re_h} = \left[\frac{\ell n(1 + B_h)}{B_h}\right]^{1.25} (1 + B_h)^{.25} \qquad (24)$$

Equation (24) was developed from Eq. (20), hence all of the data for U_∞ = constant fit Eq. (24). Implicit in Eq. (24) is the notion of local equilibrium: it is presumed that knowledge of Re_h and B will fix St/St_o, regardless of the upstream history. The validity of this hypothesis was tested by experiments in the vicinity of a step change in blowing. Such data are shown in Figure 9. The boundary layer is seen to respond very rapidly to the step, with Stanton number dropping almost all the way from the unblown value to the uniformly blown value within one plate width (4 inches in the flow direction). The boundary layer thickness at the point of the step (99% velocity thickness) was approximately one inch hence the local equilibrium is re-established in about four boundary layer thicknesses. Thus, Figure 9 shows a strong "local equilibrium" tendency, favoring the use of Eq. (24) for cases of variable blowing as well as cases of uniform blowing and opening the door for substantially local predictions of the boundary layer behavior. An example of a more complex case is shown in Figure 10, in which a linearly decreasing blowing, $F = 5 \times 10^{-5}(x)$, was combined with a sharply variable wall temperature. Whitten (1967) predicted the outcome using local equilibrium in combination with a superposition method.

Skin Friction Results for U_∞ = Constant

The principal effects of transpiration on the skin friction coefficient of a turbulent boundary layer are illustrated in Figures 11 and 12. Figure 11 shows the early results of Simpson (1967), derived from pitot probe surveys of the boundary layer. Figure 12, in Re_m coordinates, includes later results of Andersen (1972) for comparison. As can be seen, there are considerable differences in the results. Our present opinion is that

the values near the bottom of each band are more representative than those near the top. Andersen's data were taken with a rotatable, slanted, hot wire probe measuring turbulent shear stress near the wall and extrapolating to the wall using a partially integrated form of the boundary layer momentum integral equation. His data are less sensitive to interpretive differences than were Simpson's, who determined $c_f/2$ by differentiating a curve fit thru measured values of momentum thickness. Squire (1970), previously mentioned, pointed out that Simpson's momentum thickness data could be interpreted to show different values of $c_f/2$, by 10% or more, simply by choosing different coordinates in which to curve fit the momentum thickness variation.

The variation of $c_f/2$ with blowing is essentially the same as that of Stanton number: the ratio c_f/c_{f_o} can be calculated from the blowing parameter B_m, where the subscript signifies B defined with $c_f/2$ instead of St.

$$\left.\frac{c_f}{c_{f_o}}\right|_{Re_x} = \frac{\ell n(1 + B_m)}{B_m} \tag{25}$$

$$\left.\frac{c_f}{c_{f_o}}\right|_{Re_m} = \left[\frac{\ell n(1 + B_m)}{B_m}\right]^{1.25} (1 + B_m)^{.25} \tag{26}$$

where $$B_m = \frac{F}{c_f/2} \tag{27}$$

It is presumed, based on the strongly local behavior of St, that skin friction would be similarly quick to respond to a step in blowing.

Velocity and Temperature Profiles

Velocity and temperature profiles in inner coordinates are shown in Figures 13 and 14 for the case of constant velocity (about 40 fps), constant wall temperature (ΔT about 25°F), injection of air into air. The general features of the region from $y^+ = 10$ to $y^+ = 100$ can be deduced from a Couette flow analysis using a mixing length model assuming no effect of blowing on the mixing length distribution. Such an analysis leads to a

closed form "Law of the Wall" representation for the fully turbulent region. Analyses of this sort have been presented by Black and Sarnecki (1965), Stevenson (1963), Simpson (1967), and others. Thus the dramatic "uplifting" in the outer regions reflects mainly the effect of the transpiration flow on the shear stress distribution in the layer - not a drastic change in the mechanism of momentum transfer.

Figure 13 shows data from two programs (Simpson and Andersen) which used different methods of evaluating the friction factor (used in both the u^+ and the y^+ coordinate definition). The difference shown is, again, due to the difference in reported values of the friction factor. Our present opinion favors values near the high sides of the bands shown, rather than the low side.

Data inside of $y^+ = 10$ are suspect because of the possibility of probe errors due to wall displacement effects and shear effects. No definitive studies have been made concerning probe corrections in the presence of transpiration, hence no corrections were made to these data. To some extent, the situation is ameliorated by the fact that the finite difference program is only required to "bridge the gap" between $y^+ = 0$ ($u^+ = 0$) and $y^+ = 10$ (u^+ known) by some reasonable means to get into a region of reasonably well known behavior.

Relatively little has been done in terms of measuring the temperature distributions in turbulent boundary layers with transpiration. Figure 14 shows some results of Moffat (1967), Blackwell (1972), Thielbahr (1969), and Kearney (1970) for some cases of blowing and suction. The parameter t^+ is defined as follows:

$$t^+ \triangleq \frac{t-t_o}{t_\tau - t_o} \frac{\sqrt{\frac{c_f}{2}}}{St} = \bar{t} \frac{\sqrt{\frac{c_f}{2}}}{St} \qquad (28)$$

Note that t^+ includes $c_f/2$ as well as St in its definition, hence is sensitive to the hydrodvnamics as well as the heat transfer. This form follows from a Couette analysis in which the terms are made dimensionless using u_τ. The fact that t^+ includes both $c_f/2$ and St means that t^+ profiles have inherently more scatter than u^+ profiles. In fact if one examines Eq. (28) in terms of an uncertainty analysis on a simple product

form, at any value of y^+, the value of t^+ includes an uncertainty component due to $\bar{t}$, a component due to $\sqrt{\frac{c_f}{2}}$, and one due to St. If St is uncertain within $\pm 5\%$, and $c_f/2$ is uncertain within 10%, and $\bar{t}$ within 2%, then

$$\frac{\delta(t^+)}{t^+} = \left\{ \left(\frac{\delta \bar{t}}{\bar{t}}\right)^2 + \left(\frac{\frac{1}{2}\frac{\delta c_f}{2}}{\frac{c_f}{2}} \right)^2 + \left(\frac{\delta\, St}{St}\right)^2 \right\}^{1/2} \tag{29}$$

we have

$$\frac{\delta(t^+)}{t^+} = \{.0004 + .0025 + .0025\}^{1/2} = 0.073 \tag{30}$$

In the cases with high blowing, $\delta(St)$ and $\delta(c_f/2)$ remain relatively fixed (or perhaps even become larger) while the values of St and $c_f/2$ approach zero, yielding large percent-wise inaccuracies in St and $c_f/2$. These are propagated immediately into t^+.

In short, one should be more cautious in attributing significance to the details of t^+ variations than to u^+ variations, because of the added uncertainty involved. Since the major uncertainties involved appear in multiplicative terms, the slopes of the $t^+ - y^+$ figures are affected when shown in the conventional semi-log coordinates.

When air is the working fluid and the transpired fluid the values of Prandtl number and turbulent Prandtl number are both near unity. It would be expected as a consequence, that $\bar{u}$ and $\bar{t}$ would be similarly distributed within the boundary layer in a constant velocity flow. This is the case, as a review of the data of Moffat (1967) or Whitten (1967) will show. In view of this, it is reasonable to expect t^+ to vary like u^+ within the layer.

If, at every y^+:

$$\frac{u}{U_\infty} \triangleq \bar{u} \simeq \bar{t} \triangleq \frac{t-t_0}{t_\infty - t_0} \tag{31}$$

$$\text{with} \qquad u^+ \triangleq \frac{\bar{u}}{\sqrt{\frac{c_f}{2}}} \quad \text{and} \quad t^+ \triangleq \frac{\bar{t}}{St}\sqrt{\frac{c_f}{2}} \tag{32}$$

$$\text{Then} \qquad t^+ \approx u^+\left(\frac{c_f/2}{St}\right) \tag{33}$$

Thus, for the case of constant free stream velocity, we should not find great differences in the profiles, in these coordinates.

Flows Subject to Acceleration

Early in the 1960's it was observed by several studies that the Stanton number was dramatically reduced by a strong acceleration. The relationship between Stanton number and enthalpy thickness Reynolds number strongly resembled the behavior expected of a laminar boundary layer. As a result of this similarity the phenomenon was labelled "re-laminarization" and occupied a number of workers throughout the late 60's and early 70's. There was general agreement that a suitable acceleration parameter could be taken as

$$K = \frac{\nu}{U_\infty^2}\frac{dU_\infty}{dx} \tag{34}$$

though some felt that a better form would include $c_f/2$ to some power in the denominator. We used K, given by Eq. (34), as the acceleration parameter. As has earlier been shown, constant K boundary layer flows offer a possibility for asymptotic or equilibrium boundary layers. Such a possibility is attractive, experimentally, on three counts: (1) it is relatively easy to accomplish (a constant K flow can be achieved using convergent planar walls) and, (2) it produces a possibly-simpler family of responses by the boundary layer, with a better chance of revealing the fundamental effects and (3) it helps resolve the dilemna of which possible cases, out of the infinite number of possibilities, to choose. Evidence of "local" behavior already mentioned, suggests that slowly varying K conditions can be treated as quasi-equilibrium states.

Heat Transfer to an Accelerated Flow

Figures 15 thru 18 show the effects of acceleration on heat transfer for values of K between 0.57×10^{-6} and 2.55×10^{-6} with transpiration

controlled to yield constant F along the surface. The intention was to achieve and hold the asymptotic accelerated state for as long as possible, hence it was desired to start the acceleration at the particular value of momentum thickness Reynolds number appropriate for the values of K and F being used. The momentum integral equation was used as a guide to choosing the starting value of momentum thickness Reynolds number. The validity of this assumption and the accuracy of the "set point" can be judged from Figure 21 which show that momentum thickness Reynolds number did, in fact, remain substantially constant throughout the test section in a typical run.

In every case shown in Figures 15 thru 18 a flat plate, turbulent boundary layer with uniform transpiration was established in the test section and allowed to grow with length until the desired momentum thickness Reynolds number was reached. At that location, the top wall of the test section was adjusted to set in the convergence required to yield the desired value of K . Total and static pressure measurements were made at four inches intervals along the test section to check that K was, in fact, constant throughout the test region.

It might have been argued that two effects were present in these tests: (1) acceleration, and (2), high velocity flow. Flat plate tests were conducted at velocities up to 126 fps to ensure that Stanton number remained the same function of enthalpy thickness Reynolds number at the high velocity end of the test section as at the low velocity end. At 126 fps the Stanton number correlation was indistinguishable from its values at 40 fps, though the friction factor was high by 5-7% (momentum thickness method). Thus it is felt that there are no contaminating effects present: the changes in Stanton number shown in these results are those due to the acceleration level, not the velocity level.

Figures 15 thru 18 show Stanton number versus enthalpy thickness Reynolds number for the different cases studied, compared with reference curves for flat plate behavior. As a general comment, for a given enthalpy thickness Reynolds number, acceleration combined with suction reduces Stanton number, while acceleration combined with blowing increases Stanton number with respect to the transpired flat plate correlation. To illustrate this trend, note the progression of Stanton number behavior for $F = -0.002$ (moderate suction) shown in the four figures. At $K = 0.57 \times 10^{-6}$ the Stanton number

slowly falls away from the flat plate result, being low by about 10% at the end of the test section. At $K = 0.77 \times 10^{-6}$ the decline is more pronounced, with the terminal value low by almost 20%. At $K = 1.45 \times 10^{-6}$ the drop is nearly 40%, and the boundary layer seems to return only slowly to its flat plate behavior. For suction, the stronger the acceleration the greater the depression of Stanton number.

With blowing at $F = +0.004$, a more complex change in behavior is noted. With $K = 0.57 \times 10^{-6}$ the Stanton number values rise above the flat plate case by as much as 40% at the end of the acceleration, and at $K = 0.77 \times 10^{-6}$ the elevation has reached 66%. For larger values of K, however, the behavior returns toward the flat plate correlation: at $K = 1.45 \times 10^{-6}$ the elevation is only 35% and at $K = 2.55 \times 10^{-6}$ the data lie once more on the flat plate correlation. A general trade-off can be inferred, between the relaminarizing effect of acceleration and an apparent destabilizing effect of blowing. For positive values of F and K, the neutral values seem to lie along a line relating K and F such that if F exceeds $1.5 \times 10^{3} K$, the value of Stanton number will be increased by the joint effect, and if F is less than the neutral value, Stanton number will be reduced.

Figure 17 also shows data for a strong suction layer: $F = -0.004$ (strong suction) and $K = 1.45 \times 10^{-6}$ (moderate acceleration). The trajectory shows that an asymptotic suction layer was attained for these conditions, in the presence of strong acceleration. The first few data points show Stanton number diminishing from 0.005 to 0.0045, in the approach region, in a typical turbulent suction layer fashion. The acceleration begins at an enthalpy thickness Reynolds number of 400, and Stanton number immediately begins a sharp drop. With suction at $F = -0.004$, the condition of thermal equilibrium at the surface requires that the Stanton number be at least as large as $-F$ and the decline of Stanton number is stopped at that level. With Stanton number numerically equal to $-F$, and a constant wall temperature, the energy content of the boundary layer ceases to change. The increasing values of U_∞ with distance then slowly drop the value of enthalpy thickness Reynolds number, and the data points more sequentially to the left, at constant Stanton number.

No attempt has been made to devise an empirical formulation for predicting Stanton number in terms of enthalpy thickness Reynolds number, K,

and F . Complex as it is seen to be in these figures, this is still only part of the story. All of the data in these four figures are from asymptotic accelerated flows, where the flow entered the accelerating region at, or nearly at, the appropriate value of momentum thickness Reynolds number. As will shortly be seen "overshot" or "undershot" layers, where the entering values are either larger or smaller than the asymptotic values behave much differently in the accelerating region.

Figures 19 and 20 illustrate the effects of inlet conditions on the response of the boundary layer to a strong acceleration. In Figure 19, the accelerations began at momentum and enthalpy thicknesses between 800 and 1000, with the high K runs beginning at the lower values. Looking ahead to Figure 22 shows these to be nearly the asymptotic values. The solid symbols in Figure 19 show the behavior of the Stanton number within the accelerated region, and display a regular progression of slopes. With these curves as a baseline, a series of tests were run at a fixed value of $K = 2.55 \times 10^{-6}$ varying the initial momentum and enthalpy thickness Reynolds numbers. The results, in Figure 20, show that the slope of the Stanton number correlation is not a unique function of K but depends upon the initial conditions. In Figure 20, the square symbols represent a near-equilibrium combination, with momentum thickness and enthalpy thickness Reynolds numbers within 100 units of one another, and of the same approximate values as shown in Figure 19. It is worth noting that if the enthalpy thickness is kept small (in this case by delaying the heating) the response of the Stanton number to the acceleration is diminished. On the other hand, if the enthalpy thickness is held nearly constant, and the momentum thickness increased, there is relatively less change in behavior from the reference case. When both the enthalpy and momentum thicknesses are increased to large values prior to the acceleration (an "overshot" case), then the Stanton number comes down very abruptly in the accelerating region. For the strongly "overshot" entrance conditions it is not possible to obtain a long run at equilibrium conditions, hence most of the data shown are in the region where the boundary layer is still adjusting to the acceleration.

The solid line shown for comparison represents the similarity solution for a laminar wedge flow with a very thick thermal boundary layer. It seems clear, from these data, that the same relative variation of Stanton number

could be attained by different non-equilibrium combinations of enthalpy thickness Reynolds number and acceleration. The effects of a non-equilibrium combination of momentum thickness and acceleration cannot be uniquely identified by the value of K alone. Heat transfer in non-equilibrium accelerations is inherently responsive to all three variables: the acceleration parameter, the momentum thickness, and the enthalpy thickness.

The combination of acceleration and blowing has been shown, by these experiments, to be strongly non-linear in its effect on the boundary layer. Empirical descriptions of this behavior are difficult to assemble in "output" notation. To express Stanton number as a function of Re_h, K, and F in such a way as to recover all of the aspects shown in Figures 15 thru 20 would require a good deal of ingenuity. It is, however, relatively straightforward to predict this data set using a modified damping factor in a mixing length formulation. If the damping factor, A^+, is expressed as a relatively simple empirical function of F and K, the principal features of all the preceding data are recoverable within about 10%.

Momentum Transfer to an Accelerated Flow

The decision to test equilibrium accelerated flows places some constraints on the behavior of the momentum boundary layer as illustrated in Figure 21. Here, for accelerations at a value of $K = 0.75 \times 10^{-6}$, are trajectories of the boundary layer behavior for different values of F. The broken lines suggest the behavior of the skin friction and momentum thickness Reynolds number at various stations along the plate prior to the beginning of the acceleration. The vertical bar shown for each set is the last point in the unaccelerated flow. Considering the data for $F = 0.006$, after the acceleration begins, the momentum thickness Reynolds number grows only slightly, from 3000 to 3700, and does not change further with length along the plate. At the same time, the value of the skin friction coefficient rises quickly to a final value above the flat plate value and then remains unchanged. The equilibrium point thus established is characteristic of this combination of acceleration and blowing. In each of these data sets, the acceleration was begun at or near the predicted value of the equilibrium momentum thickness Reynolds number, to reduce the transient effects as much as possible. The way in which the asymptotic values of momentum thickness

Reynolds number vary with K and F is shown in Figure 22. Each symbol shown represents an experimentally achieved equilibrium state. Asymptotic values of $c_f/2$ established by these equilibrium flows are shown in Figure 23. Again, each symbol represents an experimentally achieved equilibrium state. Some confusion existed in the data sets for $K = 2.5 \times 10^{-6}$ and $F = 0$ and four different terminal states were achieved. All are shown, but symmetry with the other data sets suggests that the higher value be used.

The momentum boundary layer for an asymptotic accelerated flow has thus a relatively simple description. Being uniquely specified by F and K, there is no need for a "size dependence" and, in essence, the complexity of description is reduced by one variable. The asymptotic value of friction factor with blowing, can be predicted with reasonable accuracy by applying Eq. (26) to the unblown asymptotic value at the same K. Since F and K uniquely determine the asymptotic thickness, (see Figure 21 or 22) there is no need for a statement "...at the same momentum thickness Reynolds number..." and, in fact, such a proscription cannot be enforced in the context of comparing asymptotic boundary layers with the same value of K and different values of F.

Mean Velocity and Temperature Profiles in an Accelerating Flow

In a constant K, asymptotic boundary layer the momentum thickness Reynolds number seeks some characteristic level, as does the friction factor, and the velocity profile assumes a stationary shape in u^+, y^+ coordinates. This is illustrated in Figures 24-A, 24-B, and 24-C which show the profiles as they developed in the streamwise direction. For the two lower values of K, the momentum thickness Reynolds number was a constant throughout the length of the test section to within 10% and close to the asymptotic values shown in Figure 22. The profiles show a close similarity in both inner and outer regions. At $K = 2.6 \times 10^{-6}$ the boundary layer was "overshot", entering with a momentum thickness Reynolds number of 750 compared to the asymptotic value of 480 (from Figure 22). As can be seen, the boundary layer did not reach an asymptotic state, though the last profile (in the streamwise direction) could be taken as representative. The corresponding temperature profiles are shown in Figures 25-A, 25-B, and

25-C. For the two lower accelerations the temperature profiles remain reasonably similar, showing small changes in the outer region (for $y^+ >$ 100) which can be seen to increase in magnitude as K increases. Reviewing Figures 15 and 17 shows that the Stanton number values for these conditions were only slightly affected by the acceleration. When the value of K reaches 2.5×10^{-6}, however, as shown in Figure 25-C, the temperature profile shows a drastic difference, with the profiles strongly non-similar in the streamwise direction. The effect is felt all the way in to y^+ near 10. The Stanton number data in Figure 18 shows this combination of conditions to result in a drop in Stanton number which reaches 40% at the downstream end of the test section.

The "terminal states" of the velocity and temperature profiles are shown for high and low accelerations ($K = 0.57 \times 10^{-6}$ and 2.6×10^{-6}) in Figures 26-A and 26-B and 27-A and 27-B for various values of blowing. The phrase "terminal states" is used because, while the profiles shown for velocity are representative asymptotic profiles, those shown for temperature are simply the last measured profiles: the energy boundary layer continues to grow, a longer test section would have yielded a different "last" profile.

The temperature profiles shown for $K = 2.6 \times 10^{-6}$ display inner region similarily, out to about y^+ of 100; no such coherence is visible in the data for $K = 0.57 \times 10^{-6}$.

The velocity and temperature profiles shown in Figures 24 thru 27 illustrate the main structural features of the accelerated turbulent boundary layer. These data have been used as guides in refining the physical models used in the Stanford finite difference computer program for boundary layer calculations. This work is described in a later section.

Flows Subject to Deceleration

Decelerating flows differ from accelerating flows in that no asymptotic boundary layer state is approached, even though an equilibrium flow is established. The condition of equilibrium between the pressure-gradient force and the shear force is expressed by the parameter β given earlier (Eq. 6) and it has been shown experimentally that boundary layers for which β is constant with length display a constant value of G , the Clauser shape

factor. An extension of this observation, based on the present data set, is that G remains constant with length whenever ($\beta + B_m$) remains constant, where B_m is the momentum blowing parameter.

The experimental boundary conditions which produce flows with constant β are those for which the free stream velocity varies with distance to some power, "m". This introduces an experimental difficulty centering around the identification of the virtual origin of the boundary layer. It would not be appropriate simply to measure "x" from the leading edge of the test section unless (a) the boundary layer were of zero thickness at that point and (b) the boundary layer were fully turbulent from the leading edge onward. It is an observation of the work reported by Andersen (1972) that when "x" distance is measured from the virtual origin and velocity varies with some power of x , then equilibrium boundary layers are achieved: both β and G remain substantially constant with length along the test section, after a brief accommodation. The decision was also made, in the Stanford program, to restrict the study to flows which did not approach separation. For this reason only small negative values of "m" were used. It was anticipated that high blowing would tend to encourage separation, hence data were taken only for cases of suction and small blowing.

Since no asymptotic state is attained in a decelerating equilibrium flow, the Stanton number and friction factor values vary with boundary layer thickness Reynolds numbers and the data resemble the flat plate data in their general dependences.

Heat Transfer in Decelerating Flows

Figures 28 and 29 show the variation of Stanton number with enthalpy thickness Reynolds number for moderate and strong decelerations with blowing and suction. The solid lines through the data represent flat plate behavior. The same correlation applies to both cases of decelerated flow as applies for the flat plate case. The effects of blowing are to reduce Stanton number but, again, exactly as was observed for the flat plate case.

In terms of the surface heat transfer behavior of the boundary layer, then, one can say that adverse pressure gradients pose no new problems, within the range of conditions encountered in this study. Whatever effects the adverse pressure gradient may have on the structure of the boundary

layer, in terms of changing the sublayer thickness or the turbulent transport mechanisms, the net effect is the same as for a flat plate situation. Whatever internal correlations are proposed to describe the effects of pressure gradient on the boundary layer must, then produce this same behavior for decelerating flows.

The heat transfer characteristics for the decelerated flows reported here can be described by

$$St_o = 0.015\, Re_h^{-0.25} \tag{35}$$

$$\left.\frac{St}{St_o}\right|_{Re_h} = \left[\frac{\ell n(1 + B_h)}{B_h}\right]^{1.25} (1 + B_h)^{-.25} \tag{36}$$

Here, St_o is defined as the value of Stanton number without blowing but in the adverse pressure gradient, and St is the value of Stanton number in that same adverse pressure gradient, with blowing, at the same enthalpy thickness Reynolds number.

Momentum Transfer in Decelerating Flows

Although the heat transfer behavior in decelerating flows can be adequately described in terms of flat plate correlations, the momentum transfer cannot. The effect of an adverse pressure gradient is to decelerate the fluid in the boundary layer causing the momentum thickness to increase more rapidly than it would due to wall shear alone. The variation of $c_f/2$ with pressure gradient is shown in Figure 30 and summarized by the following recommendations, for flows in which $U_\infty = U_1 x^m$ with "m" a constant.

$$\left(\frac{c_{f_o}}{2}\right) = a\, Re_m^{-0.25} \tag{37}$$

where

U_∞ = constant	$a = 0.0120$	$(850 < Re_m < 3000)$
$U_\infty = u_1 x^{-.15}$	$a = 0.0102$	$(1500 < Re_m < 3500)$
$U_\infty = u_1 x^{-.20}$	$a = 0.0083$	$(1700 < Re_m < 4200)$
$U_\infty = u_1 x^{-.275}$	$a = 0.0059$	$(2000 < Re_m < 5000)$

Near the entrance of the test section the values of G and β were usually not stabilized, with β continuing to rise for the first two or three data points to its final value. The forms of the curves therefore reflects this accommodation: only the last six data points should be taken to represent equilibrium conditions. The data for $m = -0.275$ shows much scatter: these are difficult conditions under which to measure the friction factor. The line shown passing through the data must be regarded as only a suggestion, at best.

Blowing increases the momentum deficit of the boundary layer and would aggravate a tendency to separate due to an adverse pressure gradient, so combinations of blowing with deceleration are prone to early separation. For this reason, the blowing data shown on Figure 31 is restricted to a moderate deceleration ($m = -0.15$) and moderate blowing. The data in Figure 31 include all recorded values within the region of constant "m". In the entrance region the values of β and G were not usually stabilized, with β continuing to rise for the first two or three data points. In this region of increasing β, the value of $c_f/2$ shows a rapid drop with Reynolds number. In the region where β was substantially uniform, the variation of $c_f/2$ with Reynolds number is similar to that observed on a flat plate. In particular, the relative effects of blowing on skin friction are similar to those observed on a flat plate (though, of course, the unblown values are much different) and are once again predicted well by:

$$\left.\frac{c_f}{c_{f_o}}\right|_{Re_m} = \left[\frac{\ell n(1 + B_m)}{B_m}\right]^{1.25} (1 + B_m)^{0.25} \qquad (38)$$

where B_m is the momentum blowing parameter.

Velocity and Temperature Profiles for Decelerating Flows

Velocity and temperature profiles for moderate deceleration ($m = -0.15$) are shown in Figures 32 and 33 in wall coordinates. The velocity profile is relatively unaffected by the deceleration inside y^+ of 200 either for suction or for no blowing. Blowing at 0.004 has a very pronounced effect, however, raising the values of u^+ at every y^+ greater than about 10. The profiles of t^+ are less affected by the deceleration than are the profiles of u^+, being slightly lower across the board.

Integral Relationships for Friction Factor, Stanton Number and Shape Factor

The preceding sections have discussed data for flat plate flows (U_∞ = constant), asymptotic accelerating flows (K = constant) and equilibrium decelerating flows (m = constant). For each of these hydrodynamic situations data have been presented for different transpiration levels both positive (blowing) and negative (suction). In addition, one can envisage flows with wall temperature variations such that the thermal and momentum boundary layers might be of considerably different thicknesses. The number of combinations of these boundary conditions is very large, and it would indeed be surprising if any correlation could be contrived which would describe Stanton number or friction behavior directly and which would cover more than a small range of these conditions with any accuracy. Generality of the sort needed for that task seems inherently to require a differential predictor scheme with the experimental inputs providing information about the transport mechanisms within the boundary layer. Such is the approach taken by most heat transfer research today. The differential correlations needed to describe these experimental data are discussed in the next section and their success in prediction of complex combinations is shown in the last section.

For the present, however, it can be said that some correlations can be given which are useful for situations not too far removed from the equilibrium states represented by these data. In particular, situations involving slowly varying blowing, or slowly varying K or β even for a relatively large difference between the thermal and momentum boundary layer thicknesses.

Such correlations are shown in Figures 34 thru 36: Stanton number versus enthalpy thickness, the effects of blowing, and the variation of shape factor. In choosing the correlations conflicts had to be resolved between the desire for accuracy and the desire for range. The correlations shown are believed valid within $\pm$10% for the ranges of values covered. Figure 34 shows Stanton number versus enthalpy thickness Reynolds number for a number of different cases, all with no transpiration: flat plate, moderate and strong accelerations, and moderate to strong decelerations. All of the data shown are from the present series, and represent equilibrium states. It is noteworthy that a single correlation covers the data for all flat plate flows, all decelerating flows, and all accelerating flows less severe than $K = 1.47 \times 10^{-6}$. The recommended curve is:

$$St_o = 0.015\ Re_h^{-0.25} \qquad \text{(AIR)} \tag{39}$$

$$150 < Re_h < 6000$$

In recommending this particular form it must be admitted that certain traditions have been honored. In particular, the use of the exponent -0.25 tends to weight more heavily the data from the high Reynolds number region, but this value has a long analytic history. The skin friction data are not so conveniently described but the flat plate and the asymptotic states of accelerated flows up to $K = 2.5 \times 10^{-6}$ are reasonably well described in terms only of the momentum thickness Reynolds number by

$$\frac{c_f}{2}_o = 0.0128\ Re_m^{-.25} \qquad \begin{matrix} 0 \leq K \leq 2.5 \times 10^{-6} \\ 500 < Re_m < 5000 \end{matrix} \tag{40}$$

It should be borne in mind that for each asymptotic accelerated flow there exists only one possible value for Re_m, dependent upon the value of K: the asymptotic value, given earlier in Figure 22. When used to predict these asymptotic values of $c_f/2$ from the asymptotic values of Re_m, the equation given above tends to underpredict by about 10%.

Blowing can be discussed either in terms of the effects at a particular location (x-Reynolds number) or at a particular local state of the boundary layer (enthalpy thickness Reynolds number). The local descriptor has more generality since it can be applied in cases of non-uniform velocity. It has been found, by comparison with the data presented here and in the original source documents, that the effect of blowing (or suction) can be calculated with reasonably good accuracy using a form derivable from a Couette flow model, evaluated at constant boundary layer thickness Reynolds number:

$$\frac{c_f}{c_{f_o}} \cdot \frac{St}{St_o}\bigg|_{\substack{Re_m \\ \text{or} \\ Re_h}} \quad \Delta\ \psi \approx \left[\frac{\ell n(1+B)}{B}\right]^{1.25} (1+B)^{.25} \tag{41}$$

This relationship is recommended within the following range of conditions.

U_∞ = constant flows ($-0.01 \; F \leq 0.010$)

Decelerating flows ($-0.20 \leq m$; $-0.004 \leq F \leq +0.004$)

Accelerating asymptotic flows ($K \leq 1.75 \times 10^{-6}$; $0 \leq F \leq +0.004$)

The range of applicability of Eq. (41) can be recalled by the following notation, which suggests that three parameters are important:

$$\frac{c_f}{c_{f_0}} \approx \frac{St}{St_0} = f(U_{\infty(x)};\ B\ ;\ \text{size}) \tag{42}$$

For accelerating flows with constant K an asymptotic condition may be reached such that "size" is a unique function of K and B. For such conditions the list of variables is reduced to two, since "size" is fixed once K and B are chosen. Hence the comparison can be made between asymptotic states. For flat plate and decelerating flows, "size" is a variable and the comparisons must be made at the same boundary layer thickness Reynolds numbers. Confirmation of the validity of Eq. (41) is shown in Figure 35 which includes friction and heat transfer data for accelerating, decelerating, and flat plate cases, with blowing and with suction.

The shape factor has been found to correlate reasonably well for all values of blowing and suction and for all variations of free stream velocity if described in terms of $(B_m + \beta)$, a parametric group occurring in one form of the momentum integral equation. Figure 36 shows H versus $(B_m + \beta)$ for conditions covering accelerations and decelerations with uniform values of blowing along the surface. With the exception of 4 data points at $(B_m + \beta) = -1.0$, the remainder of the data are well organized. The errant points may well have been laminarized by the combined effects of suction and acceleration.

A MATHEMATICAL MODEL FOR SOLUTION OF THE MOMENTUM EQUATION

During the past decade enormous strides have been made in our ability to solve the partial differential equations of the boundary layer, using finite difference techniques and the power of the digital computer. To all intents and purposes mathematically exact solutions to the boundary layer equations can be obtained for virtually any kind of boundary conditions, provided that the turbulent transport processes are adequately modeled. The speed with which such solutions can be obtained has made direct solution of the boundary layer equations for particular applications a practical engineering design tool.

We are not going to be concerned here with the details of any of the several finite difference procedures in common use today, but rather with a scheme that has been used successfully to model the dominant turbulent shear stresses in transpired turbulent boundary layers.

The time averaged momentum equation of the boundary layer, particularized for the moment to constant fluid properties, and neglecting normal turbulent stresses, may be written as follows:

$$\bar{u}\frac{\partial \bar{u}}{\partial x} + \bar{v}\frac{\partial \bar{u}}{\partial y} - \frac{\partial}{\partial y}\left[\nu\frac{\partial \bar{u}}{\partial y} - \overline{u'v'}\right] + \frac{g_c}{\rho}\frac{d\bar{P}}{dx} = 0 \qquad (43)$$

If the turbulent shear stress $\overline{u'v'}$ is known at all points in the boundary layer, the momentum problem simply becomes one of solution of Eq. (43) for any desired boundary conditions, including transpiration.

Although progress continues to be made in turbulent transport theory in general, and turbulent boundary layer theory in particular, it is still fair to say that there is as yet no truly fundamental theory that may be used as a universal starting point for solution of turbulence problems. Turbulent boundary layer theory has gone through, and continues to go through, a series of stages involving successively higher orders of sophistication. Each level in this development has involved the correlation of experimental data at a more fundamental level, and has opened up the possibility for

solving successively broader ranges of problems with a single consistent set of empirical constants. The information and calculating procedures to be presented here do not represent any very bold steps toward a more general theory, but they will allow computation of equilibrium and near equilibrium boundary layers as precisely as any scheme so far devised. Higher order models are presently being investigated by numerous researchers, and hopefully will lead to theories that embrace still broader classes of applications, although probably at the price of complexity and computation cost.

We will first introduce the concept of eddy diffusivity for momentum, ε_m , as a convenient way of expressing the turbulent shear stress.

$$\overline{u'v'} = -\varepsilon_m \frac{\partial \bar{u}}{\partial y} \tag{44}$$

Already, we are in the realm of theoretical controversy, since implicit in Eq. (44) is the notion that the turbulent shear stress goes to zero in the absence of a gradient in the mean velocity profile. In spite of its short-comings, the eddy diffusivity concept has the virtue of allowing one to use the same computation program for both laminar and turbulent boundary layers. Since most real turbulent boundary layers grow out of laminar boundary layers, the advantage is obvious.

It is convenient to visualize the turbulent boundary layer as consisting of an inner wall-dominated region, and an outer region which actually occupies most of the thickness of the boundary layer. However, for most applications the inner region is, by far, the most important one, and it is on this region that we will focus primary attention.

The inner region may be subdivided into a region immediately adjacent to the wall in which viscous forces predominate (ε_m approaches zero), and a region farther out in which momentum transfer is almost entirely by turbulent transport processes, but in which the scale and intensity of the turbulence is still strongly dependent upon the proximity of the wall.

The Prandtl mixing - length theory, despite much criticism for many years, still provides a simple and remarkably adequate basis for describing the turbulent momentum transport process in the inner region, at least for equilibrium and near equilibrium boundary layers. The mixing length, ℓ , is defined such that it is related to the eddy diffusivity for momentum and the mean velocity gradient by the following equation:

$$\varepsilon_m = \ell^2 \left|\frac{\partial \bar{u}}{\partial y}\right| \tag{45}$$

Outside of the viscous-dominated region immediately adjacent to the wall, the mixing-length in the inner part of the boundary layer is found to be proportional to distance from the wall, with a proportionality factor, k , that is independent of either transpiration rate or pressure gradient. Figure (37) shows some measurements of the mixing-length for a number of cases of transpiration, both blowing and suction, with no pressure gradient and with an adverse pressure gradient. Results for favorable pressure gradients are similar. Note that all of the data in the region near the wall converge on a single linear relation with $k = 0.41$. We will model the region outside the viscous near-wall region (which latter we will now term the viscous sublayer), but inside of the outer, or "wake", region, by:

$$\ell = ky \tag{46}$$

where $k = 0.41$

The viscous sublayer immediately adjacent to the wall can be modelled in a simple way by introducing a damping function that forces the mixing-length ℓ to naught at the wall. Designating the damping function as D , the mixing-length over the entire inner region may then be expressed as:

$$\ell = kyD \tag{47}$$

The damping function D can be satisfactorily expressed in a number of different ways. A scheme which is very popular today, and which was first suggested by Van Driest (1956), is an exponential function which leads to mean velocity profiles that correspond quite well with those observed experimentally.

$$D = 1.0 - \exp\left(-y^+/A^+\right) \tag{48}$$

where y^+ is the non-dimensional distance from the wall surface, expressed in so-called "wall" coordinates, $y^+ = y\sqrt{g_c \tau_0/\rho}/\nu$, and A^+ is the effective thickness of the viscous sublayer expressed in the same way.

The effective thickness of the viscous sublayer is probably the single most important parameter in computation of turbulent boundary layers. The sublayer, though comprising a very small fraction of the total boundary layer thickness, is the region where the major change in velocity takes place, and, except for very low Prandtl number fluids, is the region wherein most of the resistance to heat transfer resides. If this region is modelled accurately only a very approximate scheme is needed throughout the rest of the boundary layer.

The thickness of the sublayer is evidently determined by viscous stability considerations. The experimental evidence is that a favorable pressure gradient (dP/dx negative) results in increased thickness, while an adverse pressure gradient has the opposite effect. Transpiration into the boundary layer (blowing) decreases the thickness, if it is expressed in non-dimensional wall coordinates, while suction has the opposite effect. Surface roughness, while not a subject of this paper, causes a thinning of the sublayer.

The effects of pressure gradient and transpiration on A^+ are conveniently expressed in terms of a non-dimensional pressure gradient parameter, p^+, and a non-dimensional blowing parameter, v_o^+, both of which can be either positive or negative. In both of these parameters the main argument is normalized with respect to the same wall coordinate parameters as is the effective sublayer thickness in A^+.

The functional dependence of A^+ upon p^+ and v_o^+ has been deduced experimentally by examination of a very large number of velocity profiles obtained as part of the Stanford project over a period of six years. Before examining these results, however, it should be mentioned that considerable progress has been made in both qualitatively and quantitatively describing this function using some relatively simple theoretical ideas and a minimum of experimental data. A number of investigators (for example, Bradshaw (1969)) have discussed the significance of a minimum value of a local Reynolds number of turbulence as being a requisite for maintenance of a turbulent boundary layer. Numerous investigators, going back to the early theoretical work on the transpired turbulent boundary layer by Rubesin (1954), have implicitly introduced this concept as a basis for defining the thickness of the viscous sublayer. The local Reynolds number of turbulence can be defined as:

$$Re_t = \ell_t \sqrt{\overline{u'v'}}/\nu = \ell_t \sqrt{g_c \tau_t/\rho}/\nu \tag{49}$$

ℓ_t , the turbulence length scale, can be considered to be effectively the same as the mixing - length $\ell = ky$. Thus,

$$Re_t = ky \sqrt{g_c \tau_t/\rho}/\nu \tag{50}$$

It should also be noted that by combining Equations (44) and (45) with (49) and (50),

$$Re_t = \varepsilon_m/\nu \tag{51}$$

Furthermore, outside of the viscous sublayer $\tau_t \approx \tau$, so Eq. (50) can also be expressed as,

$$Re_t = ky^+ \sqrt{\tau/\tau_o} \tag{52}$$

An examination by Andersen (1972) of a large amount of experimental data for transpired turbulent boundary layers for both favorable and adverse pressure gradients indicates that Re_t is approximately the same number (about 33.0) in every case at a point outside of the sublayer defined as approximately $y^+ = 2.5\ A^+$. Thus the thickness of the viscous sublayer, and by implication A^+ , is evidently characterized by a critical value of the Reynolds number of turbulence. It follows, incidently, that if Re_t falls everywhere below this value the turbulence in the boundary layer will damp out and a laminar boundary layer will result, and this is precisely what is observed in strongly accelerated flows where the shear stress decreases so rapidly with distance from the wall that Re_t never reaches 33.0. The important point here, however, is that with these facts alone it is possible to generate the functional dependence of A^+ upon p^+ and v_o^+ .

The following equation is an empirical representation of the experimental data on A^+ , but it could just as well be described as an empirical representation of Andersen's analysis. In either case the algebraic form of the equation has no particular significance.

$$A^+ = \frac{25.0}{a\left[v_0^+ + b\left(\frac{p^+}{1 + cv_0^+}\right)\right] + 1.0} \qquad (53)$$

where $a = 7.1$ if $v_0^+ \geq 0.0$, otherwise $a = 9.0$

$b = 4.25$ if $p^+ \leq 0.0$, otherwise $b = 2.0$

$c = 10.0$ if $p^+ \leq 0.0$, otherwise $c = 0.0$

Equation (53) is plotted on Figure 38 where the effects of pressure gradient and transpiration can be clearly seen. Note that a strong favorable pressure gradient forces A^+ to very high values, and that blowing lessens this effect, while suction increases it. If A^+ becomes very large the viscous sublayer simply overwhelms the entire boundary layer, and this is the "laminarization" discussed earlier. In fact most of the trends noted earlier in connection with the experimental data on Stanton number are recoverable by varying the value of A^+. The thickening of the sublayer caused by a favorable pressure gradient (accelerating flows) results in a decreased Stanton number simply because the major resistance to heat transfer is in the viscous sublayer.

Note that an adverse pressure gradient causes a decrease in sublayer thickness. Interestingly, where these results are used to compute velocity profiles for adverse pressure gradients and no transpiration, and when the velocity profiles are plotted on u^+, y^+ coordinates, they tend to fall on the same line as is obtained for no pressure gradient in the near-wall region, but outside of the sublayer. This is the "law-of-the-wall" which has long been noted to be universal for no pressure gradient and adverse pressure gradient flows. The conventional "law-of-the-wall" does not apply for strong favorable pressure gradients. The universality of the "law-of-the-wall" for adverse pressure gradients results from compensating effects of the decreased sublayer thickness and the positive pressure gradient.

A^+ as represented by Eq. (53) and Figure 38 has been evaluated under essentially equilibrium conditions, i.e., conditions under which v_0^+ and/or

p^+ are invariant or, at worst, are varying only slowly along the surface. This is a case of inner region equilibrium. It is probable that when a sudden change of external conditions is imposed, the inner region comes to equilibrium more rapidly than the outer region, although this has not been proved. In any case, under non-equilibrium conditions where v_o^+ or p^+ are changing rapidly, it has been observed that the sublayer does not change instantaneously to its new equilibrium thickness, i.e., A^+ does not immediately assume its new equilibrium value. It can be hoped that some of the higher order models of turbulence will predict this effect, but in the meantime, a reasonably satisfactory expedient is to use a rate equation of a type suggested by Launder (1968):

$$\frac{dA^+_{eff}}{dx^+} = (A^+_{eff} - A^+_{eq})/C \tag{54}$$

A^+_{eff} is the locally effective value of A^+, while A^+_{eq} is the equilibrium value obtained from Eq. (53). A value of C of about 4000 has been found to be reasonable.

All of the discussion up to now has been concerned with the inner region of the boundary layer. The outer region, comprising the greater part of the boundary layer thickness, is of considerably less importance in predicting performance, and thus can be handled successfully using more gross approximations. This statement may not be valid for strongly non-equilibrium boundary layers, especially under adverse pressure gradient conditions. Its validity for accelerating flows with and without transpiration will be demonstrated later. In any case, for equilibrium or near equilibrium boundary layers, either the assumption of a constant value of eddy diffusivity over the entire outer region, or the assumption of a constant value of mixing-length over the entire outer region yields approximately the same result. If a constant eddy diffusivity is used, an empirical correlation of eddy diffusivity as a function of either displacement or momentum thickness Reynolds number can be obtained. However, if mixing-length is used in the inner regions, it is computationally simpler to use the mixing-length concept for the entire boundary layer.

Figure 37 shows measured mixing-length data for the outer region for a number of cases of transpiration with zero and adverse pressure gradients. The adequacy of an assumption that the mixing-length is constant in the outer region may be judged from these data. A further simplification is also illustrated in this figure. The outer region mixing-length scales approximately on the total boundary layer thickness. A satisfactory computation scheme is to express the outer region mixing-length as a fixed fraction, λ, of the 99 percent boundary layer thickness.

$$\ell = \lambda \delta_{.99} \tag{55}$$

A value of $\lambda = 0.084$ works reasonably well over the entire range of experimental data discussed in this paper, including favorable and adverse pressure gradients, blowing and suction. One then simply evaluates ℓ from Eq. (47) until the value obtained equals that given by Eq. (55), and then uses the latter value for the remainder of the boundary layer.

There is some evidence that the effective value of λ is larger than 0.084 for boundary layers in which the momentum thickness Reynolds numbers is less than 5500. This may be a result of the fact that at low Reynolds numbers the sublayer is a larger fraction of the boundary layer and the approximation of a constant mixing-length over the remainder of the boundary layer is less valid. For strong blowing, even at low Reynolds numbers, λ again appears to be close to 0.084, and this is consistent with the above explanation because the sublayer is then thinner. The following equation has been found to describe the observed low Reynolds behavior of λ quite well:

$$\lambda = 0.250\ Re_m^{-1/8}\ (1. - 67.5\ F) \tag{56}$$

$$\text{IF}\quad \lambda < 0.084;\quad \lambda = 0.084$$

A Mathematical Model for Solution of the Energy Equation

The time-averaged energy equation of the boundary layer, particularized to constant fluid properties and negligible viscous dissipation, and neglecting turbulent conduction in the stream-wise direction, may be written as:

$$\bar{u}\frac{\partial \bar{t}}{\partial x} + \bar{v}\frac{\partial \bar{t}}{\partial y} - \frac{\partial}{\partial y}\left[\alpha\frac{\partial \bar{t}}{\partial y} - \overline{t'v'}\right] = 0 \qquad (57)$$

This equation can be solved for any desired boundary conditions providing the velocity field has been established first by solution of the momentum equation, and provided that we have information on the turbulent heat transfer rate, $\overline{t'v'}$.

Analogous to the method of solution of the momentum equation, we will introduce the concept of eddy diffusivity for heat, ε_h .

$$\overline{t'v'} = -\varepsilon_h \frac{\partial \bar{t}}{\partial y} \qquad (58)$$

Although it might be fruitful to attempt to evaluate either $\overline{t'v'}$ or ε_h on the basis of assumptions that are independent of the turbulent shear stress, it seems plausible that there is some kind of relationship between $\overline{t'v'}$ and $\overline{u'v'}$, or ε_h and ε_m . Therefore most analysts have found it convenient to introduce the concept of a turbulent Prandtl number, Pr_t , defined as follows:

$$Pr_t = \frac{\varepsilon_m}{\varepsilon_h} \qquad (59)$$

Introducing Eq. (58) and (59) into Eq. (57) we obtain:

$$\bar{u}\frac{\partial \bar{t}}{\partial x} + \bar{v}\frac{\partial \bar{t}}{\partial y} - \frac{\partial}{\partial y}\left[(\alpha + \varepsilon_m/Pr_t)\frac{\partial \bar{t}}{\partial y}\right] = 0 \qquad (60)$$

If Pr_t were known, Eq. (60) could be solved for any desired boundary conditions so long as the momentum equation had been previously solved. Evaluation of the turbulent Prandtl number can thus solve one of the central problems of turbulent heat transfer.

A very simple physical model of the turbulent momentum and energy transfer processes leads to the conclusion that $\varepsilon_h = \varepsilon_m$, i.e., $Pr_t = 1.00$ (the "Reynolds Analogy"). Slightly more sophisticated models suggest that $Pr_t > 1.00$ when the molecular Prandtl number, Pr , is less than unity. Still other models suggest that Pr_t equals 0.7 or 0.5 in turbulent wakes.

The experimental data are not abundant, but Figures 39, 40, 41, and 42 show the measurements, respectively of Simpson, Whitten and Moffat (1970),

Kearney (1970), and Blackwell (1972) with air as a working substance. These were all evaluated from measurements of the slopes of mean velocity and temperature profiles, together with estimates of shear stress and heat flux profiles, and the experimental uncertainty is high, especially near the wall ($y^+ < 20$) and near the outer edge of the boundary layer. The data on Figure 39 are all for constant free-stream velocity, but cover a wide range of blowing and suction conditions. The data on Figure 40 are for accelerated flows with a considerable range of blowing. Figure 41 shows three separate test runs with no transpiration, but first with no pressure gradient, and then two successively stronger cases of equilibrium adverse pressure gradients. Finally Figure 42 shows three test runs for an adverse pressure gradient with three cases of successively stronger blowing.

Despite the very considerable scatter of data, a few conclusions seem definitely warranted. First, the turbulent Prandtl number, at least for air, apparently has an order of magnitude of unity. Thus the Reynolds Analogy ($Pr_t = 1.0$) is not a bad approximation.

The second conclusion is that Pr_t seems to go to a value higher than unity very near the wall, but is evidently less than unity in the wake or outer region. The situation very close to the wall is especially vexing because it is extremely difficult to make accurate measurements in this region, and yet it seems evident that something interesting and important is happening in the range of y^+ from 10.0 to 15.0 . The behavior of Pr_t at values of y^+ less than about 10.0, is highly uncertain but fortunately not very important because molecular conduction is the predominant transfer mechanism in this region. At the other extreme, in the wake region Pr_t does not need to be known precisely because the heat flux tends to be small there.

Another conclusion, for which the evidence is not yet very strong, is that there is some small effect of pressure gradient on Pr_t . Figure 41 suggests that an adverse pressure gradient tends to decrease Pr_t . Although the scatter of his data was very large, Kearney (1970) reported that there seemed a tendency for Pr_t to be increased by a favorable pressure gradient (an accelerating flow).

The results on Figure 39 suggest that transpiration does not influence Pr_t unless there is an effect very close to the wall that is hidden in the

experimental uncertainty in this region. This conclusion is also implied by the results on Figure 42.

Many analysts have been content to assume that turbulent Prandtl number is a constant throughout the boundary layer, and indeed the assumption that $Pr_t = 0.9$, for air, will generally yield satisfactory predictions of overall heat transfer rates. However, it is found that the assumption of a constant Pr_t will yield temperature profiles that do not correspond well with experiment except in the regions very close to the wall, and near the outer edge of the boundary layer. Temperature profiles can be much more accurately predicted if some attempt is made to introduce a variation of Pr_t with y^+ that at least approximates the variation seen in the experimental data. Both of the following equations, neither of which have any theoretical basis, have been used with reasonable success by the authors for calculations for air:

$$Pr_t = 1.43 - 0.17\, y^{+\,1/4} \tag{61}$$

$$\text{IF } Pr_t < 0.86 \; ; \; Pr_t = 0.86$$

$$Pr_t = 0.90 + 0.35[1 + \cos(\pi y^+/37)]; \; y^+ < 37 \tag{62}$$

$$= 0.90 \; ; \; y^+ > 37$$

$$= 0.60 \; ; \; y^+ > (\lambda\, \delta_{.99}/k)$$

A pressure gradient effect has not been included in these empirical equations because of insufficient information but, in the section to follow, one effect of this omission will be illustrated.

SOME EXAMPLES OF BOUNDARY LAYER PREDICTIONS

The quality of boundary layer predictions that can be made using the mixing-length model and associated empirical functions will now be demonstrated. Four examples have been chosen for illustration. The first is the case of the simple impermeable wall with no pressure gradient, and this is of course both an equilibrium momentum boundary layer and an equilibrium thermal boundary layer. The second is an adverse pressure gradient equilibrium boundary layer. The third is an adverse pressure gradient boundary layer with strong blowing which is not precisely an equilibrium boundary layer, but shows near-equilibrium characteristics. The final example is a strongly accelerated boundary layer with strong blowing, but in which both blowing and acceleration are abruptly stopped at different points along the surface to yield non-equilibrium conditions.

A modification of the Spalding/Patankar (1967) finite difference program was used for all predictions, although any good finite difference procedure should yield similar results.

Figure 43 shows $c_f/2$ as a function of momentum thickness Reynolds number for the simple impermeable wall with no pressure gradient. Shown for comparison is the recommendation of Coles (1962), which is based on an extensive examination of the available data, and also two sets of data from the Stanford project, the earlier results of Simpson, and the more recent results of Andersen. The predicted friction coefficients coincide closely with Coles', and indeed the auxilliary functions were chosen to force this coincidence.

The corresponding heat transfer results are shown on Figure 44 where comparison is made with two sets of data from the Stanford project, the results of Whitten (1967) and of Blackwell (1972). The Blackwell data at Re_h below 2000 are a little lower than would be expected for a corresponding equilibrium thermal boundary layer, because the thermal boundary layer started out at the beginning of the test section much thinner than the momentum boundary layer.

It should also be added that all of these results were obtained using low velocity air with temperature difference from 25 to 35 degrees F . Although the influence of the temperature dependent fluid properties has not really been systematically investigated, and indeed small temperature dif-

ferences were deliberately used to avoid this problem, calculations with the computer program using real properties suggest that the temperature-difference effect is to reduce Stanton number by about 1 or 2 percent. This effect has not been considered in any of these results; the predictions have been made using constant properties, and the experimental data have not been corrected for any variable properties effect.

Note that if the friction coefficient prediction on Figure 43 is acceptable, the heat transfer prediction on Figure 44 is entirely dependent upon the turbulent Prandtl number function employed, because everything else in the model is identical, and in fact both predictions were made simultaneously.

In the upper part of Figure 45 both friction and heat transfer results are shown for an adverse pressure gradient test run with no transpiration. For this case U_∞ was varied by,

$$U_\infty = U_1 x^m \tag{63}$$

where $m = -0.15$. Both the Clauser shape factor, G , and β were found to be essentially constant for the experimental data over most of the test section, so this is believed to be an equilibrium momentum boundary layer.

The prediction program also produced essentially constant values of G and β . The friction prediction is excellent, but the heat transfer prediction is about 5% low. Experimental uncertainty may account for this difference, but it is also quite possible that we see here evidence of a pressure gradient influence on turbulent Prandtl number. A 10 percent decrease of Pr_t throughout the boundary layer would make the difference.

In the lower part of Figure 45 are the results for an adverse pressure gradient test with rather strong blowing. Because F was held constant (.004) this is not an equilibrium boundary layer, either momentum or thermal. For an equilibrium boundary layer it would be necessary for v_0 , and thus F , to decrease with x . However, the departure from equilibrium is not great and the predictions for both $c_f/2$ and St are seen to be quite good.

The scheme described not only predicts $c_f/2$ and St quite adequately, but does equally well for velocity and temperature profiles. Figure 46 shows a pair of profiles for the adverse pressure gradient, strong blowing case dis-

cussed above. These are presented in dimensional coordinates so that normalization will not tend to mask anything, and are presented for a point 70 inches downstream so that a small percentage drift of the predictions would show as a large effect. The results shown on this figure would be hard to improve upon.

The final illustration, Figure 47, shows an example of prediction of a very difficult case. In this run the flow starts at constant free-stream velocity but with relatively strong blowing, $F = 0.004$. This flow is then subjected to a very strong acceleration starting at $X = 2$ ft. In approximately the middle of the accelerated region the blowing is removed entirely. Then at about $X = 3.4$ ft. the acceleration is removed, and for the remainder of the test section there is no blowing and no change in free-stream velocity.

An important thing to note here is that the model responds remarkably to the abrupt changes in boundary conditions, and predicts the resulting non-equilibrium boundary layer very well indeed. Of particular significance is the abrupt rise in Stanton number following the removal of blowing. The ability of the prediction to follow the data at this point is heavily dependent upon the use of the rate equation and lag constant, Eq. (54). This shows very graphically the importance of the sublayer and the fact that the sublayer does not instantaneously assume its new equilibrium thickness after an abrupt change of boundary conditions. There may well be significant non-equilibrium effects in the outer part of the boundary layer, but these have a relatively minor influence on overall heat transfer rate.

REFERENCES

Andersen, P. S. (1972), "The Turbulent Boundary Layer on a Porous Plate: An Experimental Study of the Fluid Mechanics for Adverse Free Stream Pressure Gradients," Ph.D. Thesis, Stanford University.

Black, T. J., and Sarnecki, A. J. (1965), "The Turbulent Boundary Layer with Suction or Injection," A.R.C. R & M 3387.

Blackwell, B. F. (1972), "The Turbulent Boundary Layer on a Porous Plate: An Experimental Study of the Heat Transfer Behavior with Adverse Pressure Gradients," Ph.D. Thesis, Stanford University.

Bradshaw, P. (1967), "The Turbulence Structure of Equilibrium Boundary Layers," Jn. of Fl. Mech., Vol. 29, Part 4, pp. 625-645.

Bradshaw, P. (1969), "A Note on Reverse Transition," Jn. of Fl. Mech., Vol. 35, Part 2, pp. 387-390.

Clauser, F. H. (1954), "Turbulent Boundary Layers in Adverse Pressure Gradients," Jn. of Aero. Sci., Vol. 21, p. 91.

Coles, D. E. (1962), "The Turbulent Boundary Layer in a Compressible Fluid," Rand Corporation Report R-403-PR.

Kearney, D. W. (1970), "The Turbulent Boundary Layer: Experimental Heat Transfer with Strong Favorable Pressure Gradients and Blowing," Ph.D. Thesis, Stanford University.

Launder, B. E., and Jones, W. P. (1968), "On the Prediction of Laminarization," Presented at the ARC Heat and Mass Transfer Subcommittee Meeting of April 5, 1968.

Mickley, H. S., Ross, R. C., Squyers, A. L., and Stewart, W. E. (1954), "Heat, Mass and Momentum Transfer for Flow over a Flat Plate with Blowing or Suction," NACA TN 3208.

Mickley, H. S., and Davis, R. S. (1957), "Momentum Transfer for Flow over a Flat Plate with Blowing," NACA TN 4017.

Moffat, R. J. (1967), "The Turbulent Boundary Layer on a Porous Plate: Experimental Heat Transfer with Uniform Blowing and Suction," Ph.D. Thesis, Stanford University.

Orlando, A. F., Moffat, R. J., and Kays, W. M. (1974), "Heat Transfer in Turbulent Flows Under Mild and Strong Adverse Pressure Gradient Conditions for an Arbitrary Variation of the Wall Temperature," Heat Transfer and Fluid Mechanics Institute, 1974.

Rubesin, M. W. (1954), "An Analytical Estimation of the Effect of Transpiration Cooling on the Heat-Transfer and Skin Friction Characteristics of a Compressible, Turbulent Boundary Layer," NACA TN 3341.

Simpson, R. L. (1967), "The Turbulent Boundary Layer on a Porous Plate: An Experimental Study of the Fluid Dynamics with Injection and Suction," Ph.D. Thesis, Stanford University.

Simpson, R. L., Whitten, D. G., and Moffat, R. J. (1970), "An Experimental Study of the Turbulent Prandtl Number of Air with Injection and Suction," Int. Jn. of Heat and Mass Transfer, Vol. 13, pp. 125-143.

Spalding, D. B., and Patankar, S. V. (1967), "Heat and Mass Transfer in Boundary Layers," Morgan-Grampian: London.

Squire, L. C. (1970), "The Constant Property Turbulent Boundary Layer with Injection; a Reanalysis of Some Experimental Results," Int. Jn. Heat and Mass Transfer, Vol. 13, No. 5, p. 939.

Stevenson, T. N. (1963), "A Law of the Wall for Turbulent Boundary Layers with Suction or Injection," Cranfield College of Aero. Report 166.

Thielbahr, W. H. (1969), "The Turbulent Boundary Layer: Experimental Heat Transfer with Blowing, Suction, and Favorable Pressure Gradient," Ph.D. Thesis, Stanford University.

Van Driest, E. R. (1956), "On Turbulent Flow Near a Wall," Heat Transfer and Fluid Mechanics Institute.

Whitten, D. G. (1967), "The Turbulent Boundary Layer on a Porous Plate: Experimental Heat Transfer with Variable Suction, Blowing, and Surface Temperature," Ph.D. Thesis, Stanford University.

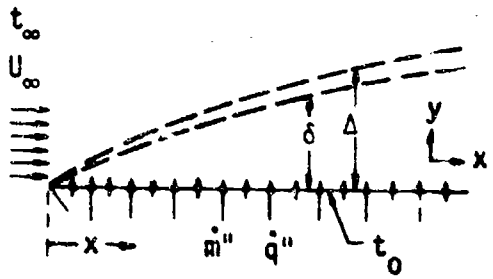

Fig. (1) The physical situation.

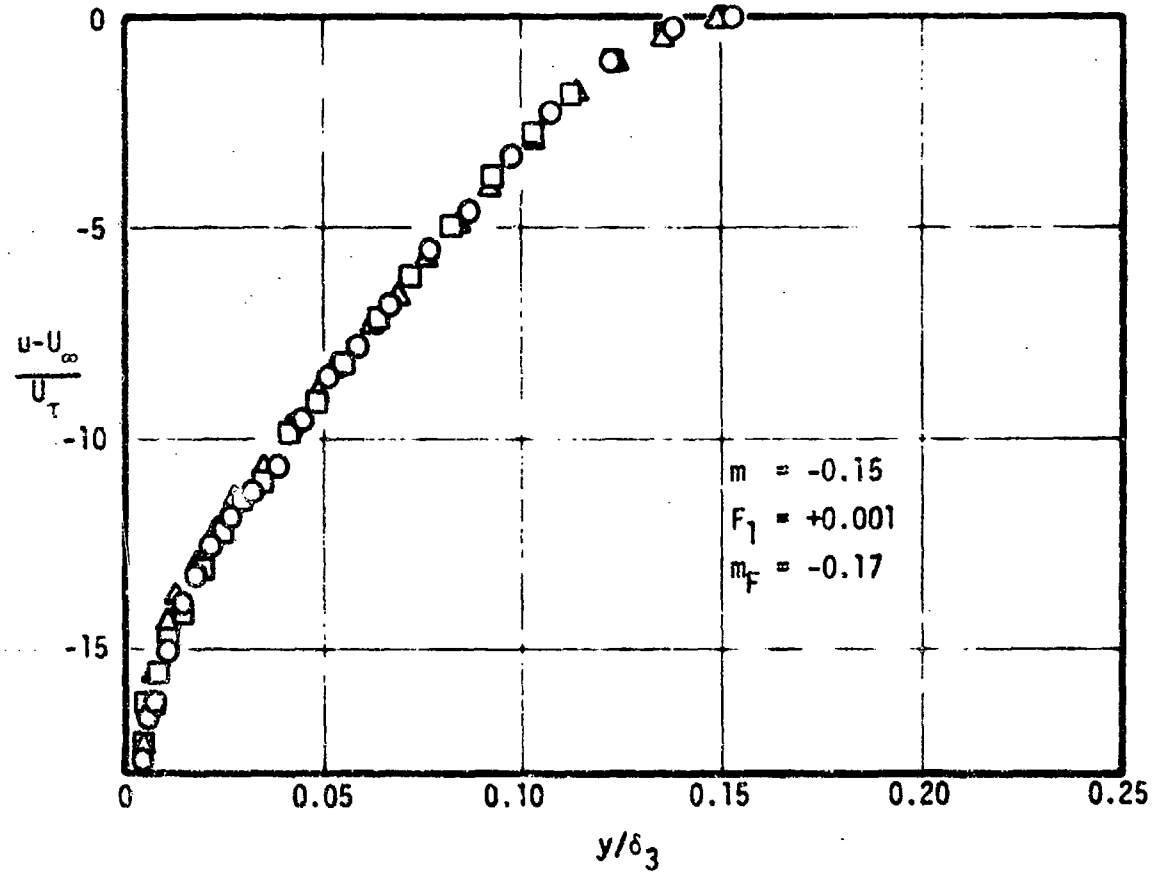

Fig. (2) Defect profiles for an equilibrium boundary layer.

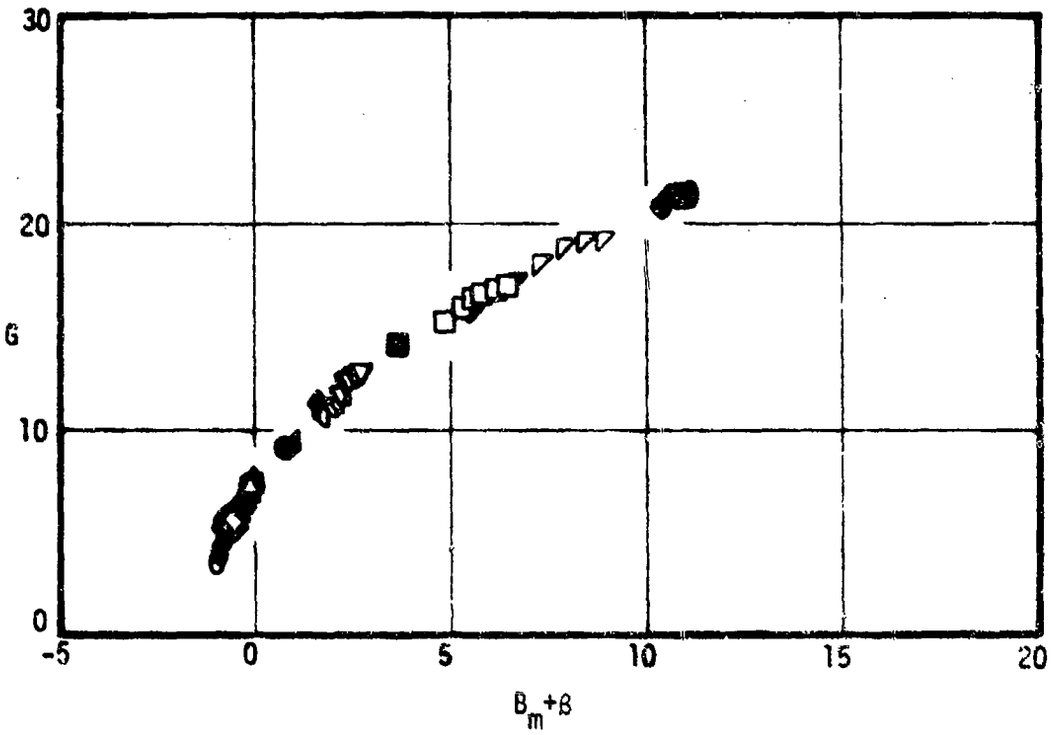

Fig. (3) The Clauser shape factor, G , versus $B_m + \beta$.

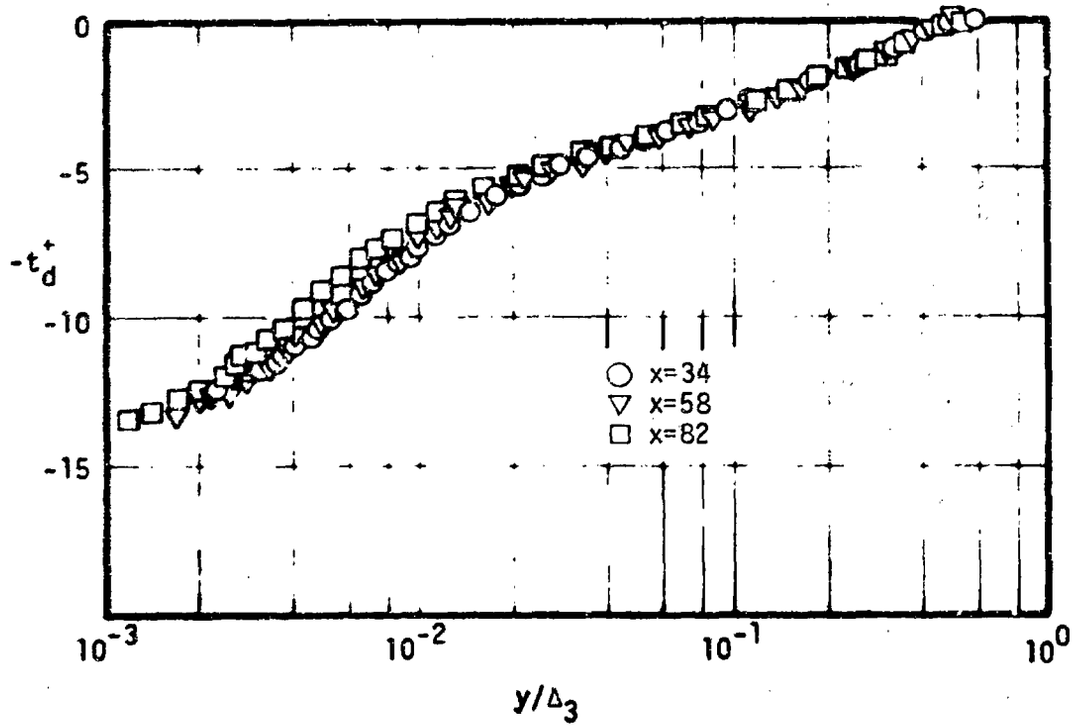

Fig. (4) Temperature defect profiles for a decelerating flow, m = -0.2 .

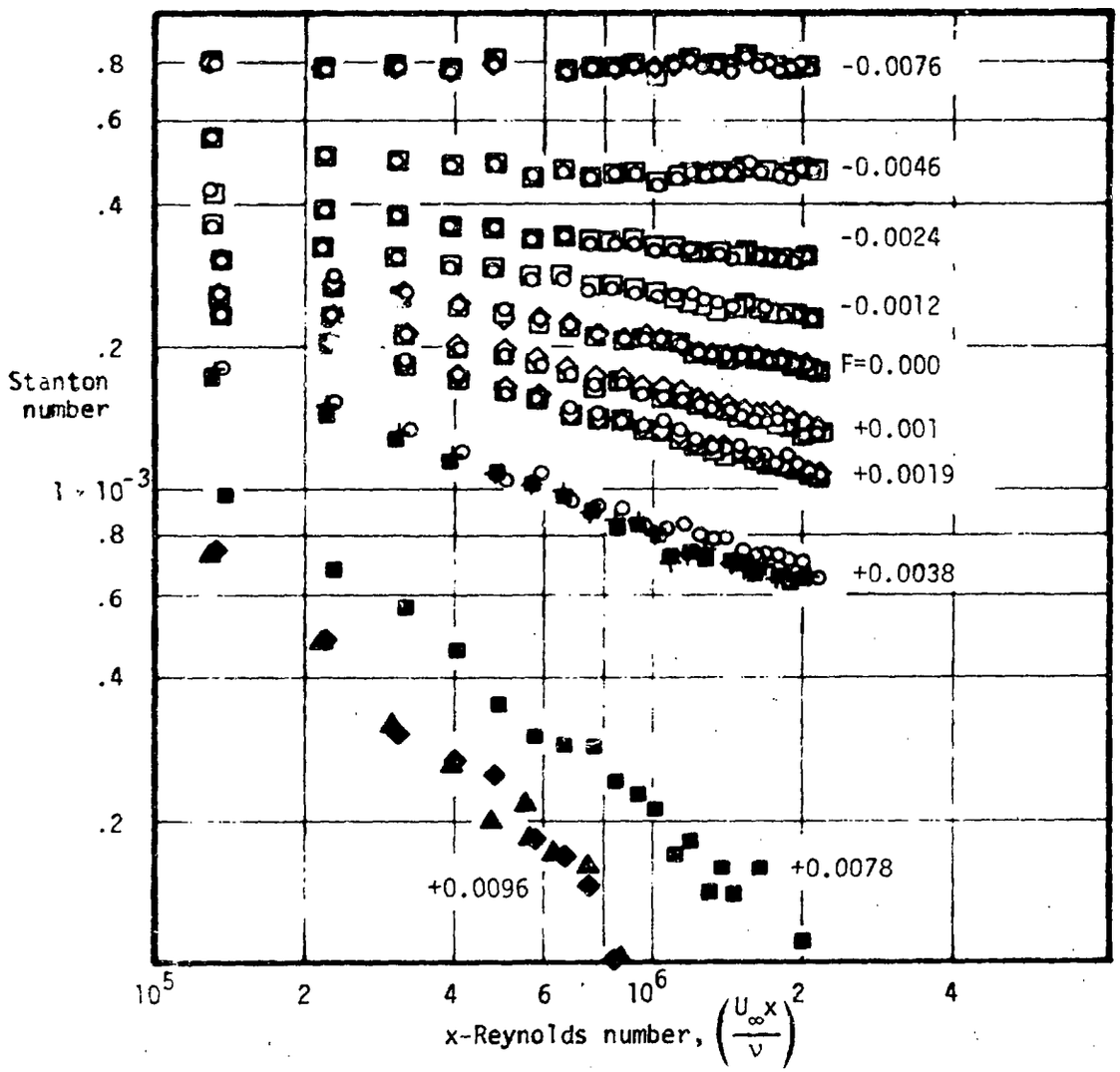

Fig. (5) The variation of Stanton number with x-Reynolds number at constant F.

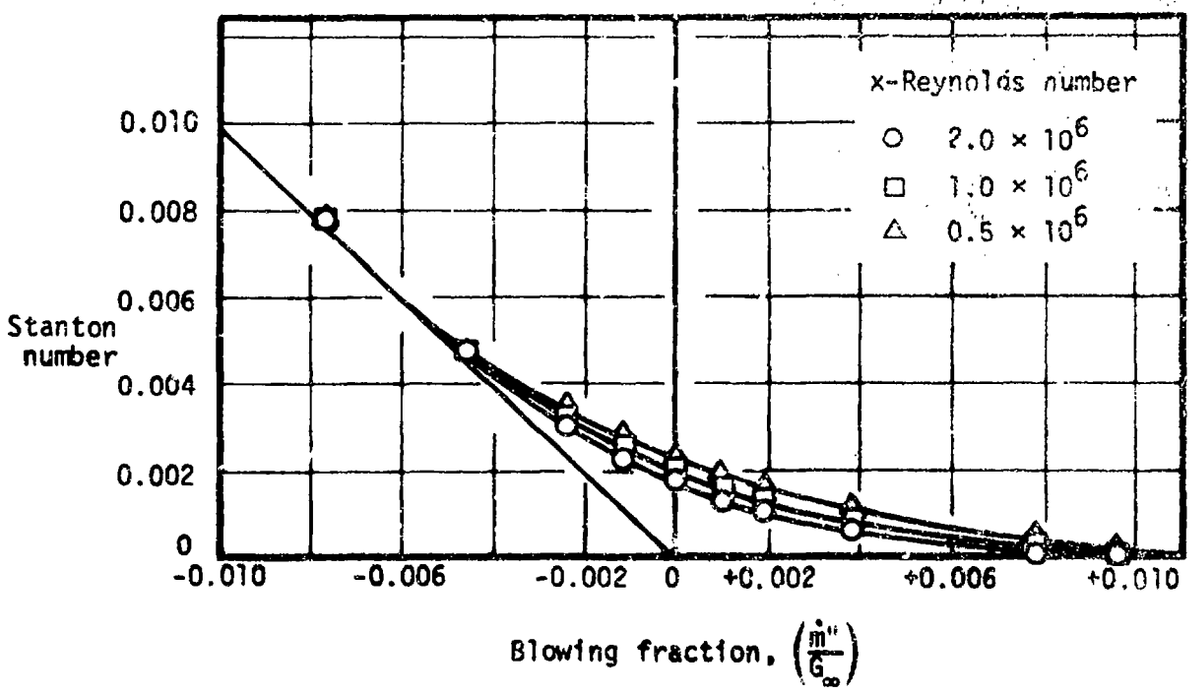

Fig. (6) The variation of Stanton number with F at constant x-Reynolds number.

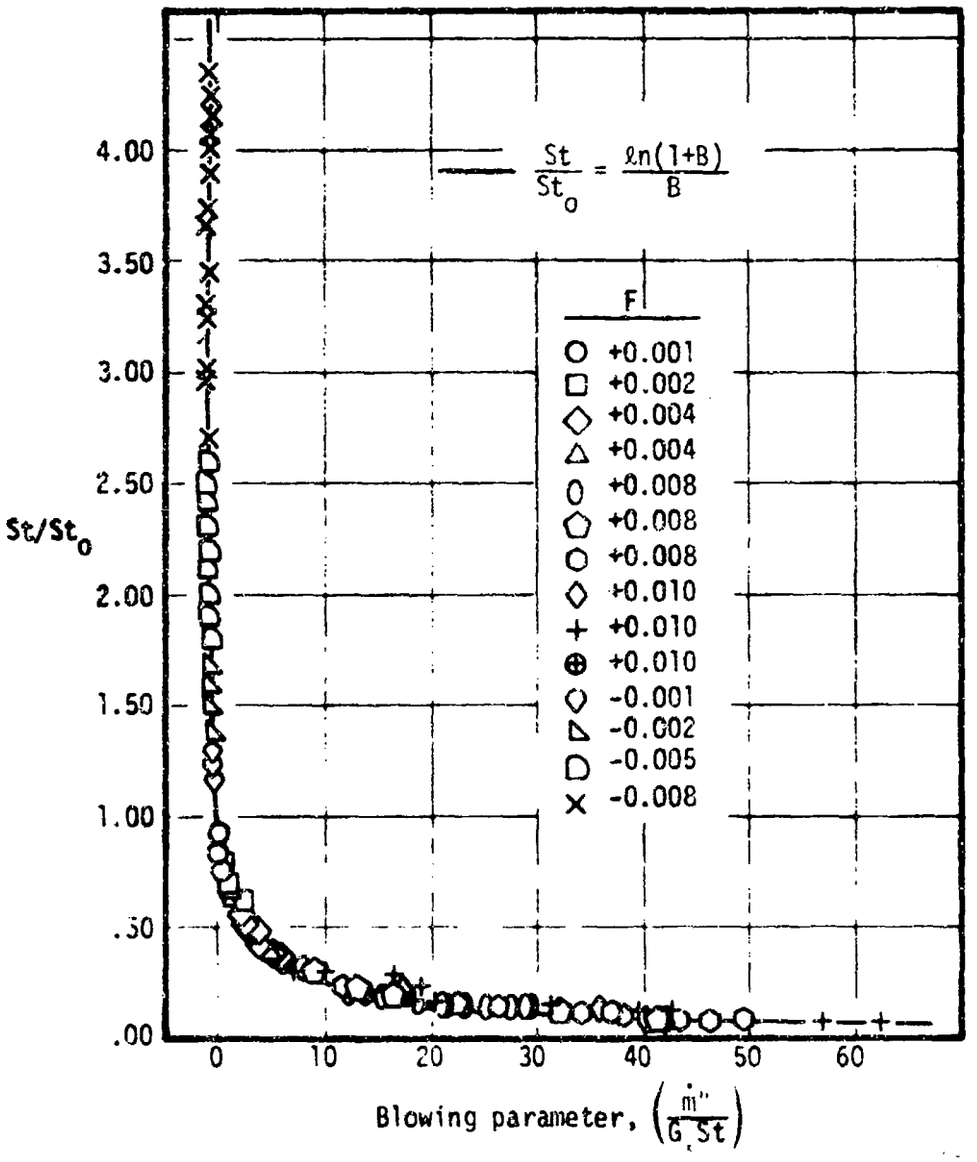

Fig. (7) The ratio St/St_o versus the heat transfer blowing parameter, B_h.

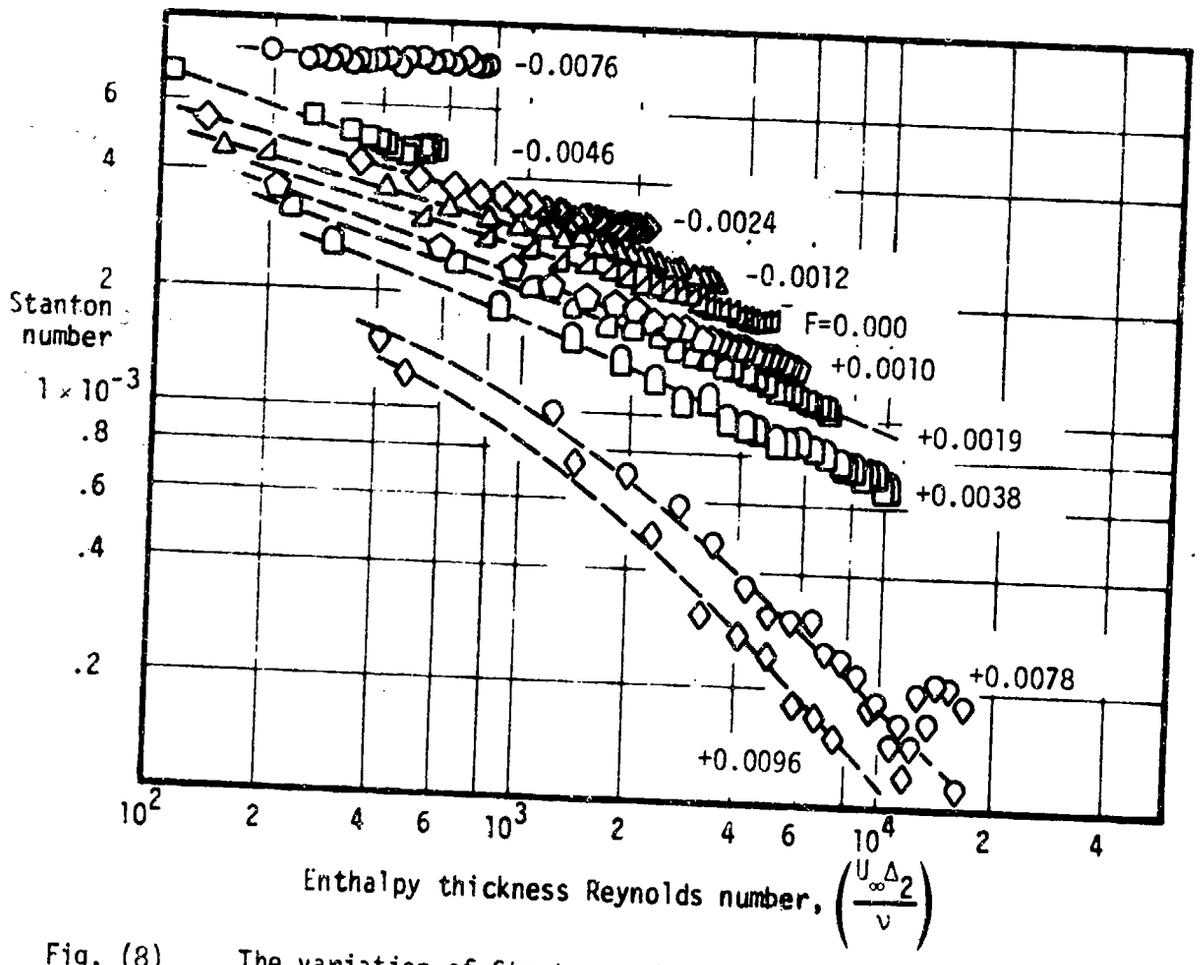

Fig. (8) The variation of Stanton number with enthalpy thickness Reynolds number at constant F .

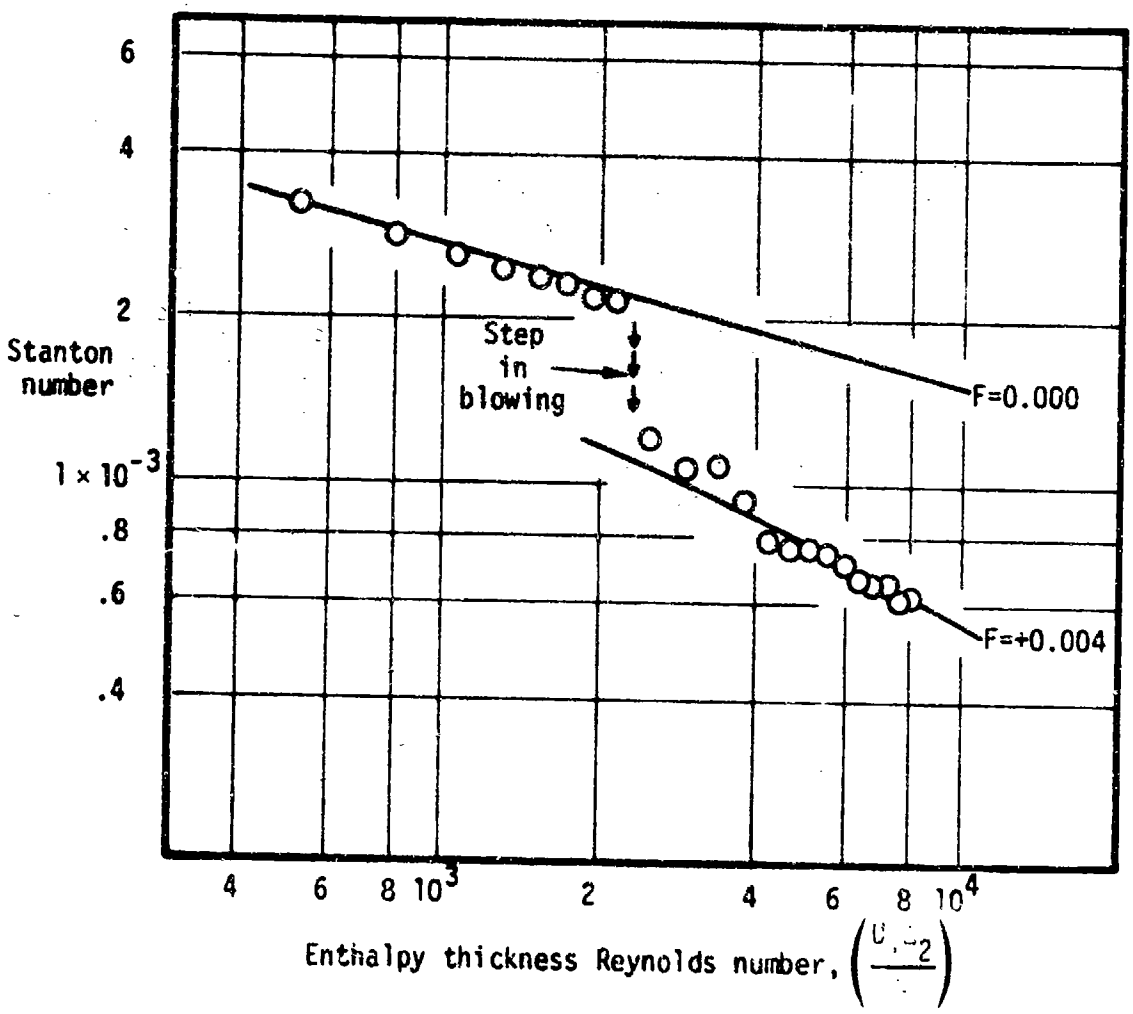

Fig. (9) The response of Stanton number to a step increase in blowing.

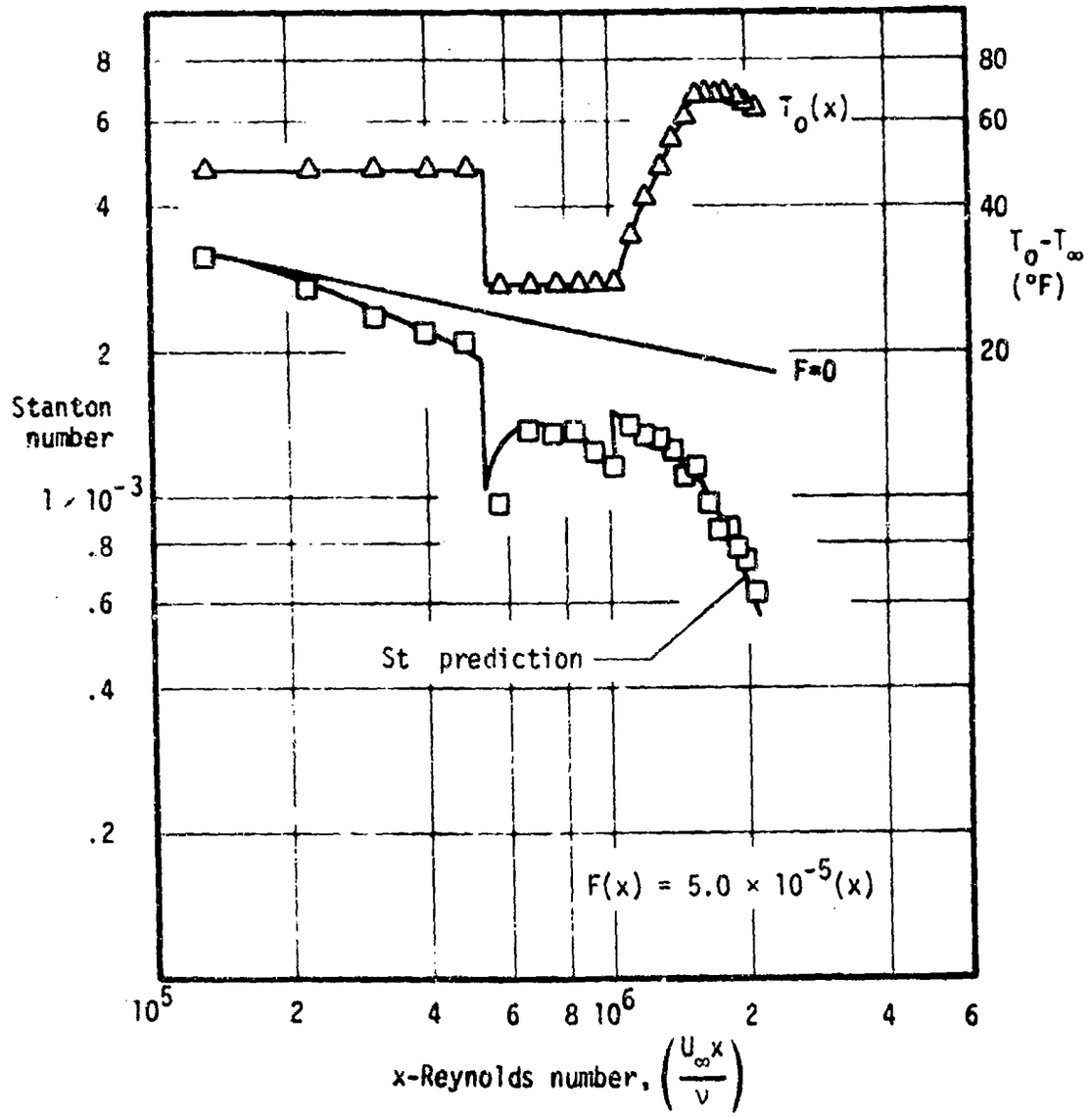

Fig. (10) A demonstration case: linearly varying blowing with arbitrary wall temperature.

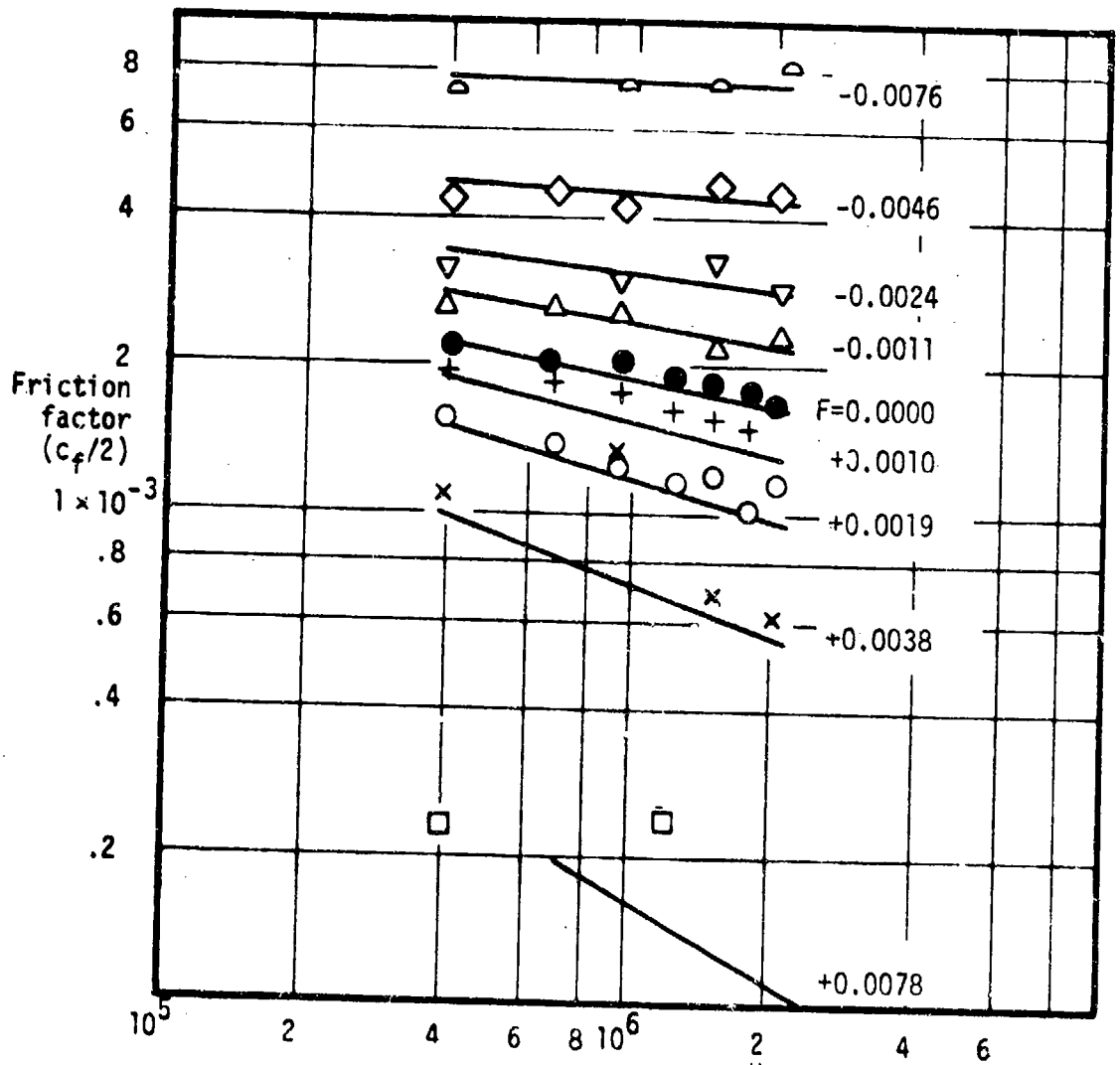

Fig. (11) The variation of friction factor, $c_f/2$, with x-Reynolds number at constant F.

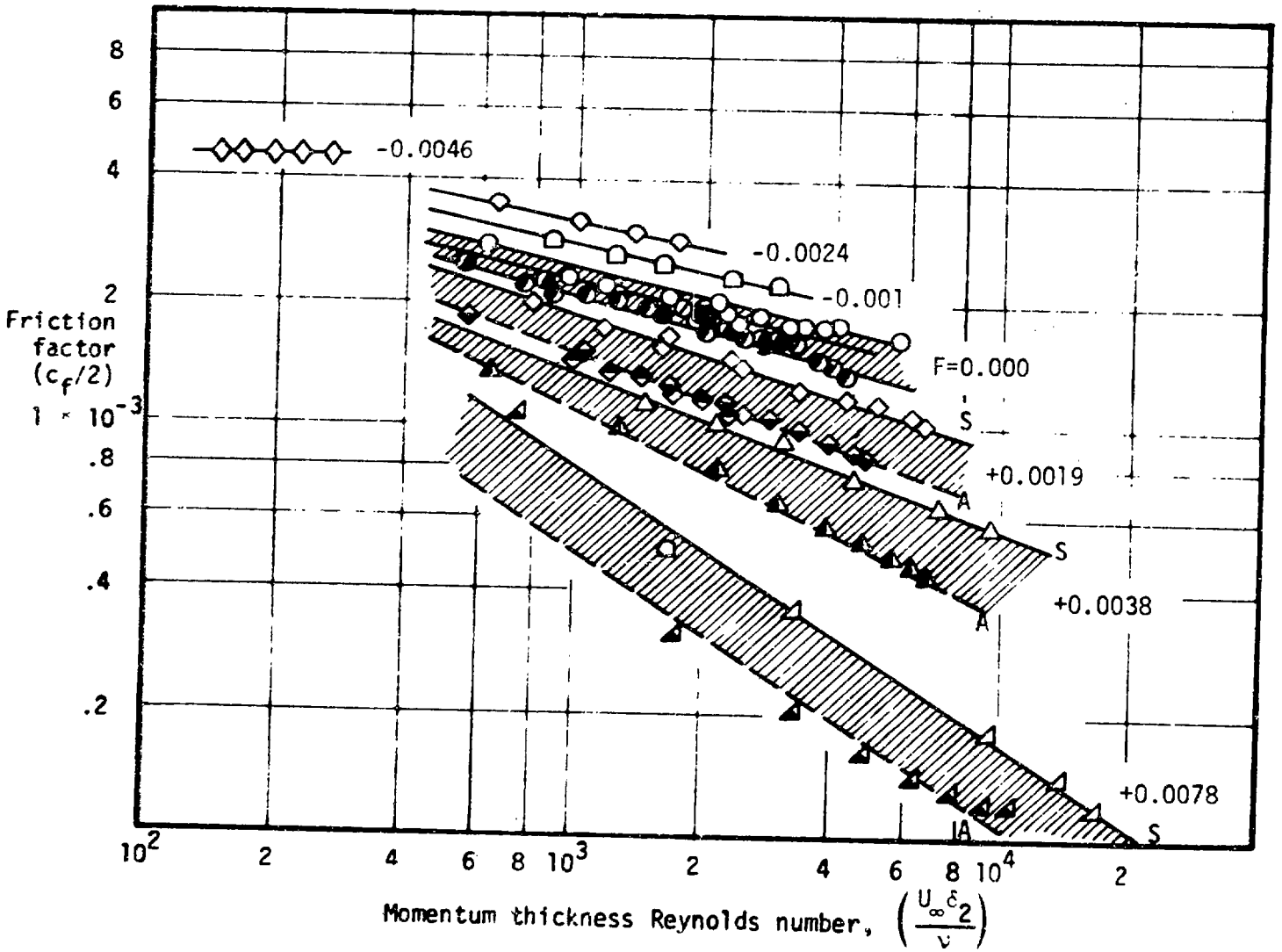

Fig. (12) The variation of friction factor, $c_f/2$, with momentum thickness Reynolds number at constant F .

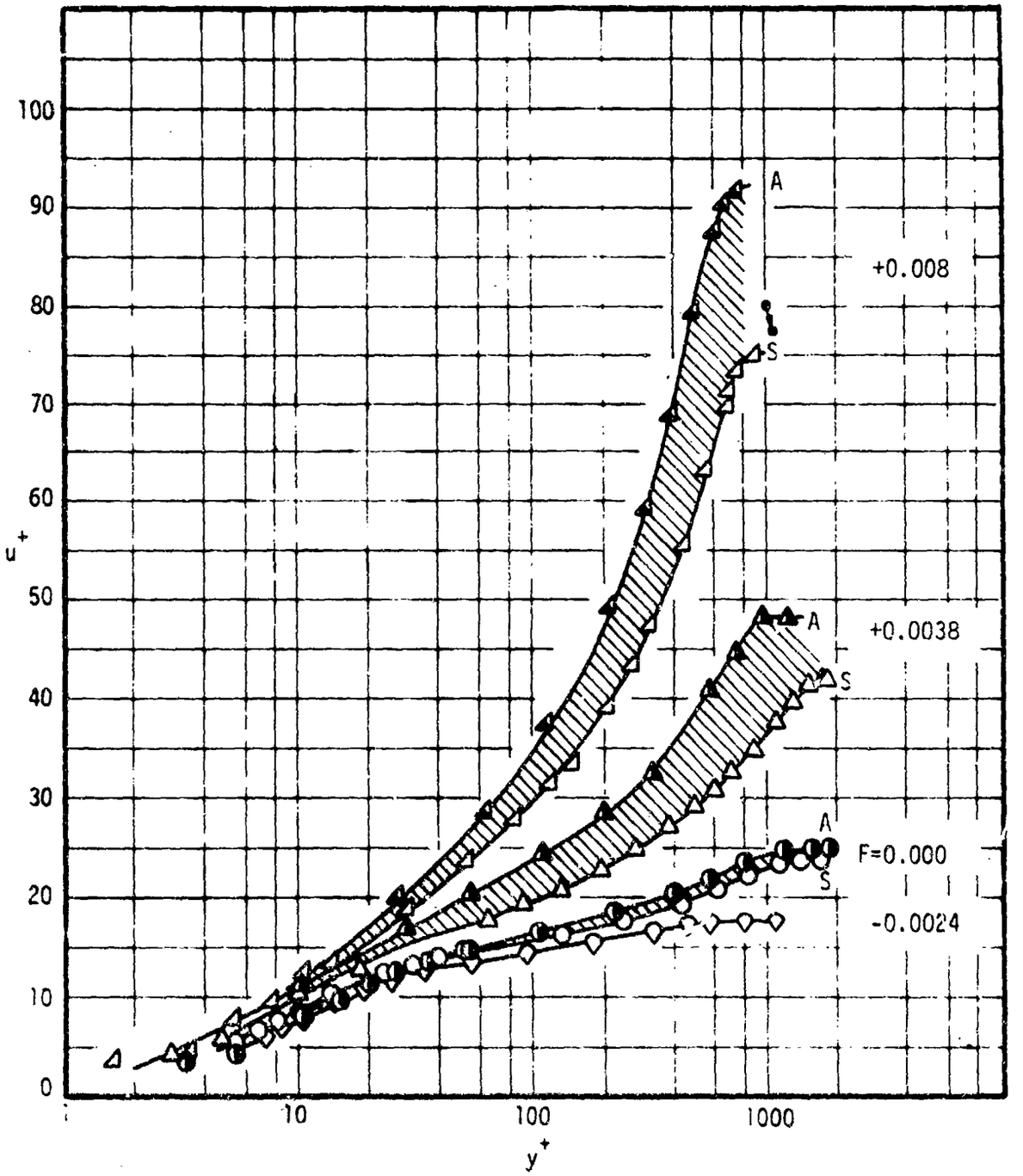

Fig. (13) Velocity profiles with blowing and suction, constant F and U_∞ .

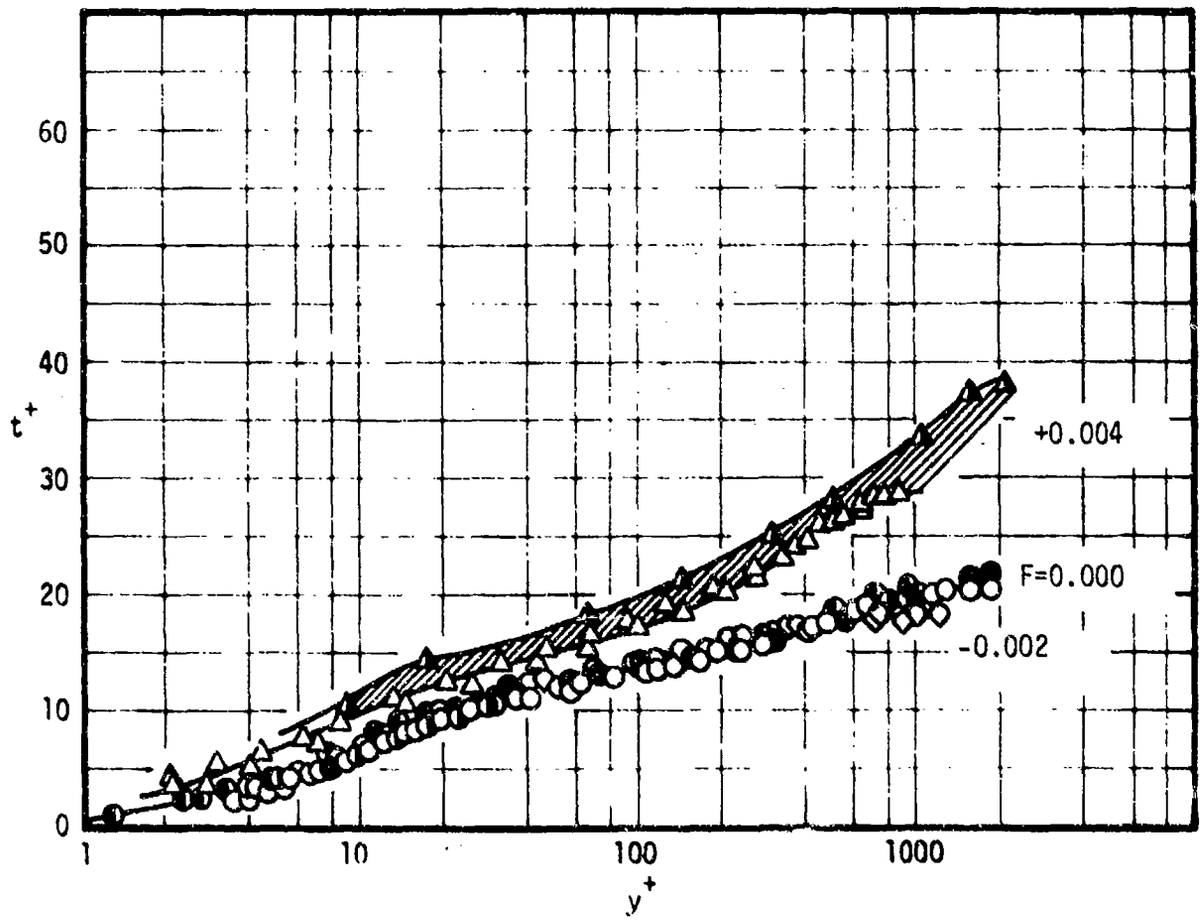

Fig. (14) Temperature profiles with blowing and suction, constant f and U_∞ .

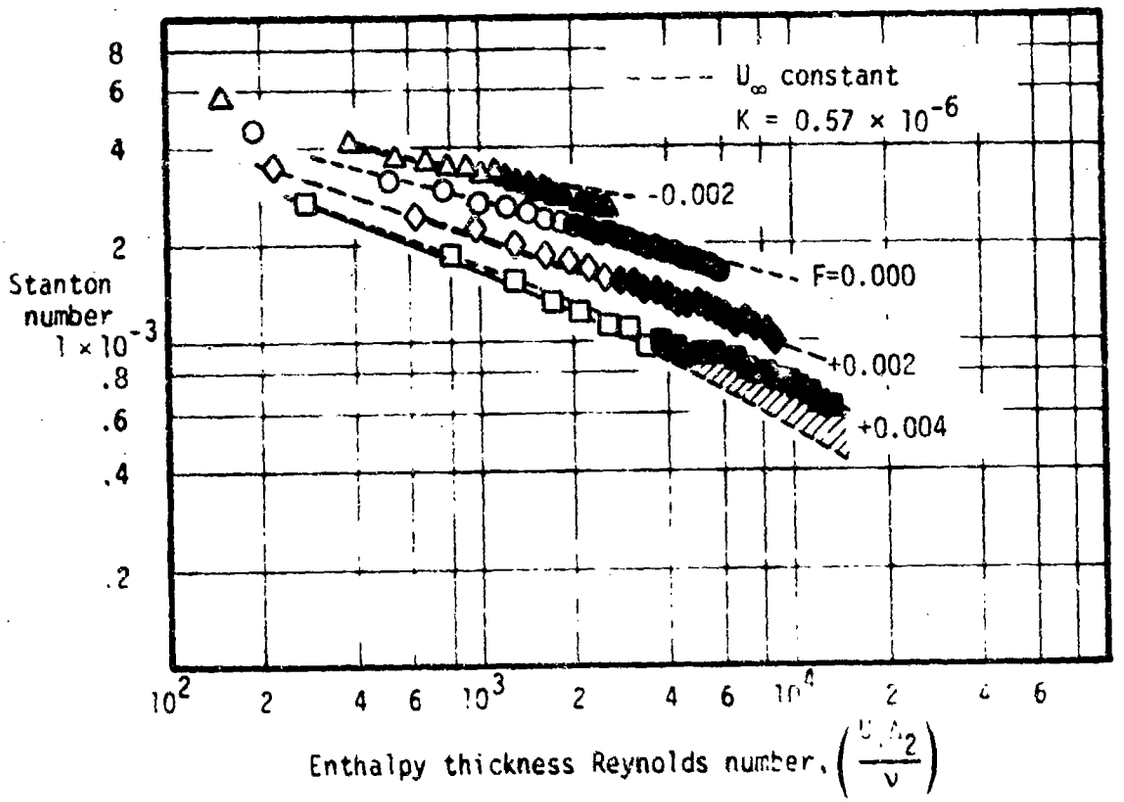

Fig. (15) The variation of Stanton number with enthalpy thickness Reynolds number at constant F for mild acceleration.

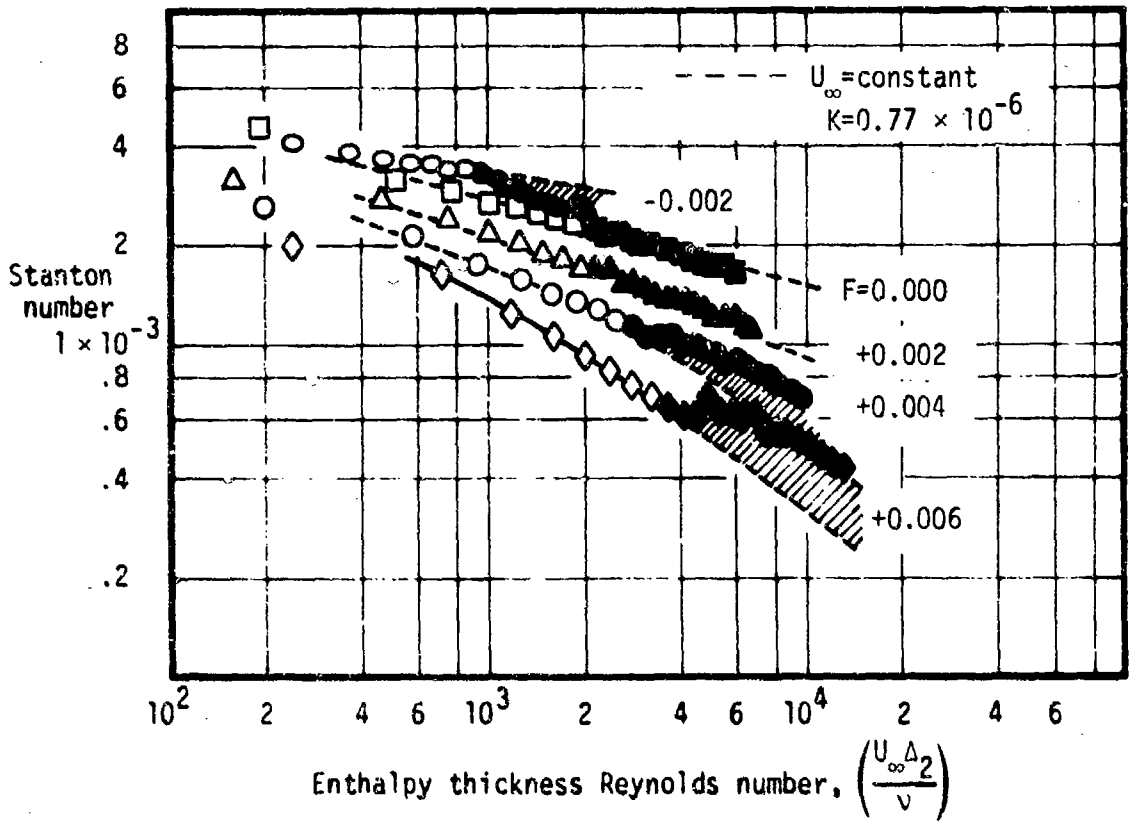

Fig. (16) The variation of Stanton number with enthalpy thickness Reynolds number at constant F for moderate acceleration.

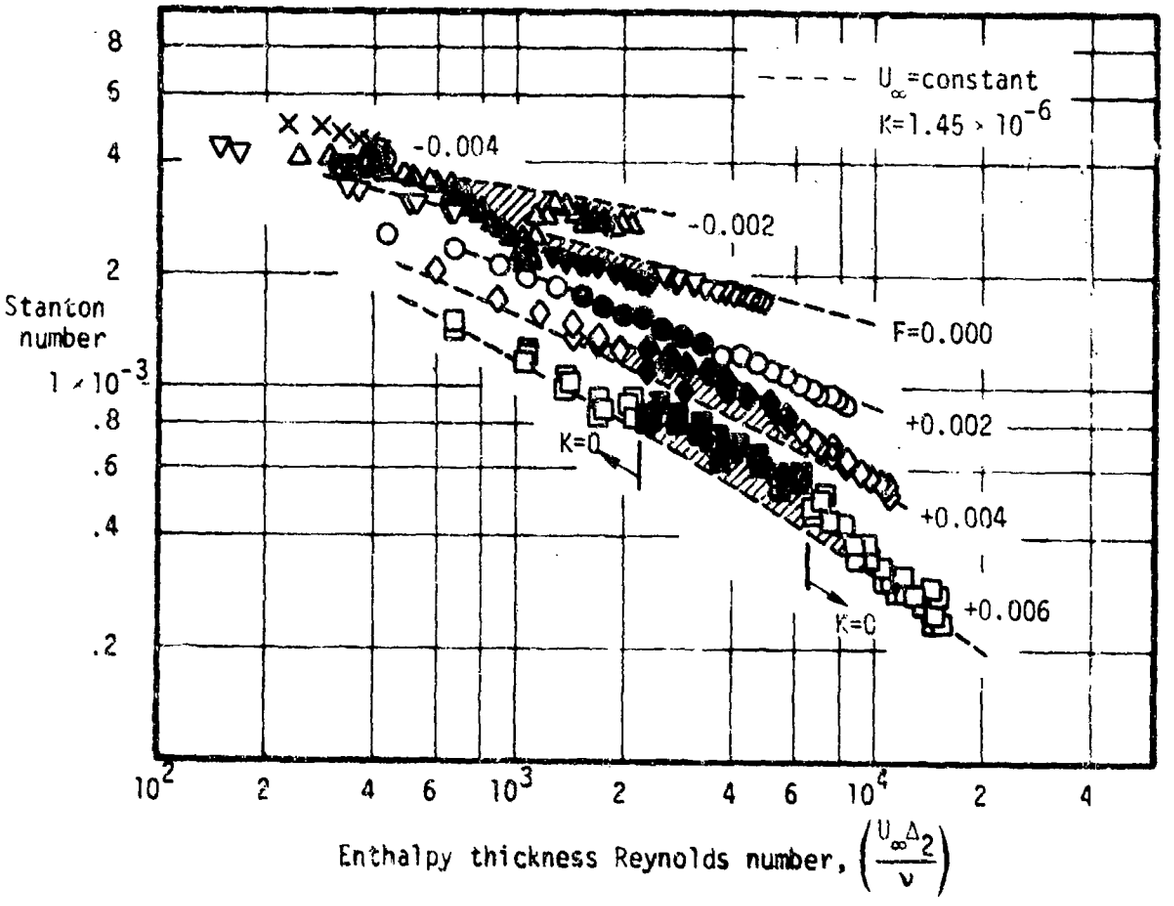

Fig. (17) The variation of Stanton number with enthalpy thickness Reynolds number at constant F for strong acceleration.

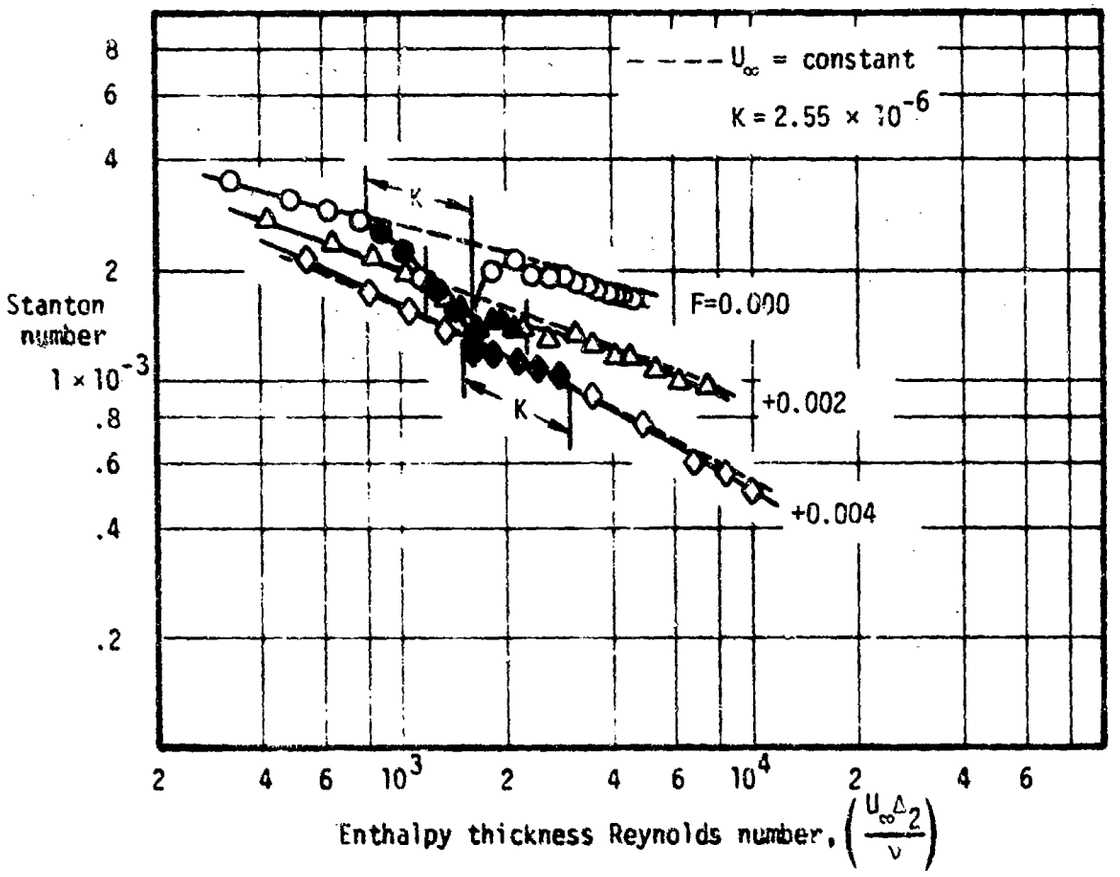

Fig. (18) The variation of Stanton number with enthalpy thickness Reynolds number at constant F for very strong acceleration.

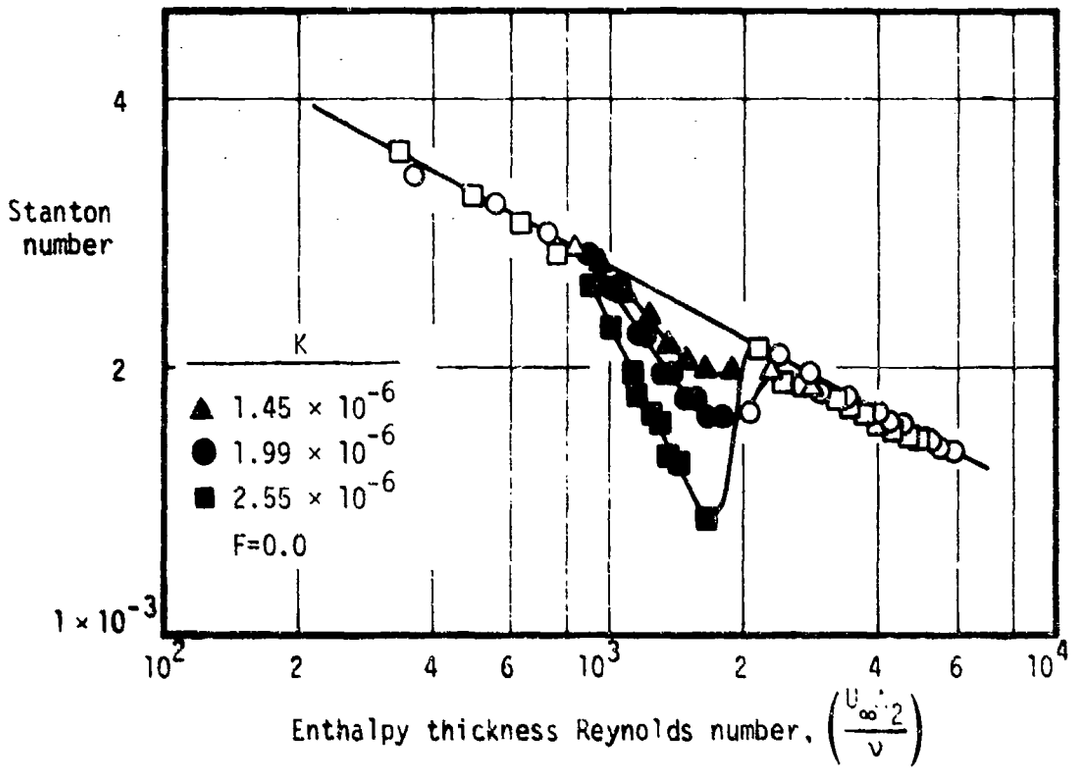

Fig. (19) The effects of acceleration on Stanton number with no transpiration.

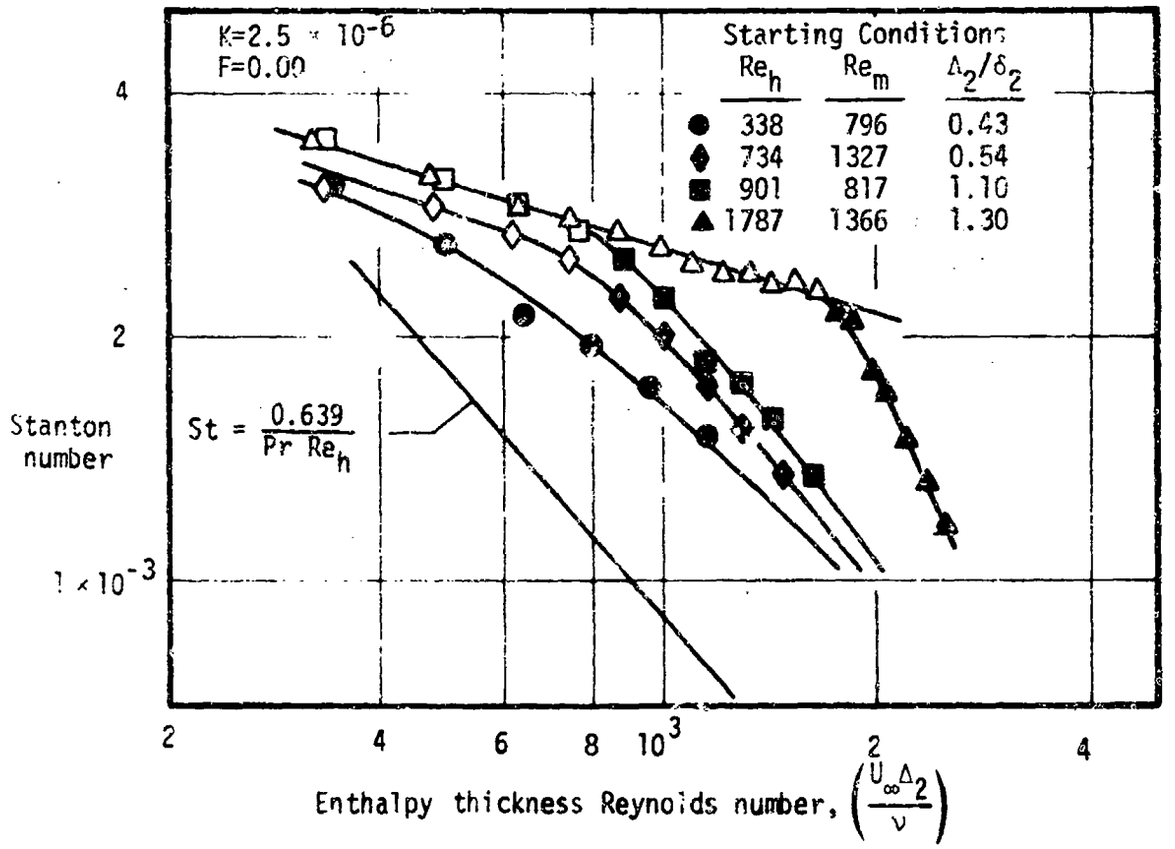

Fig. (20) The effects of initial boundary layer thickness on Stanton number during strong accelerations with no transpiration.

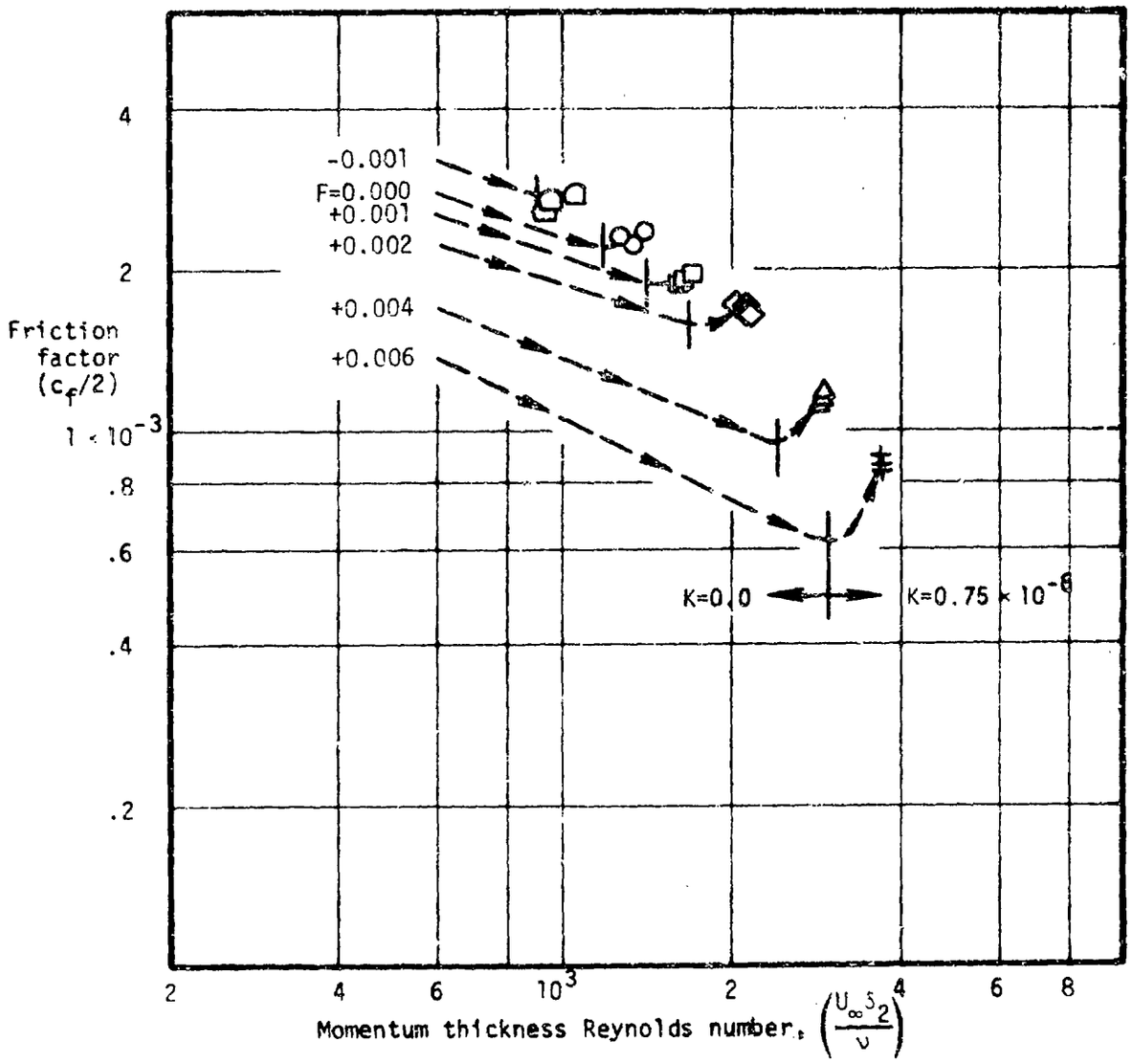

Fig. (21) The behavior of friction factor and momentum thickness Reynolds number after initiation of an asymptotic acceleration condition.

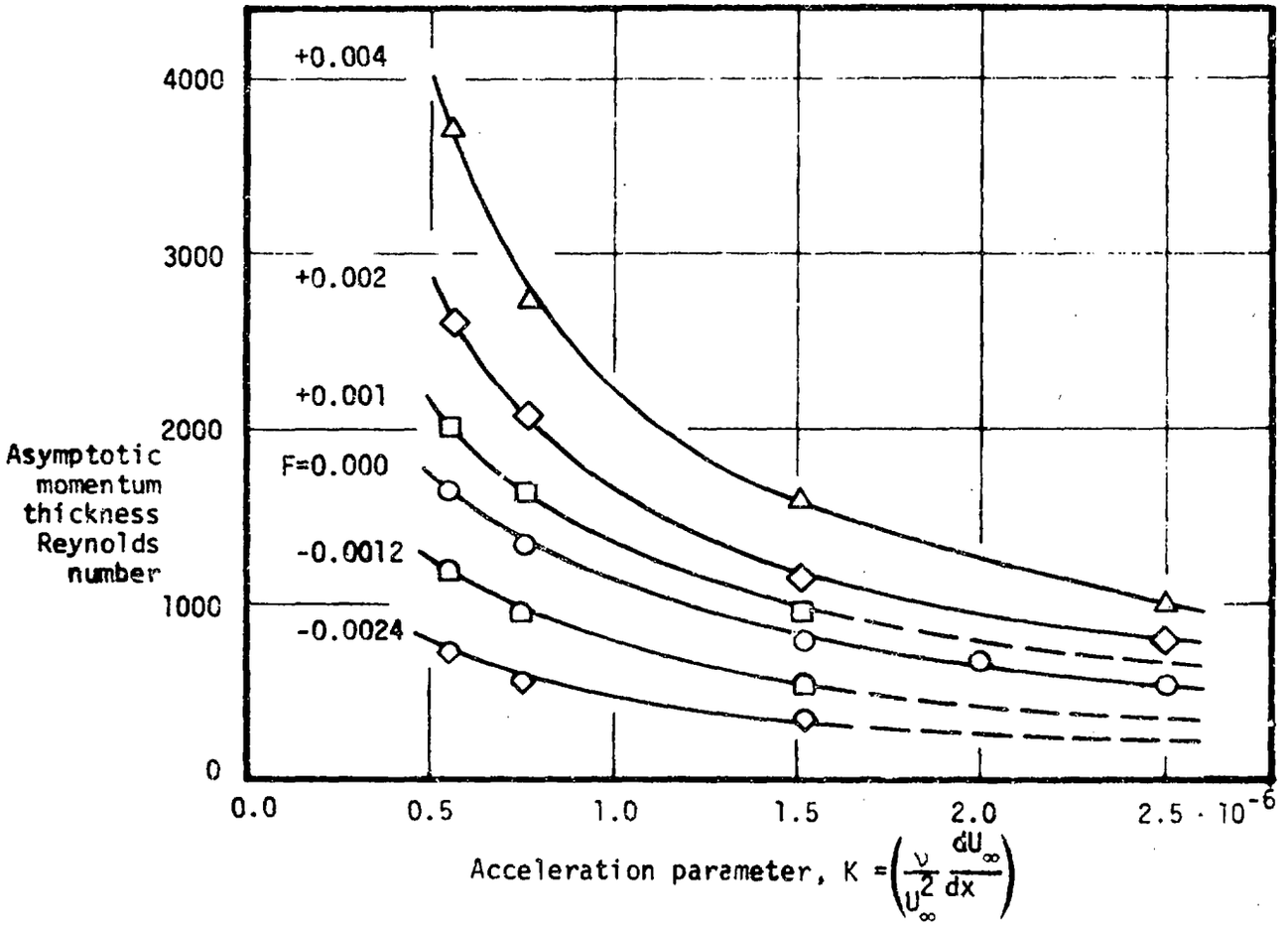

Fig. (22) The asymptotic values of momentum thickness Reynolds number for various values of K and F.

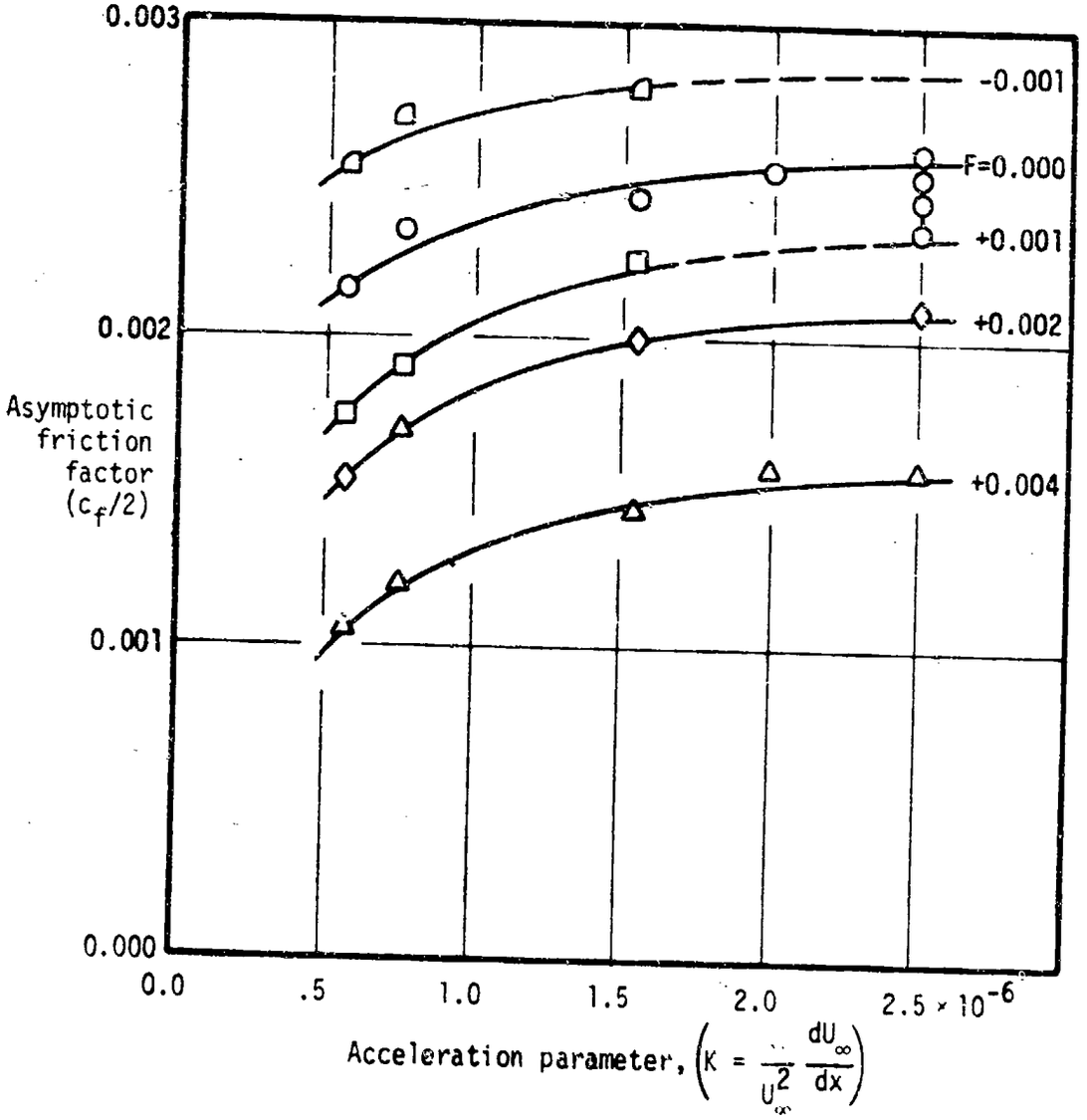

Fig. (23) The asymptotic values of friction factor, $c_f/2$, for various values of K and F.

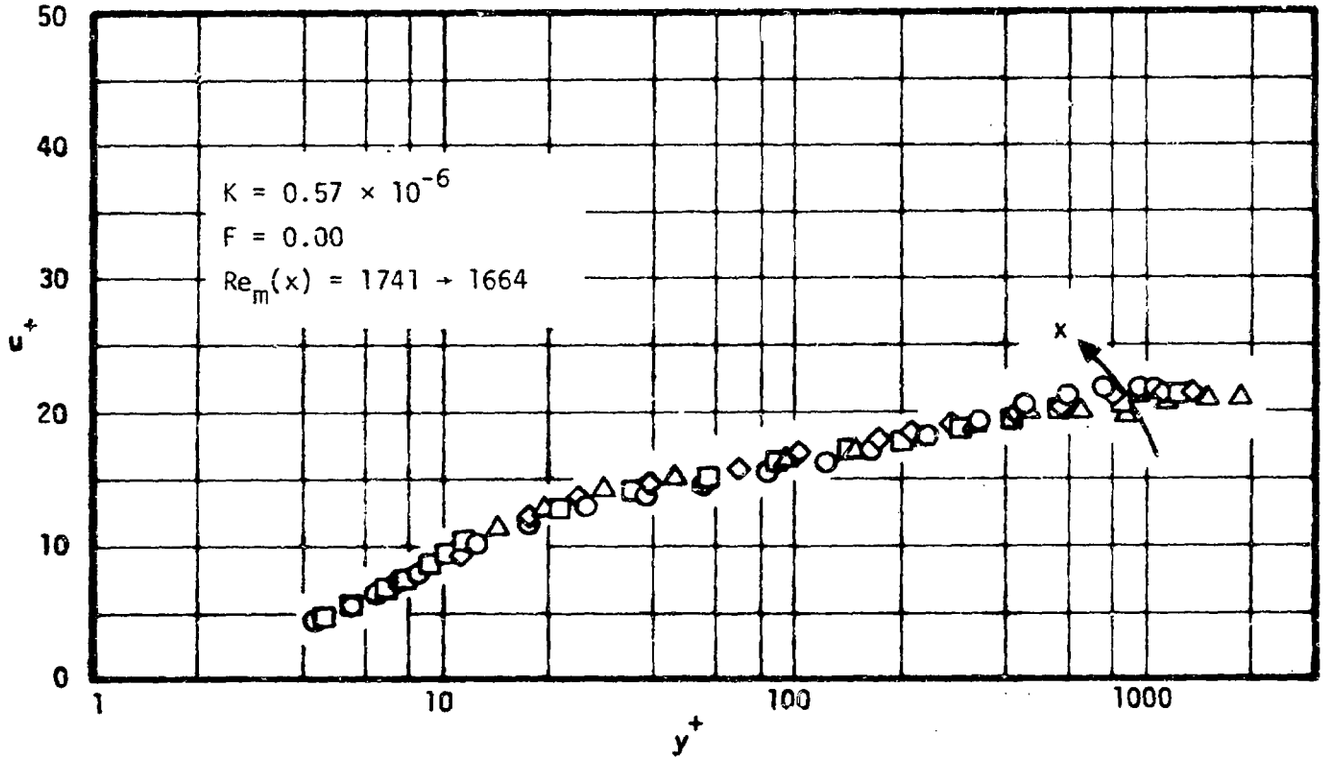

Fig. (24a) Sequential velocity profiles within an equilibrium acceleration at $K = 0.57 \times 10^{-6}$ with $F = 0.00$.

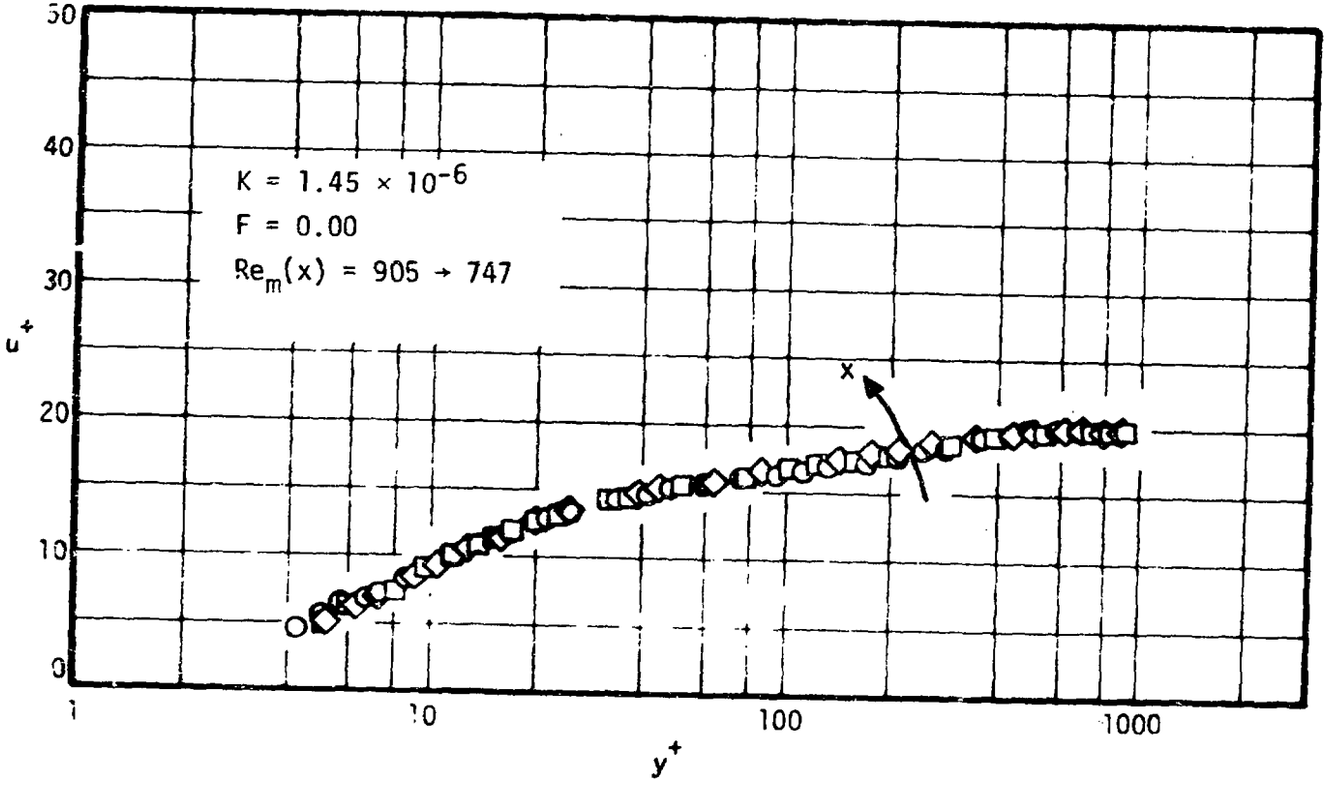

Fig. (24b) Sequential velocity profiles within an equilibrium acceleration at $K = 1.45 \times 10^{-6}$ with $F = 0.00$.

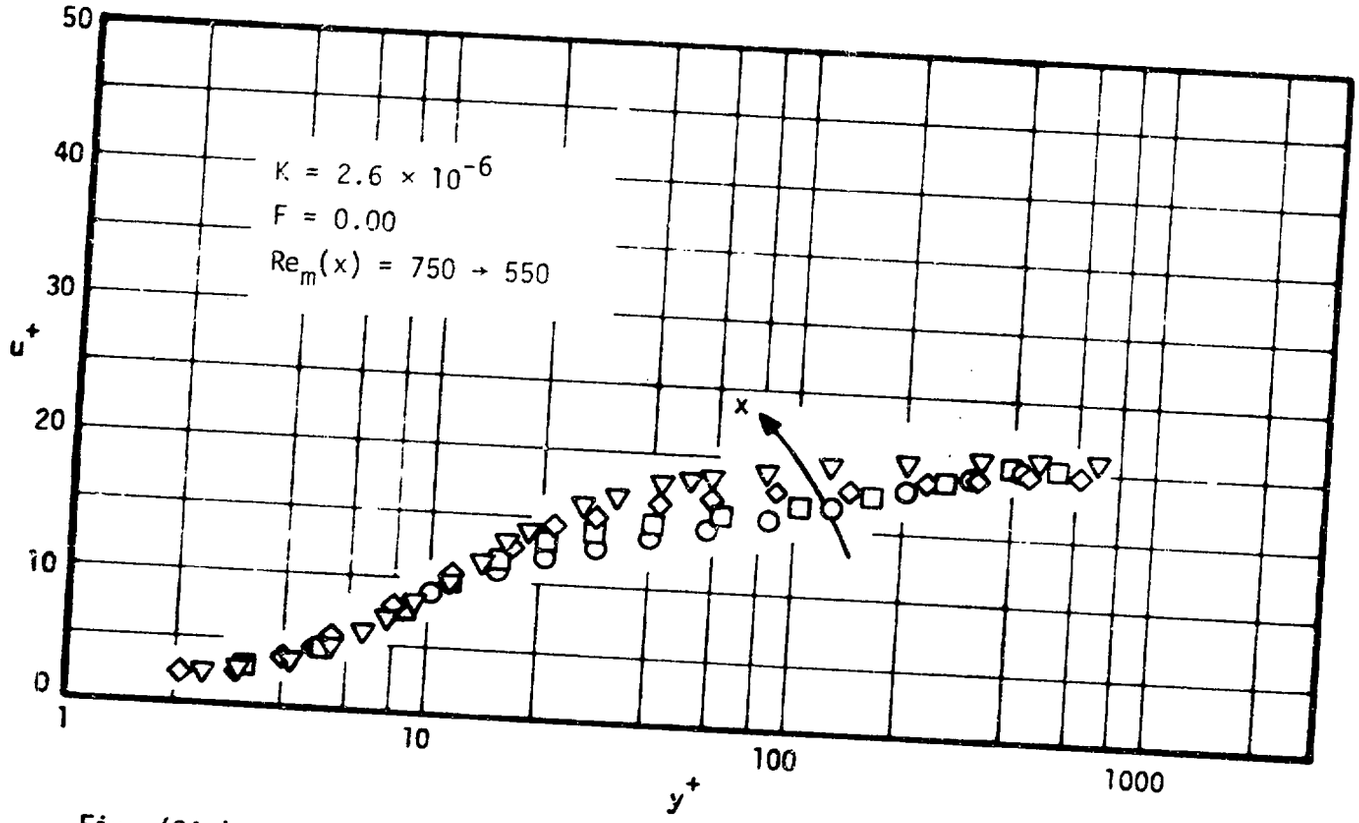

Fig. (24c) Sequential velocity profiles within a strong acceleration ($K = 2.6 \times 10^{-6}$) with significant changes in momentum thickness Reynolds number and a large reduction in Stanton number.

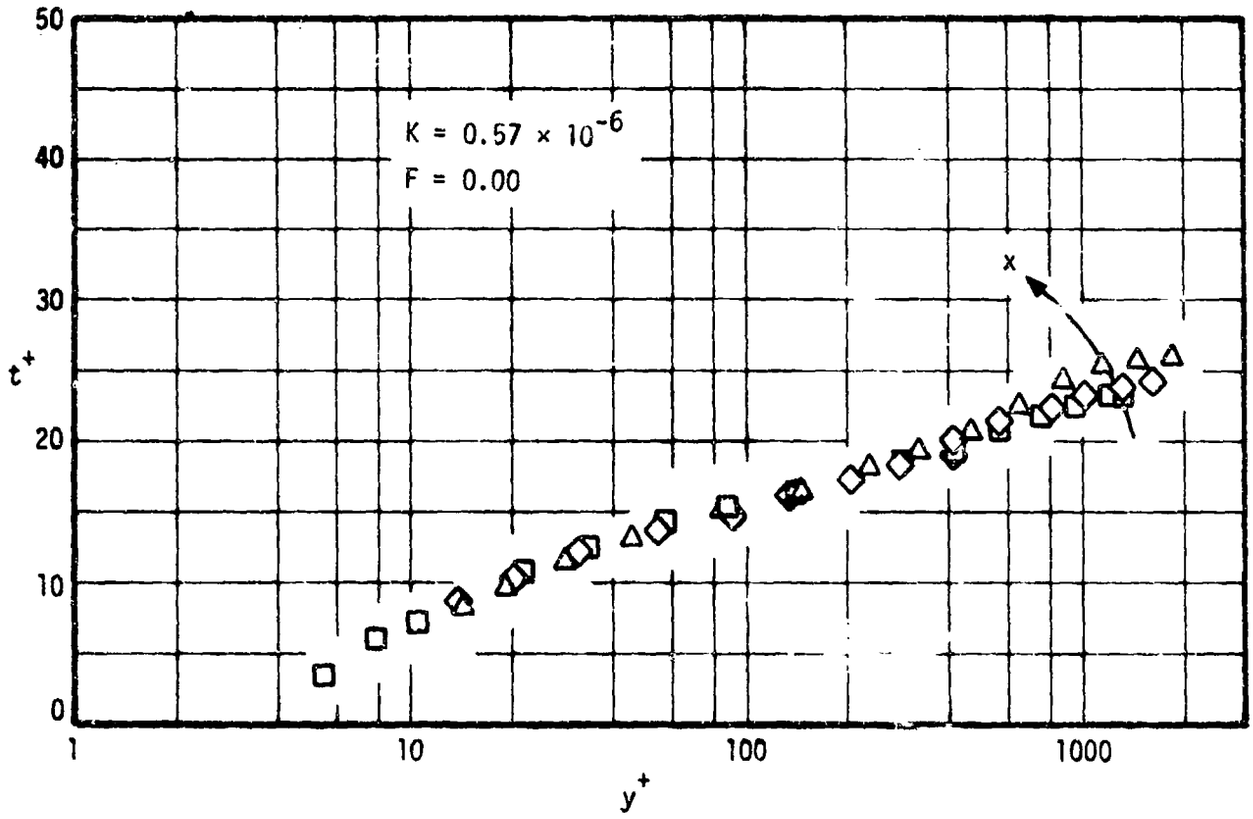

Fig. (25a) Sequential temperature profiles within an equilibrium acceleration at $K = 0.57 \times 10^{-6}$ with $F = 0.00$.

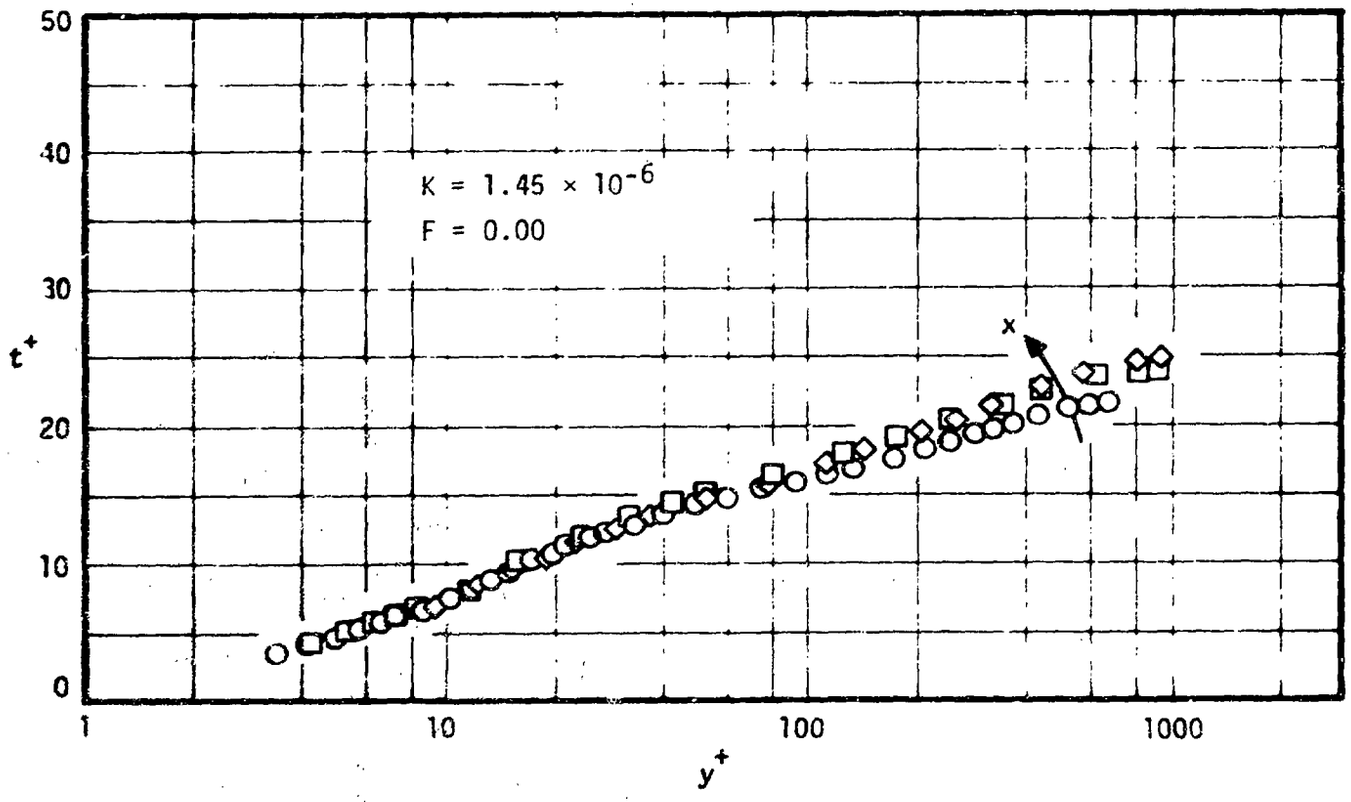

Fig. (25b) Sequential temperature profiles within an equilibrium acceleration at $K = 1.45 \times 10^{-6}$ with $F = 0.00$.

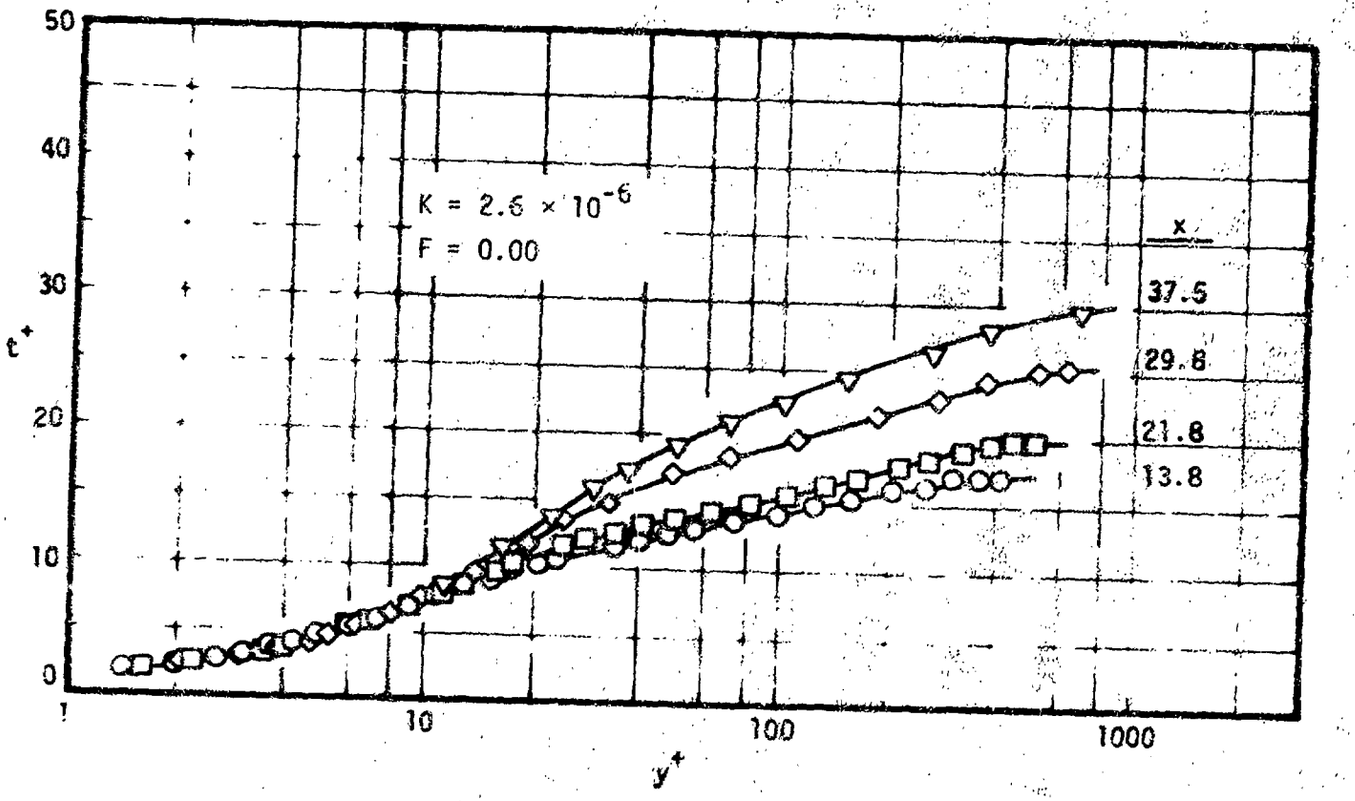

Fig. (25c) Sequential temperature profiles within a strong acceleration ($K = 2.6 \times 10^{-6}$) with significant changes in momentum thickness Reynolds number and a large reduction in Stanton number.

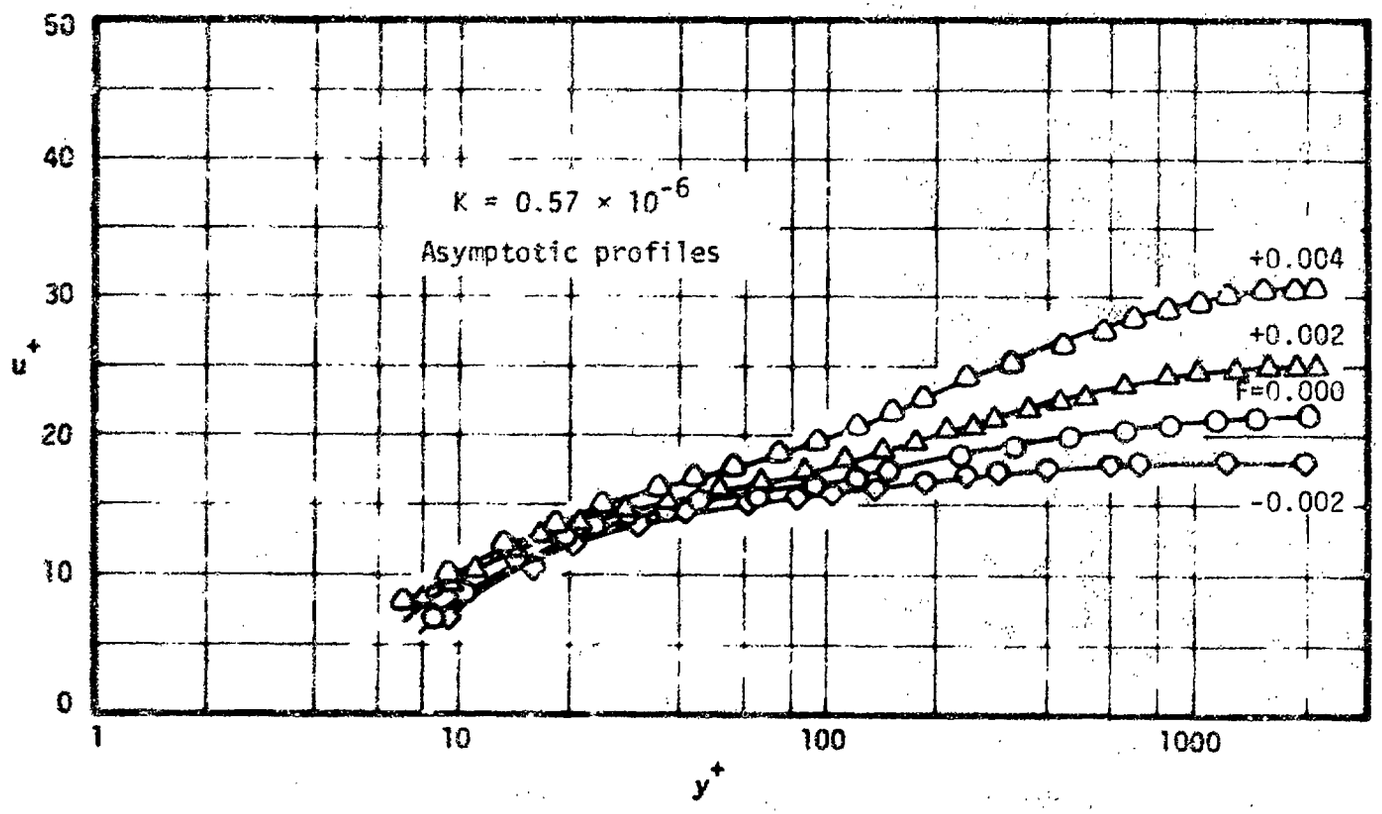

Fig. (26a) Asymptotic velocity profiles for mild acceleration with transpiration.

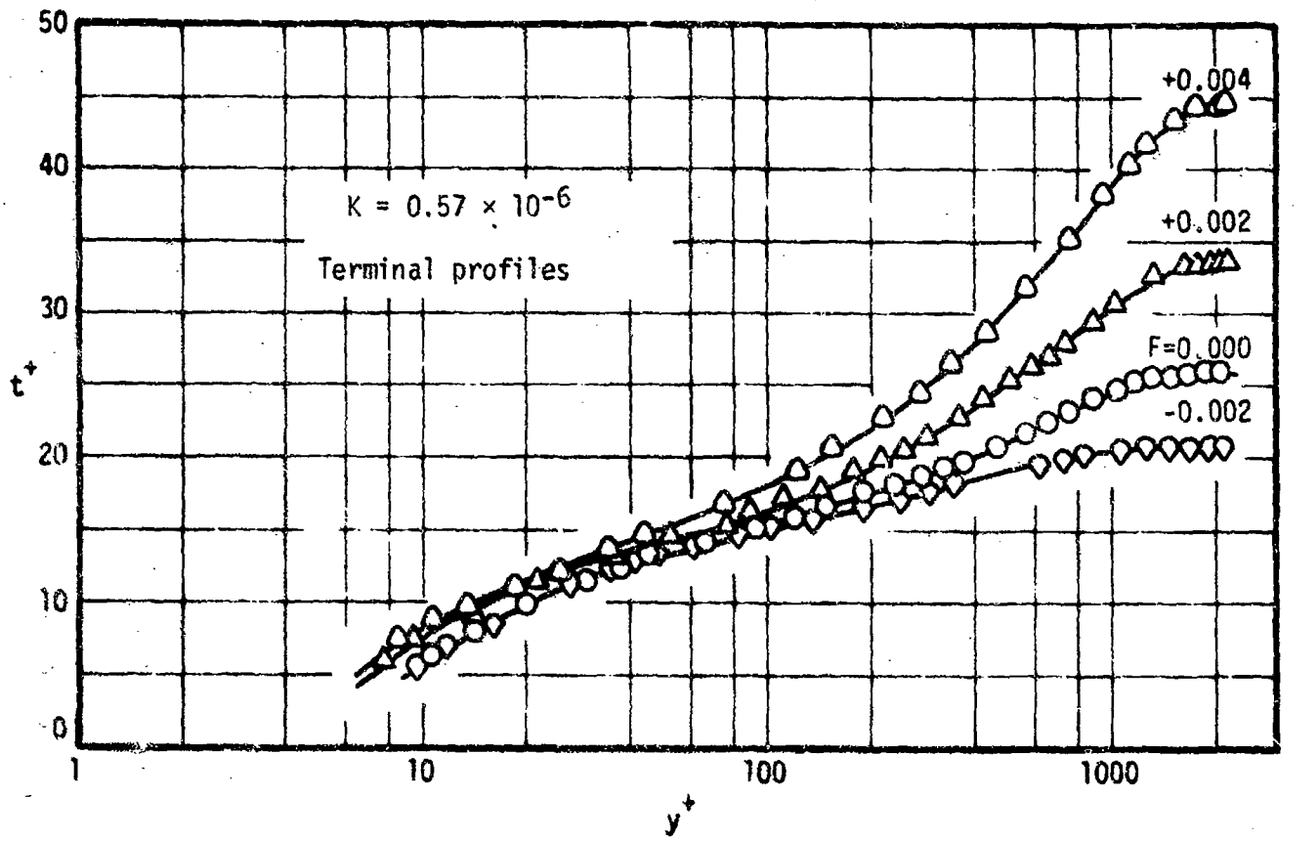

Fig. (26b) Terminal temperature profiles observed for mild acceleration with transpiration.

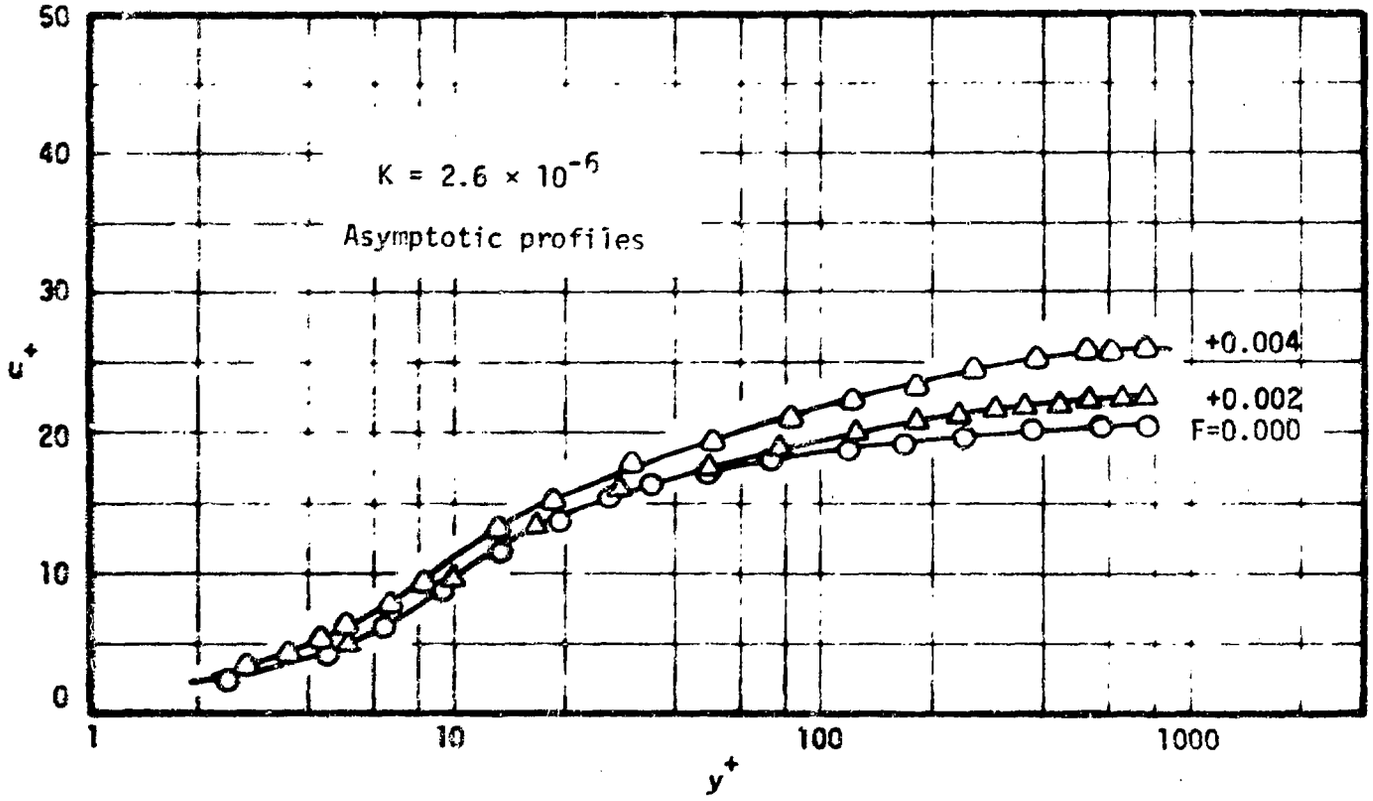

Fig. (27a) Asymptotic velocity profiles for strong acceleration with transpiration.

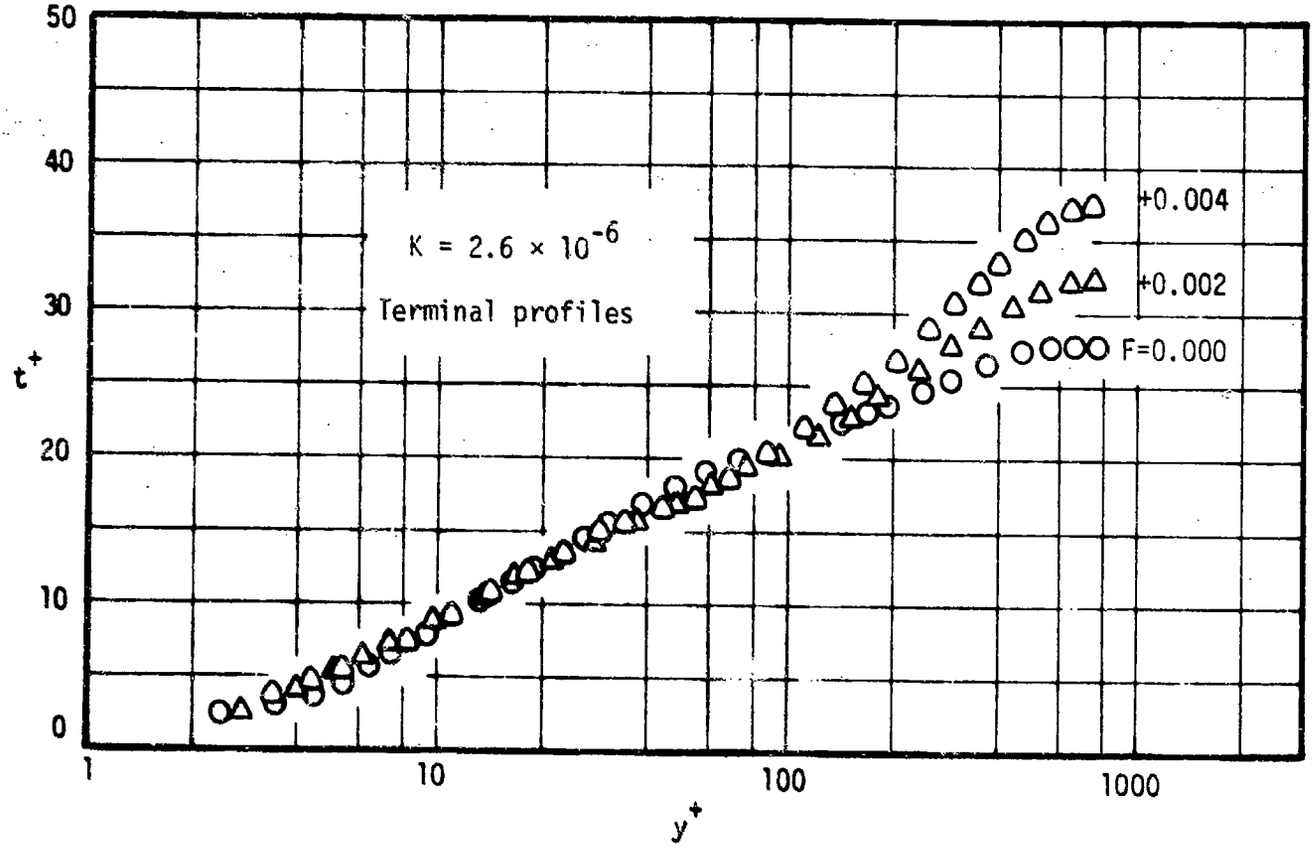

Fig. (27b) Terminal temperature profiles observed for strong acceleration with transpiration.

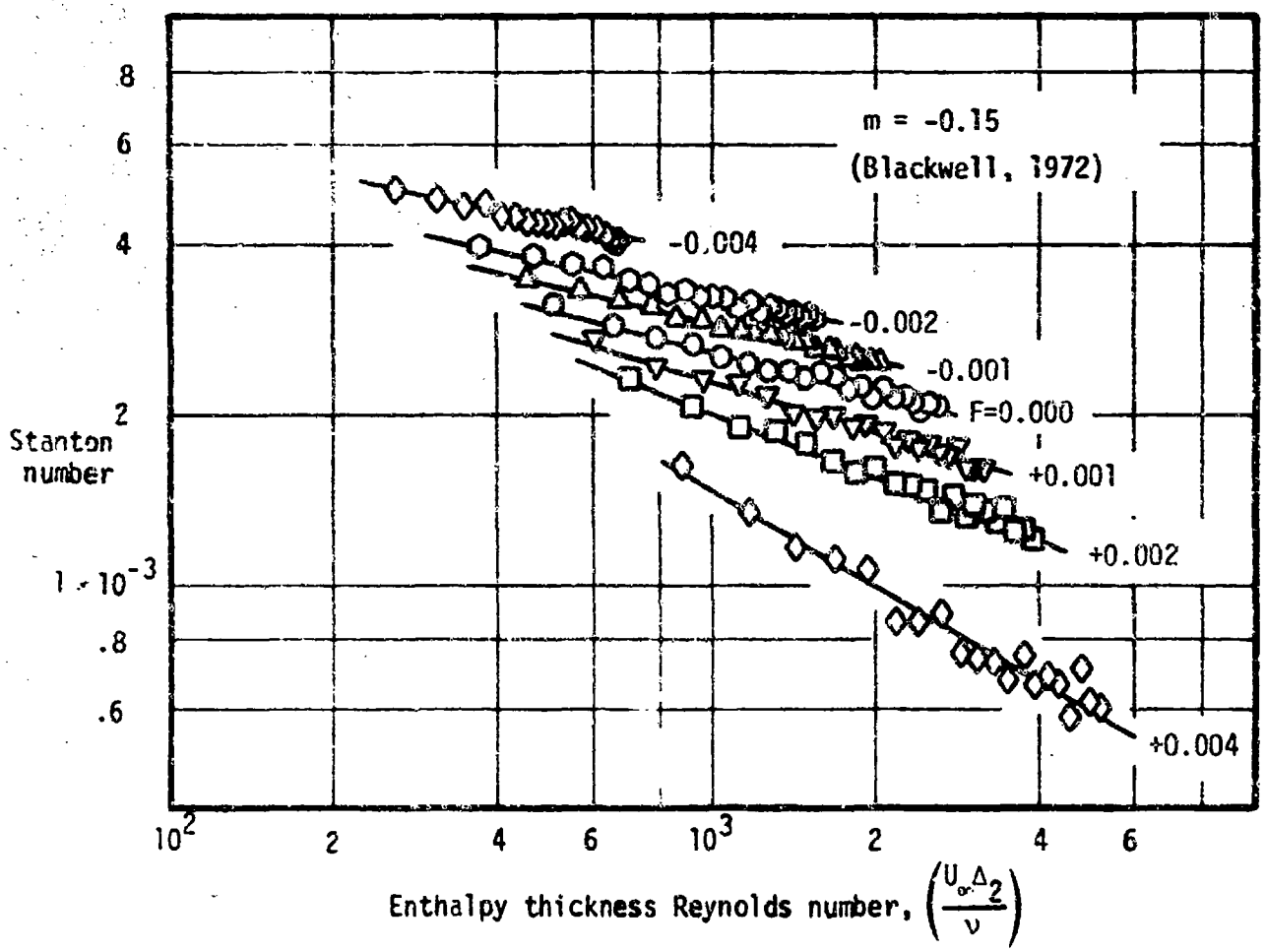

Fig. (28) The variation of Stanton number with enthalpy thickness Reynolds number for mild deceleration, with transpiration.

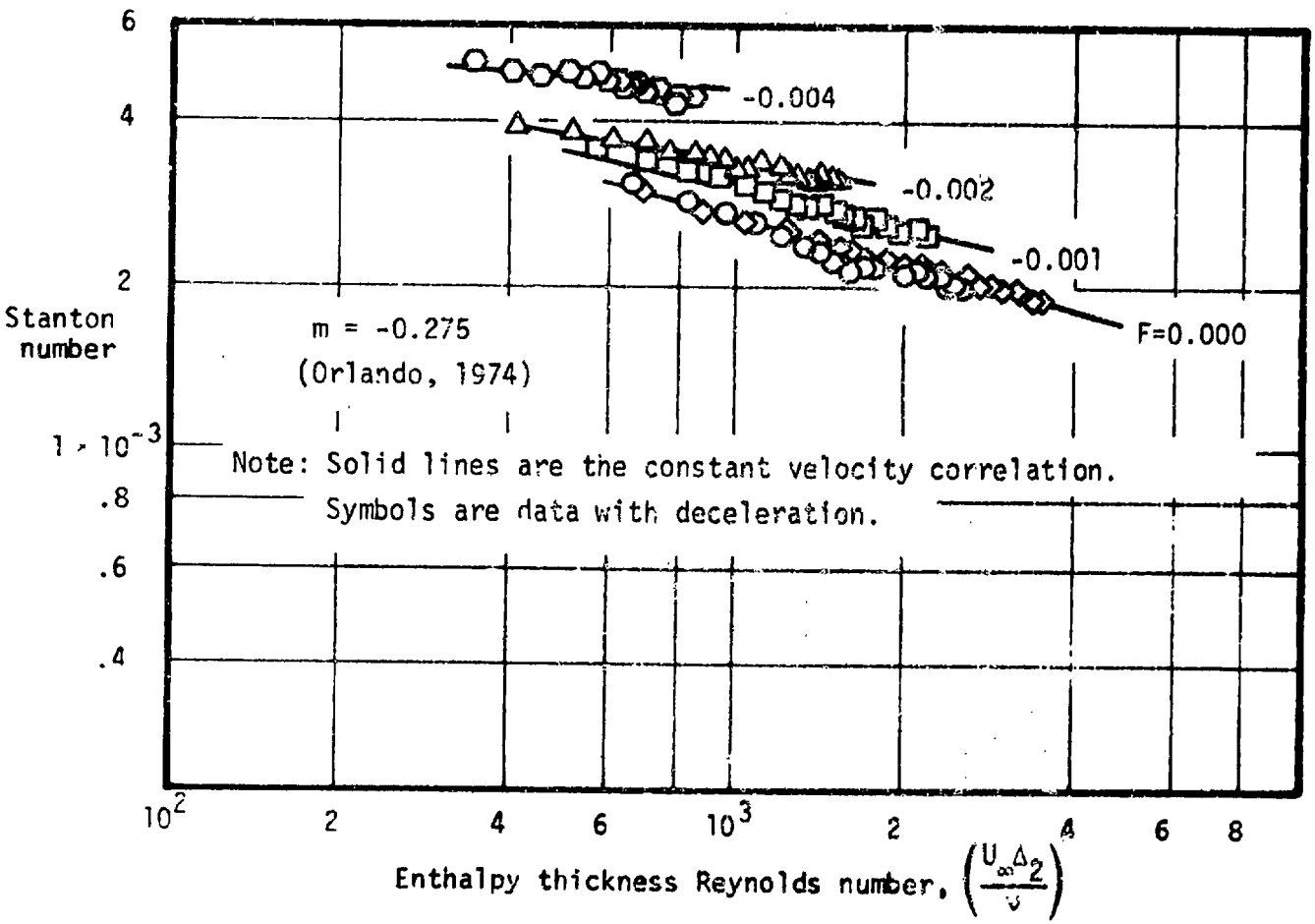

Fig. (29) The variation of Stanton number with enthalpy thickness Reynolds number for strong deceleration with transpiration.

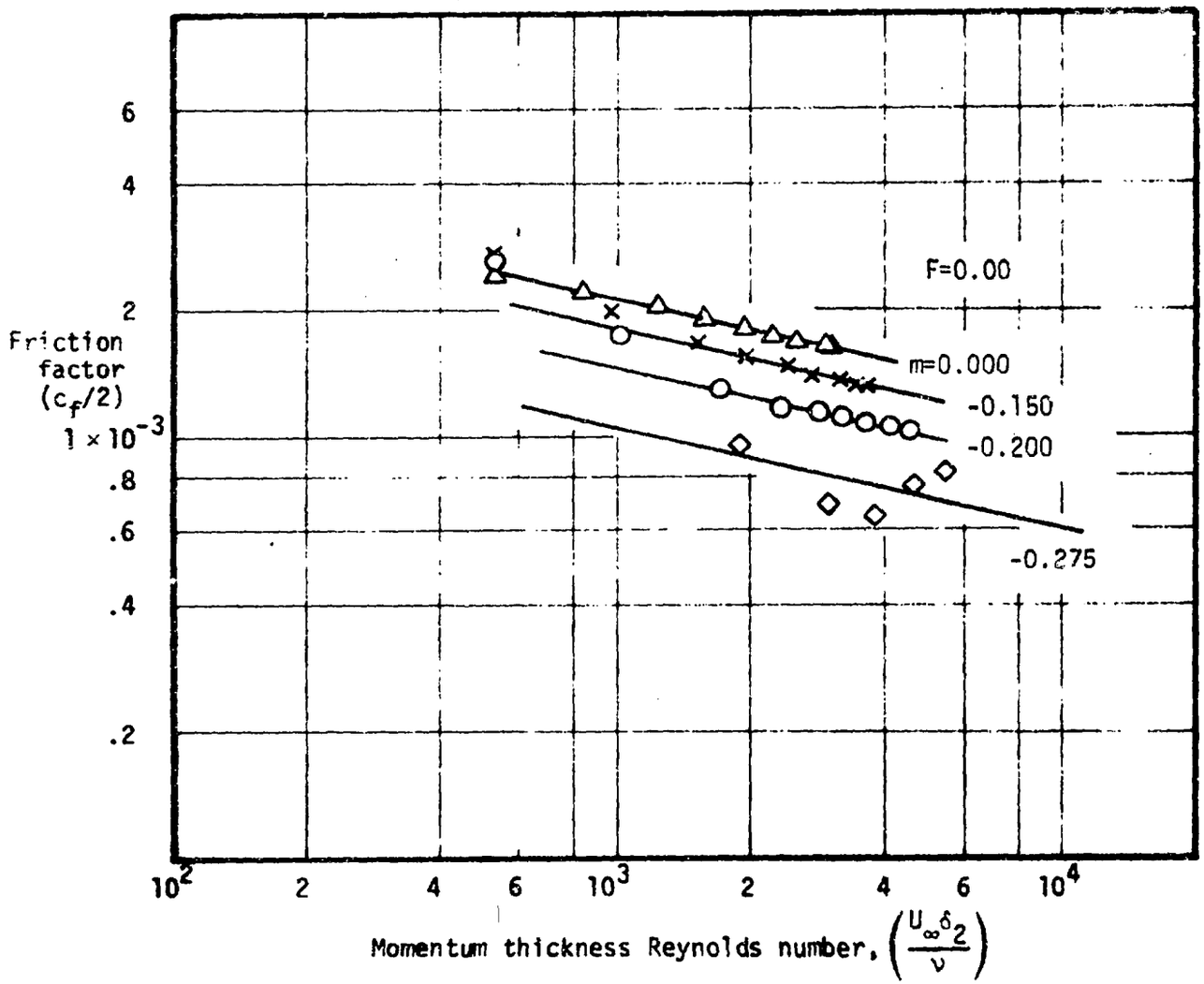

Fig. (30) The variations of friction factor, $c_f/2$, with momentum thickness Reynolds number for three decelerating flows.

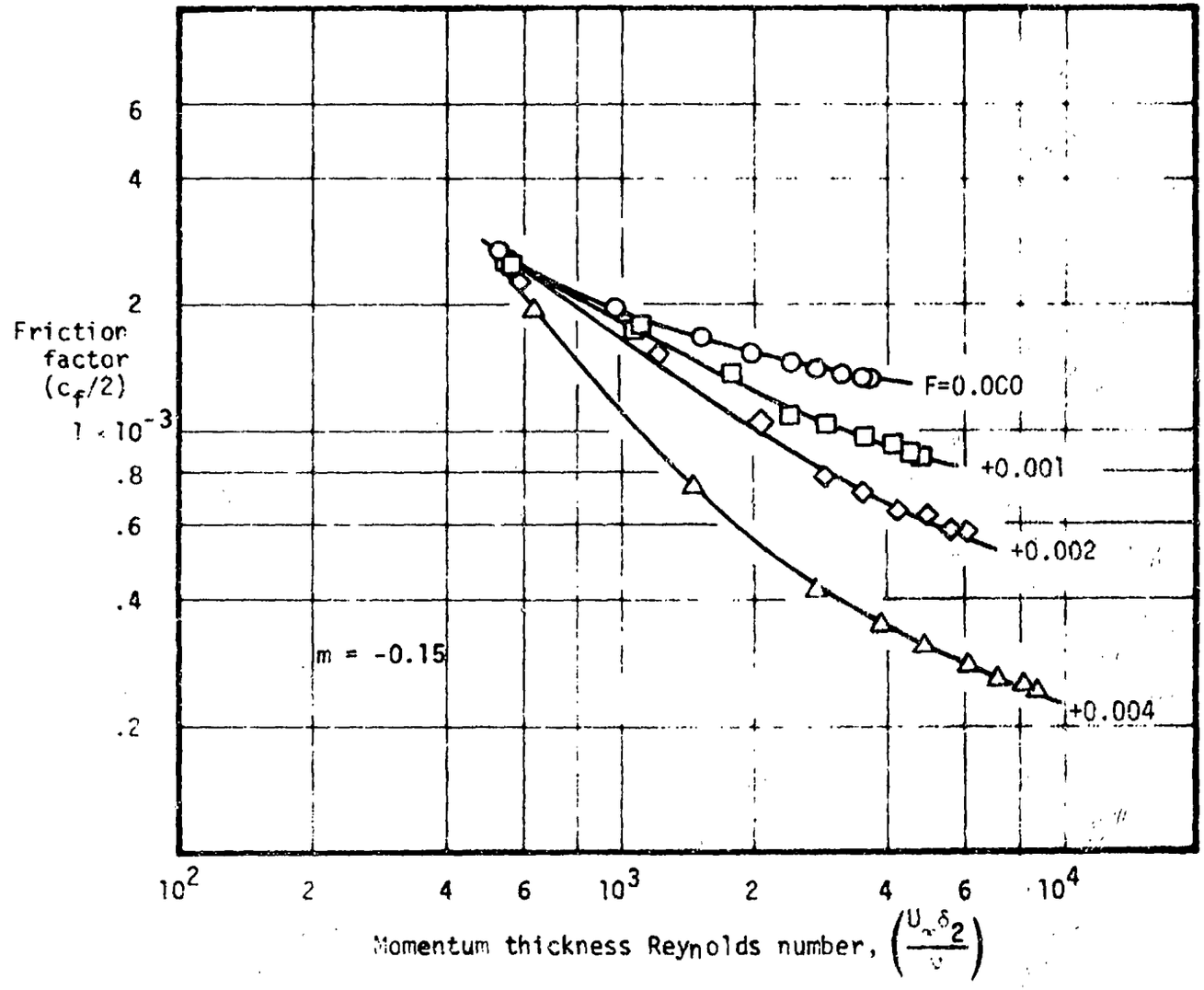

Fig. (31) The variation of friction factor with momentum thickness Reynolds number for mild deceleration with transpiration.

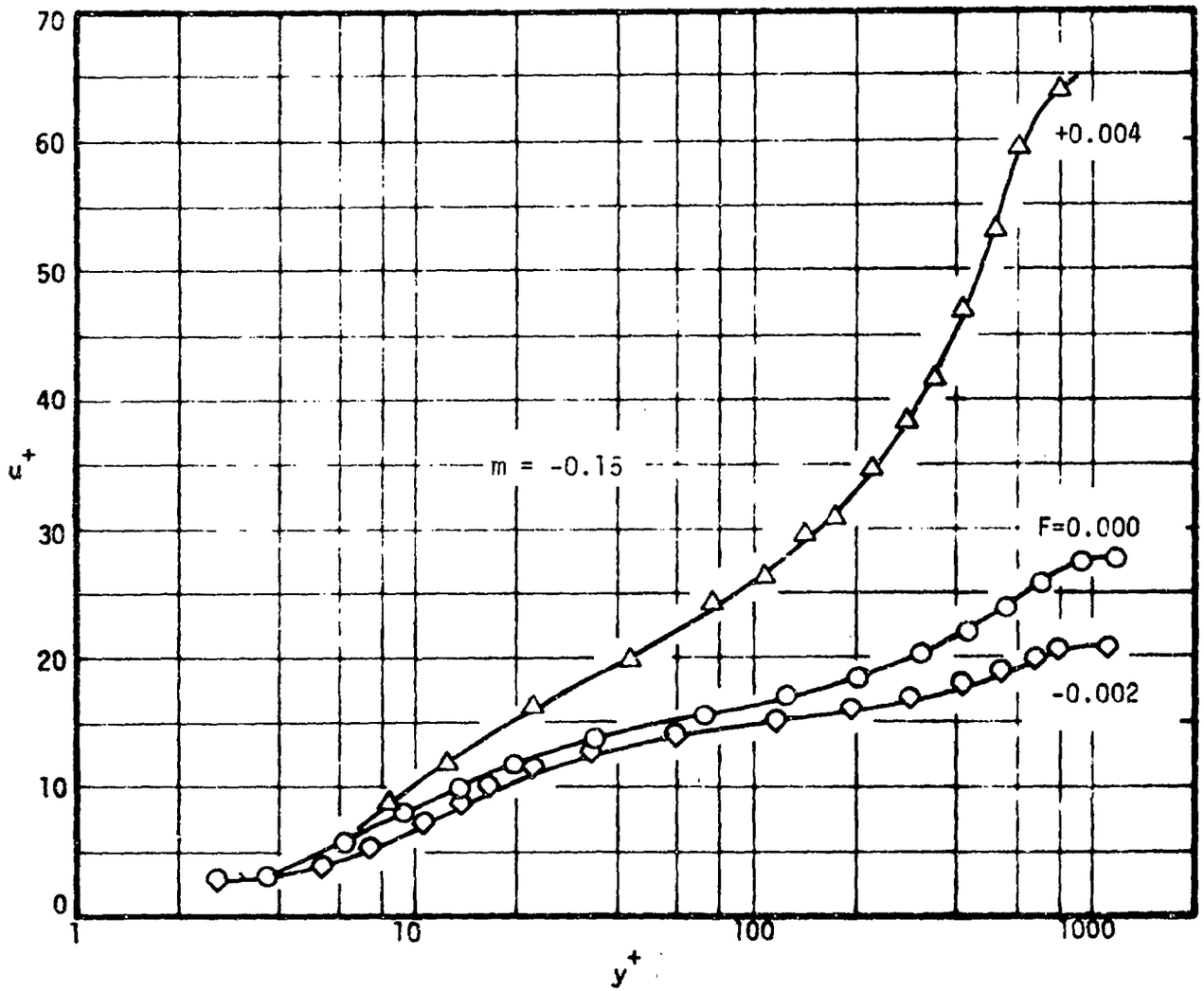

Fig. (32) Velocity profiles for mild deceleration with transpiration.

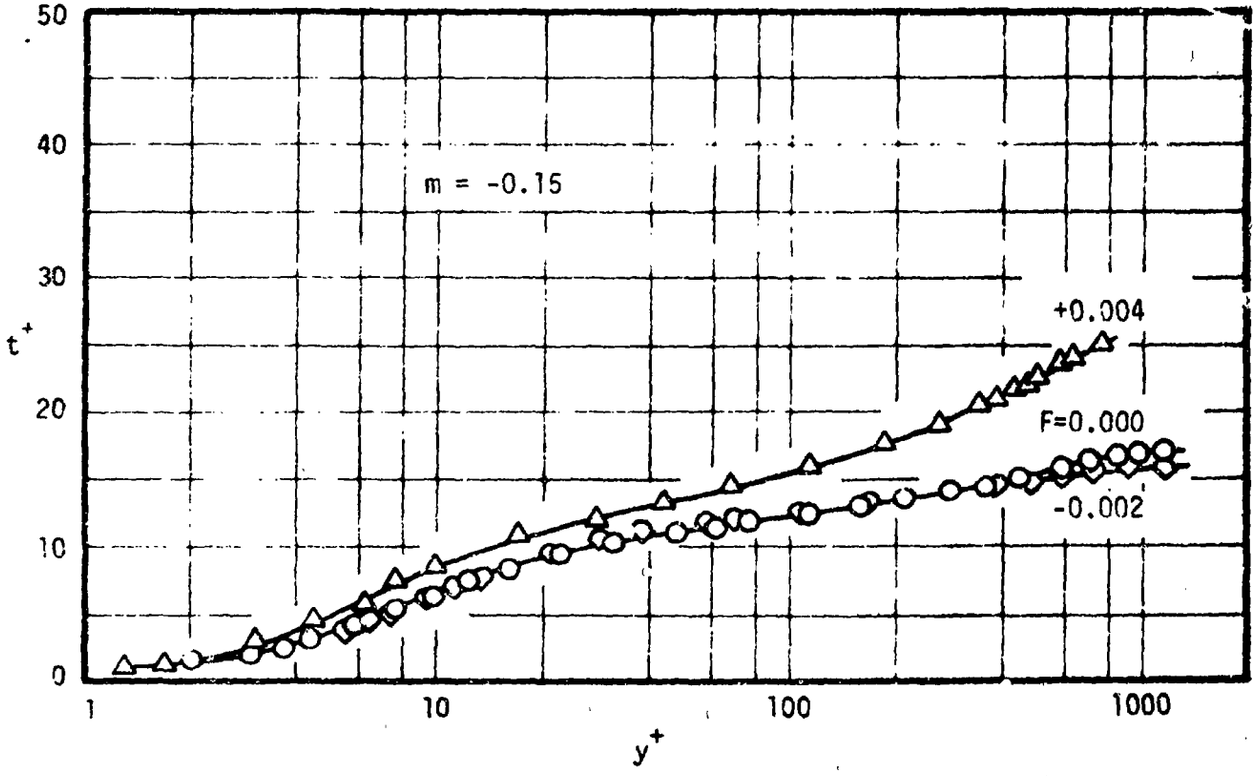

Fig. (33) Temperature profiles for mild deceleration with transpiration.

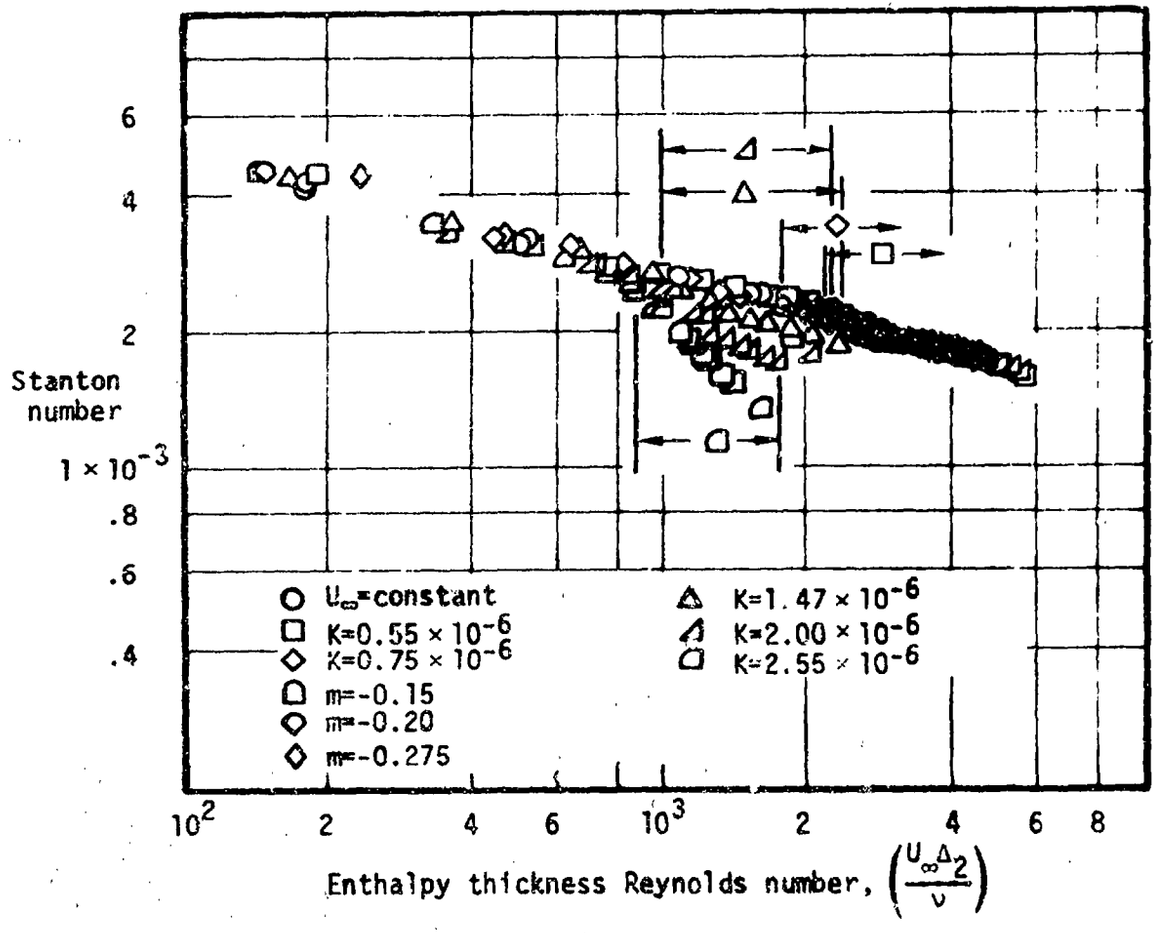

Fig. (34) A summary of Stanton number behavior for all flows tested.

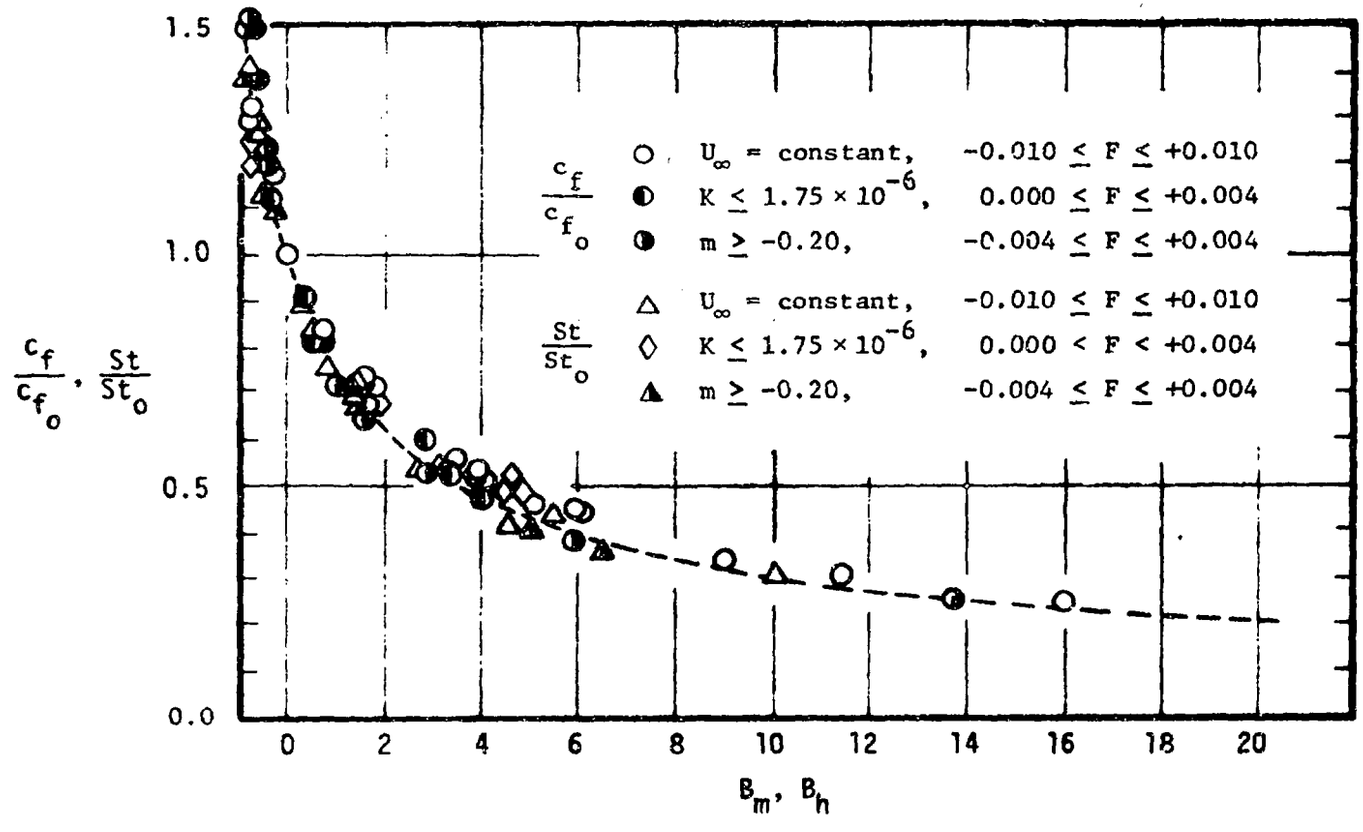

Fig. (35) A summary of the effects of transpiration on Stanton number and friction factor for all flows tested.

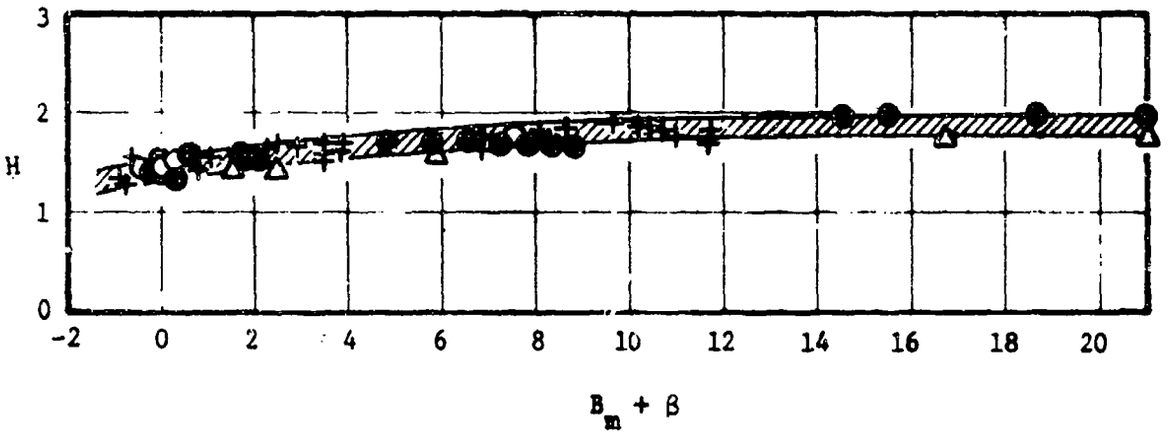

Fig. (36) The variation of shape factor, H , with $B_m + \beta$ for all flows tested.

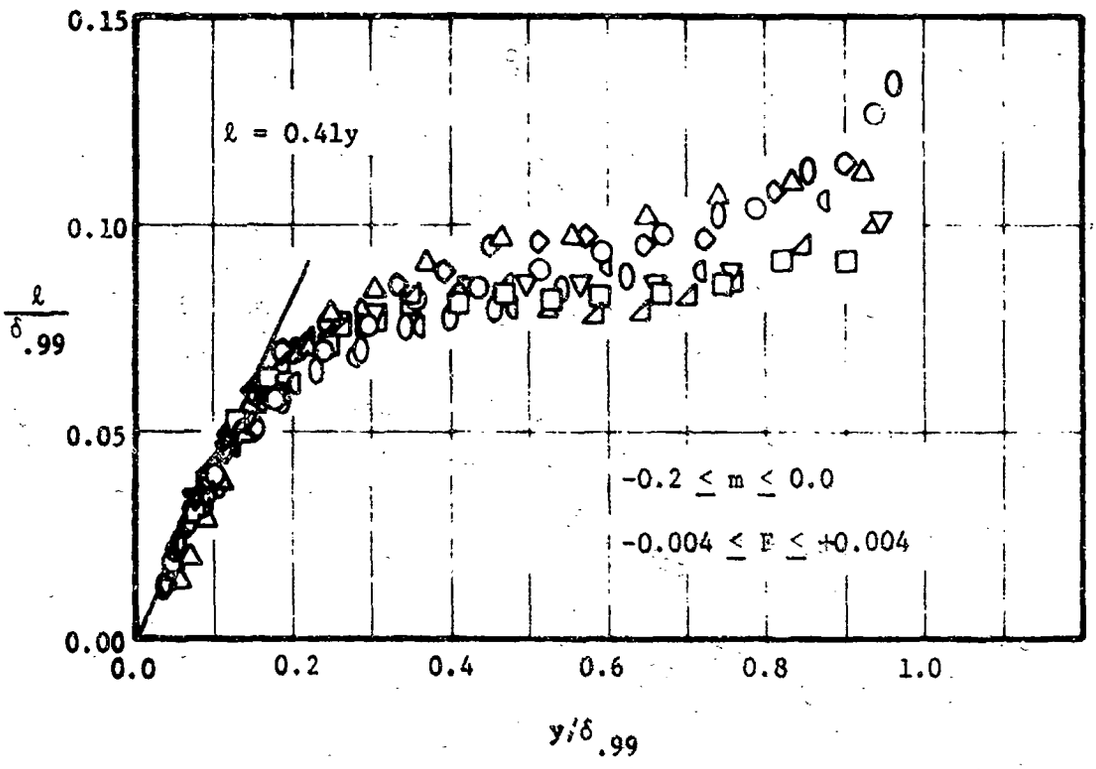

Fig. (37) The behavior of the mixing length for flat plate and decelerating flows with transpiration.

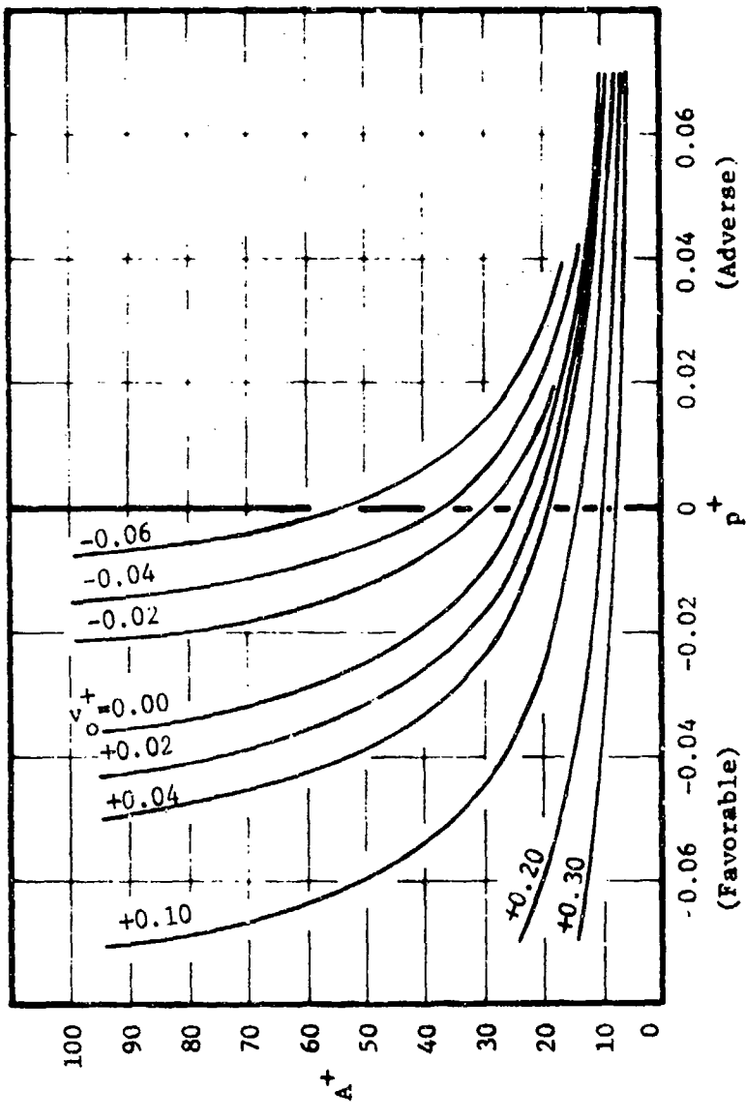

Fig. (38) The variation of the damping constant, A^+, as a function of v_o^+ and p^+.

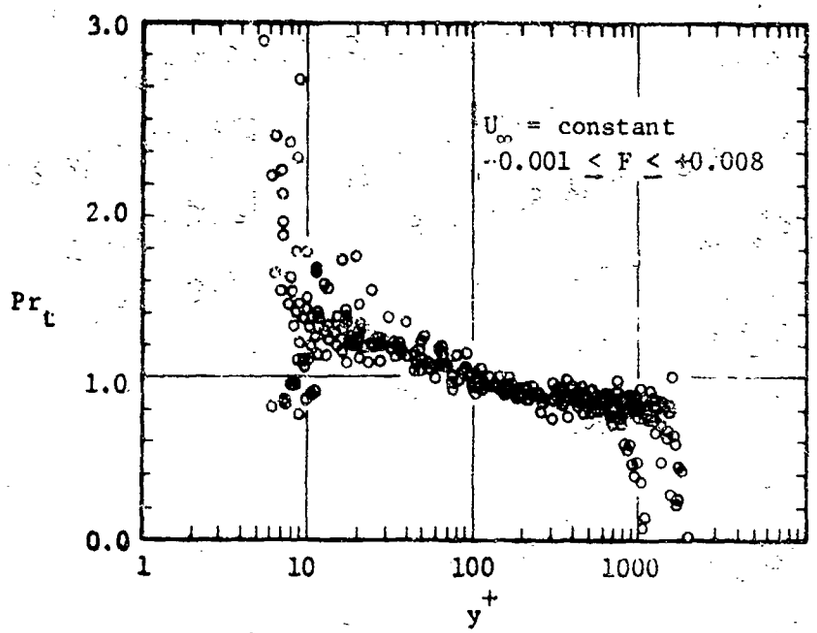

Fig. (39) The variation of turbulent Prandtl number within the boundary layer for flat plate flows with transpiration.

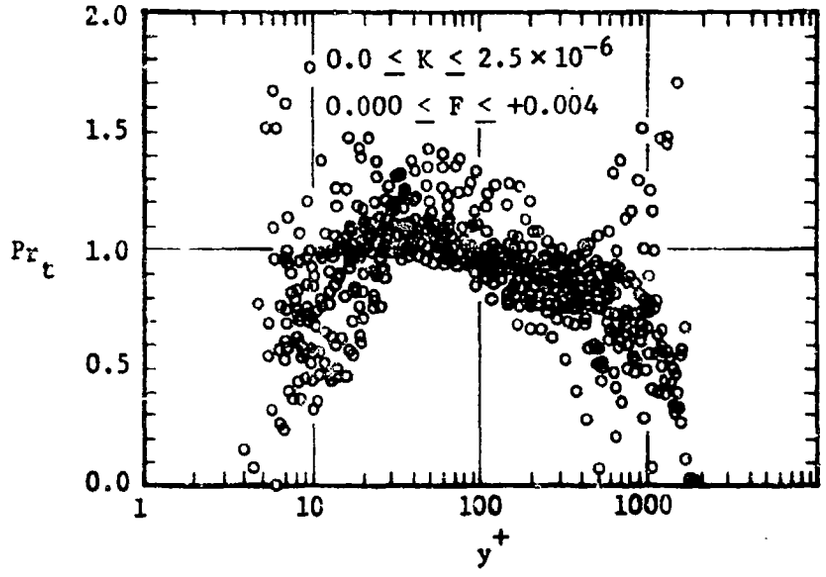

Fig. (40) The variation of turbulent Prandtl number within the boundary layer for accelerating flows with transpiration.

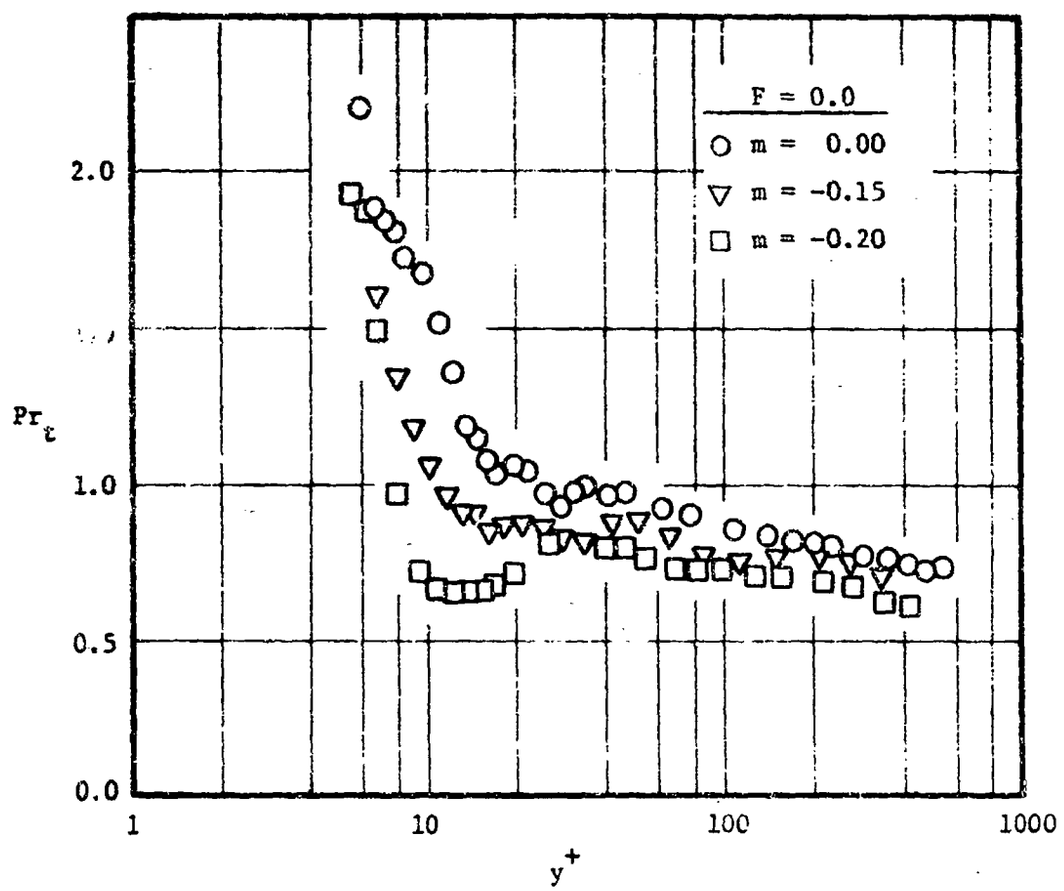

Fig. (41) The variation of turbulent Prandtl number within the boundary layer for decelerating flows without transpiration.

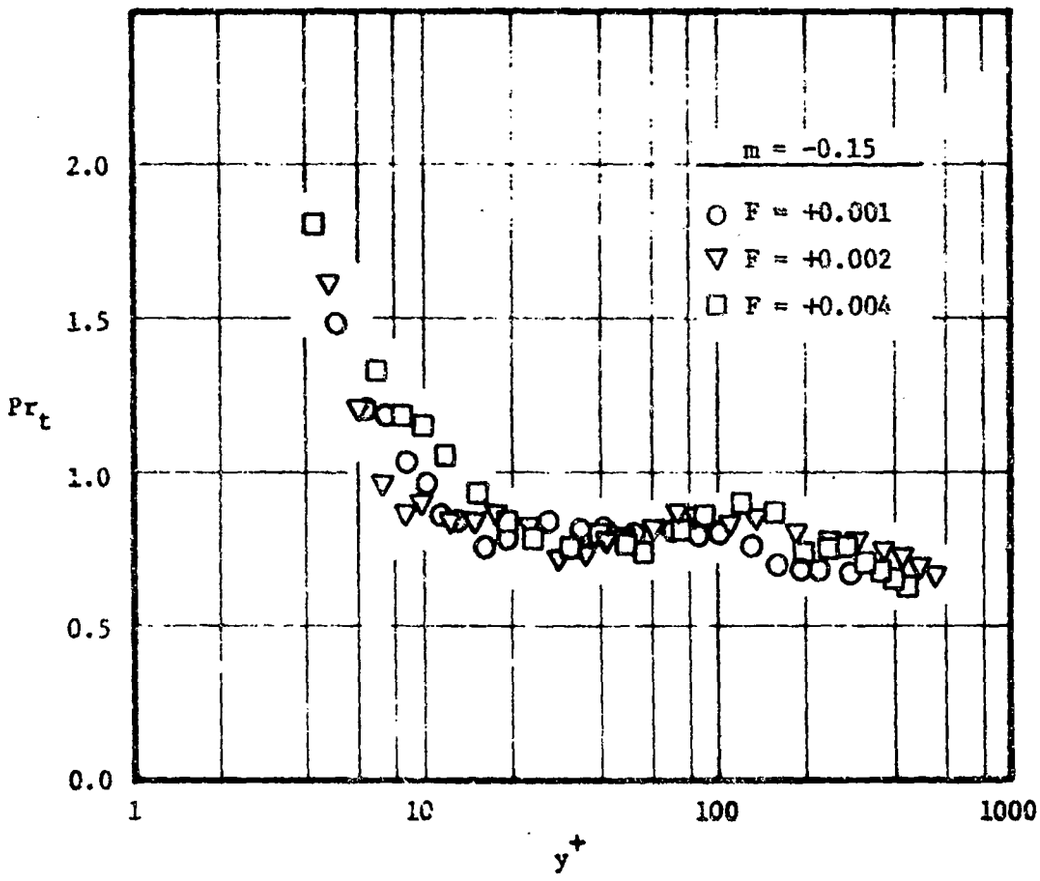

Fig. (42) The variation of turbulent Prandtl number within the boundary layer in a mild deceleration, with transpiration.

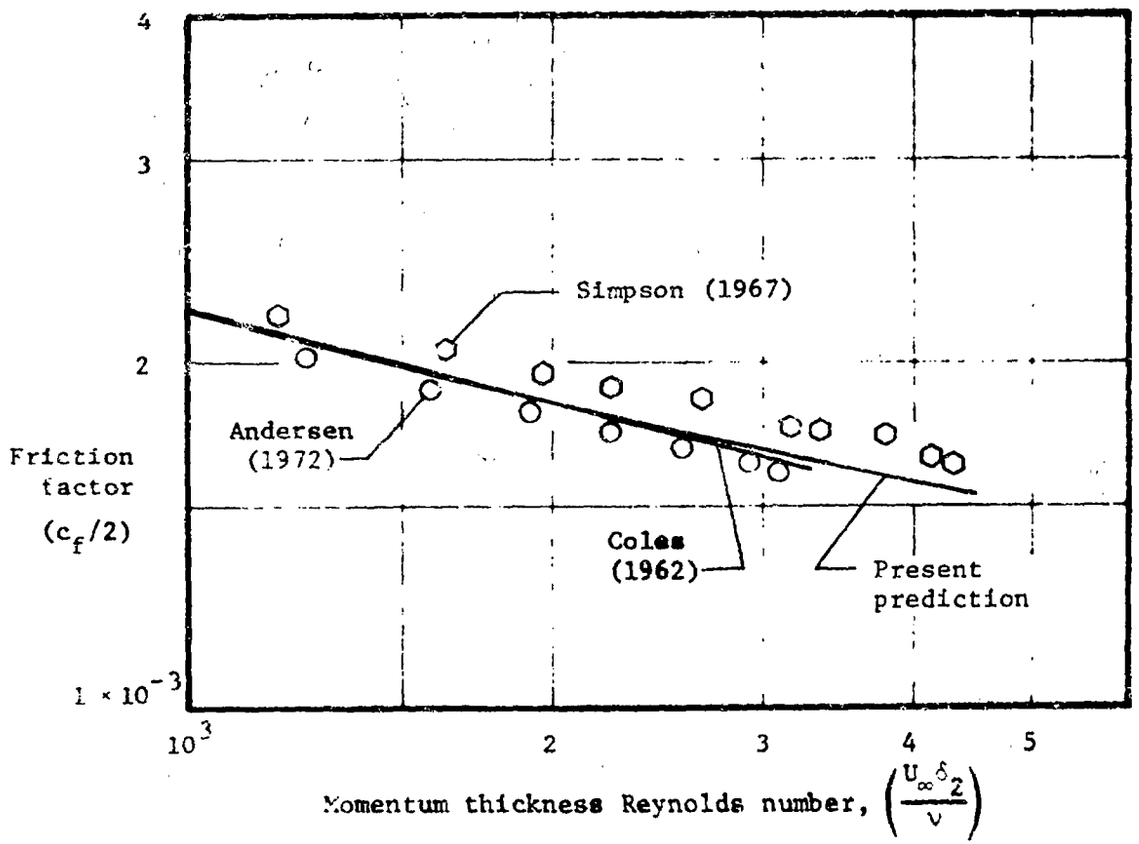

Fig. (43) A comparison of measured and predicted values of friction factor for a flat plate flow without transpiration.

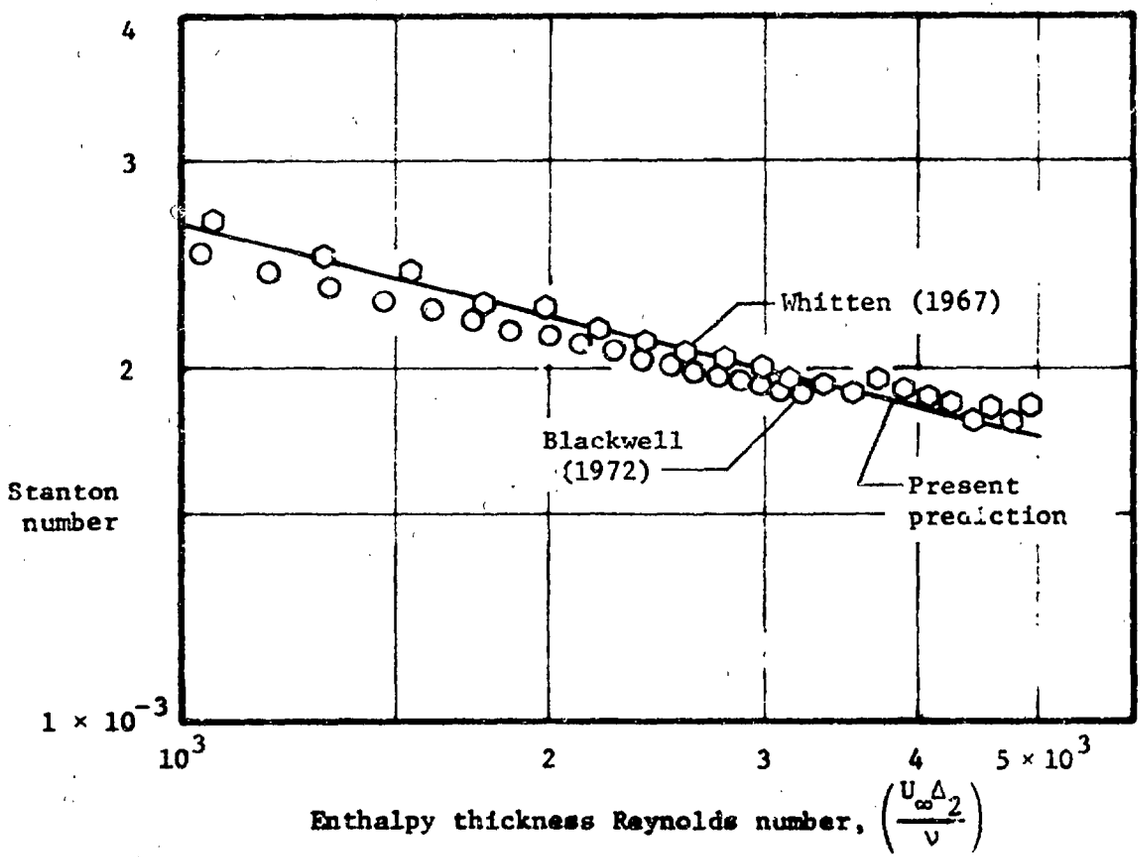

Fig. (44) A comparison of measured and predicted values of Stanton number for a flat plate flow without transpiration.

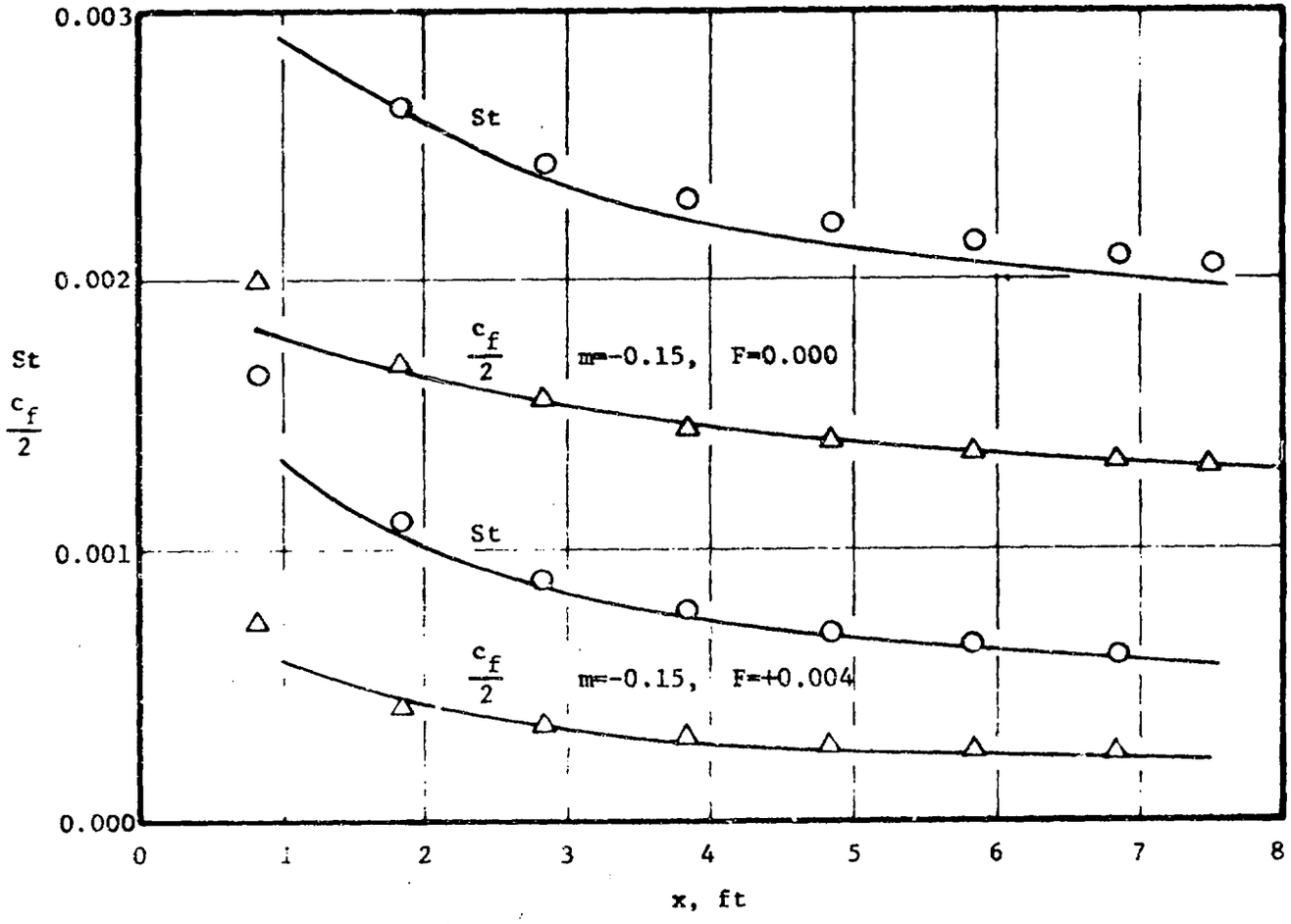

Fig. (45) A comparison of measured and predicted values of Stanton number and friction factor in a mild deceleration with transpiration.

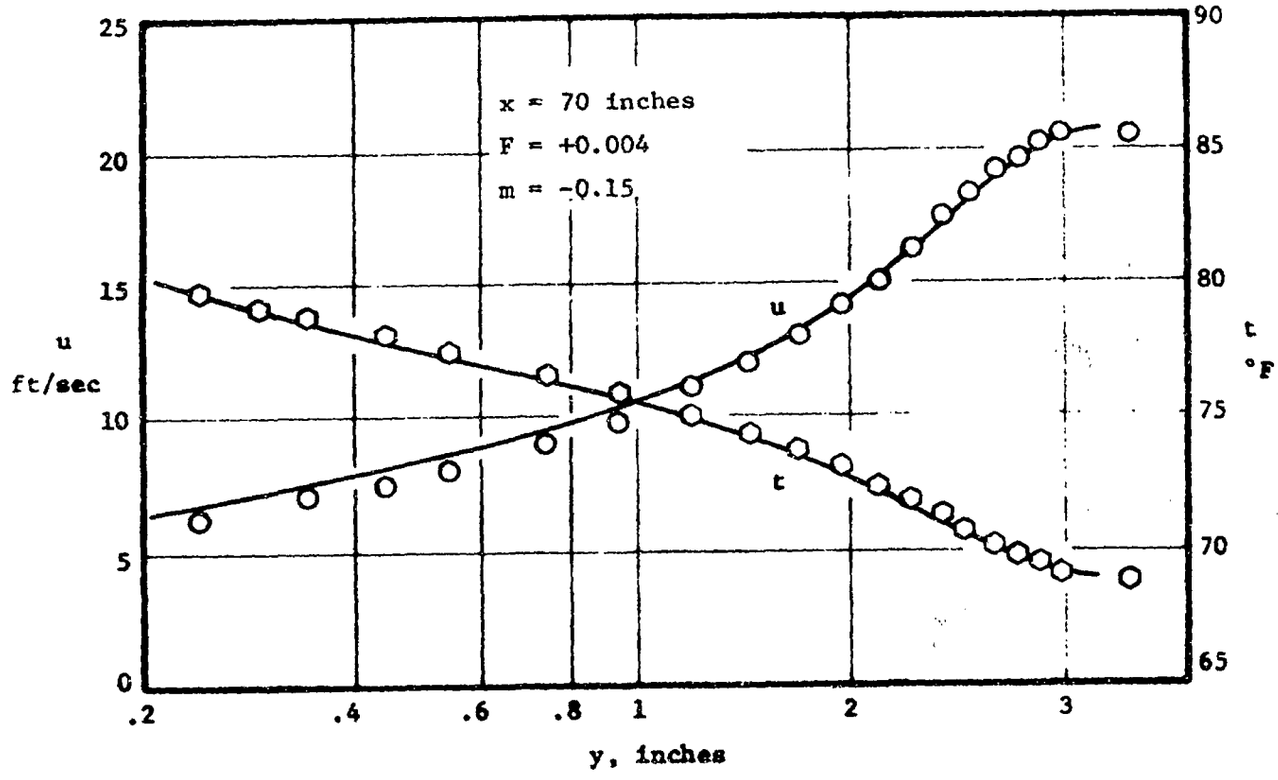

Fig. (46) A comparison of measured and predicted profiles of velocity and temperature for mild deceleration with transpiration.

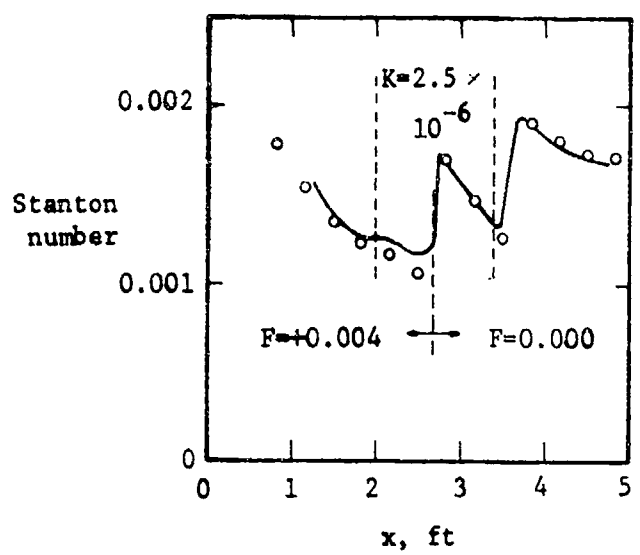

Fig. (47) A comparison of measured and predicted Stanton numbers for a step decrease in blowing within a strong acceleration.